SEPARATION OF ARSENIC, BORON AND LITHIUM FROM WATER BY USING FUNCTIONAL RESINS, FIBERS AND INORGANIC ION EXCHANGER λ-MnO₂

Gülşah ÖZKULA

Supervisor: Assoc. Prof. Dr. Müşerref ARDA

Co-Supervisor: Prof. Dr. Nalan KABAY (Chem. Eng. Dept.)

Department of Chemistry

Department Code: 405.03.01
Date of Presentation: 27.06.2014

Bornova-İZMİR

2014

Sayın **Gülşah ÖZKULA** tarafından **Yüksek Lisans** tezi olarak sunulan "**Separation of Arsenic, Boron and Lithium From Water by Using Functional Resins, Fibers and Inorganic Ion Exchanger λ-MnO$_2$**" başlıklı bu çalışma E.Ü. Lisansüstü Eğitim ve Öğretim Yönetmeliği ile E.Ü. Fen Bilimleri Enstitüsü Eğitim ve Öğretim Yönergesi'nin ilgili hükümleri uyarınca tarafımızdan değerlendirilerek savunmaya değer bulunmuş ve **27.06.2014** tarihinde yapılan tez savunma sınavında aday oybirliği/oyçokluğu ile başarılı bulunmuştur.

Jüri Üyeleri:		**İmza**
Jüri Başkanı	: Doç. Dr. Müşerref ARDA	……………………...
Raportör Üye	: Prof. Dr. Nalan KABAY	....
Üye	: Prof. Dr. H. İsmet GÖKÇEL	....
Üye	: Prof. Dr. Özdemir EGEMEN	....
Üye	: Doç Dr. Nur AKSUNER	....

EGE ÜNİVERSİTESİ FEN BİLİMLERİ ENSTİTÜSÜ

ETİK KURALLARA UYGUNLUK BEYANI

E.Ü. Lisansüstü Eğitim ve Öğretim Yönetmeliğinin ilgili hükümleri uyarınca Yüksek Lisans Tezi / Doktora Tezi olarak sunduğum "**Separation of Arsenic, Boron and Lithium From Water by Using Functional Resins, Fibers and Inorganic Ion Exchanger λ-MnO₂**" başlıklı bu tezin kendi çalışmam olduğunu, sunduğum tüm sonuç, doküman, bilgi ve belgeleri bizzat ve bu tez çalışması kapsamında elde ettiğimi, bu tez çalışmasıyla elde edilmeyen bütün bilgi ve yorumlara atıf yaptığımı ve bunları kaynaklar listesinde usulüne uygun olarak verdiğimi, tez çalışması ve yazımı sırasında patent ve telif haklarını ihlal edici bir davranışımın olmadığını, bu tezin herhangi bir bölümünü bu üniversite veya diğer bir üniversitede başka bir tez çalışması içinde sunmadığımı, bu tezin planlanmasından yazımına kadar bütün safhalarda bilimsel etik kurallarına uygun olarak davrandığımı ve aksinin ortaya çıkması durumunda her türlü yasal sonucu kabul edeceğimi beyan ederim.

27/06/2014

Gülşah ÖZKULA

ÖZET

FONKSİYONEL REÇİNE, FİBER VE ANORGANİK İYON DEĞİŞTİRİCİ λ-MnO$_2$ İLE SULARDAN ARSENİK, BOR VE LİTYUM AYRILMASI

ÖZKULA, Gülşah

Yüksek Lisans Tezi, Kimya Anabilim Dalı

Tez Danışmanı: Doç. Dr. Müşerref ARDA

İkinci Danışmanı: Prof. Dr. Nalan KABAY (Kimya Mühendisliği Bölümü)

Haziran 2014, 123 sayfa

Dünya nüfusunun artması ve buna karşılık su kaynaklarının sabit kalması ile suya olan ihtiyaç her geçen gün artmaktadır. Bu nedenle, yeni su kaynaklarının bulunması ve su arıtım yöntemlerinin geliştirilmesi gerekmektedir. Jeotermal su kullanımı da bu duruma alternatif bir çözüm getirmektedir.

Jeotermal sular, zengin mineral içeriğe sahiptir. Jeotermal sulardaki bor elementi bitkilerin bazı metabolik aktiviteleri için gereklidir; ancak bor derişiminin belirli düzeyin üzerinde olması bitkilerde olumsuz etkilere yol açmaktadır. Jeotermal sulardan lityum kazanımı cep telefon bataryaları, nükleer füzyon yakıtı gibi endüstriyel uygulamalar için önemlidir.

Bu çalışmada, bor seçimli şelatlayıcı reçine Amberlite PWA10 ve graft polimerizasyon yöntemi ile Japonya'da sentezlenen kompozit fiberin (PE-PP-NMDG) jeotermal sudan bor giderme performansları kesikli ve kolon çalışmaları ile incelenip karşılaştırılmıştır. Ayrıca, bor seçimli reçine ve fiber adsorbanların bor sorpsiyonunun kinetik olarak tepkime derecesi ve hız tayin basamağının belirlenmesi için bazı matematiksel modeller kullanılmıştır. Lityum kazanım çalışmalarında ise lityum seçimli inorganik adsorban λ-MnO$_2$, iyon değişim-membran filtrasyon yönteminde kullanılmıştır.

Tez kapsamında, Şili'de bulunan Concepcion Üniversitesi'nde N-metil-D-glukamin grubu içeren poli(N-(4-vinil benzil)-N-metil gulukamin) P(VbNMDG) reçinesi ve kuaterner amonyum grubu içeren poli[(Ar-vinilbenzil) trimetil amonyum klorür] P(ClVBTA) reçineleri sentezlenmiş ve bu iki reçinenin sulardan arsenik gideriminde kullanılabilirliği incelenmiştir. Bunun için adsorpsiyon çalışmaları yapılarak, elde edilen sonuçlar kinetik ve adsorpsiyon izoterm modellerine uygulanmıştır.

Anahtar sözcükler: Bor, lityum, arsenik, iyon değiştirici reçine, iyon değiştirici fiber, iyon değişim-membran filtrasyon hibrit yöntemi, jeotermal su, lityum seçimli adsorban.

ABSTRACT

SEPERATION OF ARSENIC, BORON AND LITHIUM FROM WATER BY USING FUNCTIONAL RESINS, FIBERS AND INORGANIC ION EXCHANGER λ-MnO$_2$

ÖZKULA, Gülşah

MSc in Chemistry
Supervisor: Assoc. Prof. Dr. Müşerref ARDA
Co-Supervisor: Prof. Dr. Nalan KABAY (Chemical Engineering Department)
June 2014, 123 pages

Due to the growing of world population, water resources remain unchanged, thus, the demand for water increases every day. Therefore, finding new water resources and developing water purification methods become necessary. The utilization of geothermal water can be an alternative solution on this respect.

Geothermal waters have a high mineral content. Boron which exists in geothermal water is required for some metabolic activities of plants, but if the concentration of boron is high, it leads to adverse effects. Lithium recovery from geothermal waters is important for industrial applications such as production of cell phones batteries and nuclear fusion.

In this study, boron selective chelating resin Amberlite PWA-10 and composite fiber synthesized in Japan with graft polymerization were investigated and compared according to their performance for boron removal from geothermal water. Moreover, mathematical models were used to investigate the rate order and rate determining step of boron sorption for boron selective resin and composite fiber adsorbents. Also, lithium recovery studies were carried out by ion exchange-membrane filtration methods using lithium selective inorganic adsorbent λ-MnO$_2$.

Besides, poly(N-(4-vinyl benzyl)-N-metyl glucamine, P(VbNMDG) resin and poly[(Ar-vinylbenzyl) trimetyl ammonium chloride], P(ClVBTA) resin which contains quarternary ammonium group were synthesized at Concepcion University, Chile. The sorption performances of these resins for arsenic were investigated. For this, adsorption studies were carried out and the results of these studies were applied to the kinetic and adsorption isotherm models.

ACKNOWLEDGEMENT

I would like to express my gratitude to my supervisors Assoc. Prof. Dr. Müşerref ARDA and Prof. Dr. Nalan KABAY as they encouraged me throughout this M.Sc study. I would like to thank them for their great guidance, valuable and helpful advices and every opportunities given to me during this study.

I would like to thank 7FP-MC-IRSES Project (CHILTURPOL 2 Grant No 269153) for the opportunity to study at University of Concepcion for 3 months period. I would like to thank Prof. Dr. Bernabe RIVAS, Dr. Bruno URBANO and Dr. Julio SANCHEZ from University of Concepcion, for their valuable guidances and supports during my studies at University of Conception, Chile.

I wish to thank Prof. Dr. Mithat YÜKSEL and Prof. Dr. Ümran YÜKSEL for all kind of helps, valuable suggestions and support.

I would like to thank Mr. Katakai, Japan for sending us ion exchange fiber samples.

I would like to thank Prof. Dr. H. İsmet GÖKÇEL, Prof. Dr. Özdemir EGEMEN and Assoc. Prof. Dr. Nur AKSUNER for reading my thesis and giving kind advices on it.

I wish to thank Dr. İdil YILMAZ İPEK for her suggestions and kind help. I am very thankful to Dr. Özgür ARAR for his kind suggestions and great support.

I would like to thank to Mehmet AKÇAY for AAS analyses.

I also wish to thank my friends Şebnem Gül İLARSLAN, Seyhan SOLAK, Yeşim SOYOĞLU, Gökhan SERT, Eren YÖRÜKOĞLU, Özge KUŞKU, Cüneyt KAYA, Suna YÜKSEL, Samuel BUNANİ and Kadir DEMİRAK for their support, great assistance and patience.

Finally, I would like to thank my family for their great support and confidence in me.

Gülşah ÖZKULA

CONTENTS

CONTENTS (continued)

CONTENTS (continued)

LIST OF FIGURES

LIST OF FIGURES (continued)

LIST OF FIGURES (continued)

LIST OF FIGURES (continued)

LIST OF FIGURES (continued)

LIST OF FIGURES (continued)

LIST OF FIGURES (continued)

LIST OF FIGURES (continued)

LIST OF TABLES

LIST OF TABLES (continued)

NOMENCLATURE

Symbol	Explanation
C	concentration of the solute in water (mg/L)
C_o	initial concentration of the solute in water (mg/L)
C_e	equilibrium concentration (mg/L)
q_e	amount of boron sorbed at equilibrium (mg/g)
q_t	amount of boron sorbed at time t (mg/g)
b	Langmuir constant
k_F	Freundlich constant
k_1	rate constant of pseudo first-order sorption (min^{-1})
k_2	rate constant of pseudo second-order sorption (g/mg min)
a	stoichiometric coefficient
C	total concentration of both exchanging species (M)
C_{Ao}	concentration of species A in bulk solution (M)
D	diffusion coefficient in solution phase (m^2/s)
D_r	diffusion coefficient in solid phase (m^2/s)
D_{eR}	effective diffusion coefficient in solid phase (m^2/s)
K_{li}	rate constant for film diffusion (infinite solution volume condition) (L/s)
K_{mA}	mass transfer coefficient of species A through the liquid film (m/s)

NOMENCLATURE (continued)

Symbol	Explanation
k_s	reaction constant based on surface (m/s)
K	rate constant (L/s)
r_o	average particle radius (mm)
T	time (s)
X	fractional attainment of equilibrium or extent of resin conversion
δ	film thickness (mm)
X	suspension resin concentration (mg/L)
Qs	rate of replacement of saturated and fresh resin (mL/min)
Qp	flow rate of permeate and feed (mL/min)

Abbreviations

RO	reverse osmosis
UF	ultrafiltration
MF	microfiltration
ED	electrodalysis
IX	ion exchange
WHO	World Health Organization

1. INTRODUCTION

1.1. Boron

Boron is metalloid, situated in group 3A of the periodic table. In its own properties, it is located somewhere between aluminum and carbon. The stable isotopes of boron are of mass 10 and 11 with estimated 20:80% ratio (Tu et al., 2010). Elemental boron has a high melting point, good hardness and is a rather poor conductor of electricity. Boron has various oxidation states in its compounds but the most significant and common is +3. It appears in lower oxidation states +1,0 or less than 0, but these states are found in compounds such as e.g. higher borates only (Tu et al., 2010; Power and Woods, 1997).

Boron is a ubiquitous element in rocks, soil and water, and although it is widely distributed in nature, it occurs in nature only in low and very low concentrations (Jay Murray, 1995). The average content of boron in the earth crust is 10 mg/L (Badruk et al., 1999). In soils its average concentration is in the range of 10-20 mg/L. There are large areas of the world suffering for deciency of this element. The content of boron in rocks is 5 mg/L in basalts to 100 mg/L in sedimentary shale. Seawater contains an average of 4.6 mg/L boron with variation of concentration from 0.5 to 9.6 mg/L. The concentration of boron in fresh water is usually from less than 0.01 mg/L to 1.5 mg/L and increases signicantly in areas where soils are boron enriched — the western part of the U.S., and a ground stretching from the Mediterranean Sea to Kazakhstan (Sarp, 2006).

In nature, boron is found mostly in the form of over 200 minerals with different amounts of calcium, sodium or magnesium. Among them the most popular are: borax, tincal, colemanite, ulexite and kernite (Sahin, 2002). Boron can ocur in nature in the form of: undissociated orthoboric acid, partially dissociated borate anions in the form of polyborates, complexes of transition metals and fluoroborate complexes (Wyness et al., 2003). These forms are present in surface waters mostly — the boron in surface waters in Europe varies from less than 10 mg B/L to greater than 1000 mg B/L (Neal et al., 1998). It is also found in ground water, brackish water or hot springs, especially at geothermal or tectonic areas. In general, the amount of boron in fresh water depends on such factors as the geochemical nature of the drainage area, proximity to marine coastal regions and imputes from industrial and municipal effluents (Loizou et al., 2010).

Boric acid is a very weak acid with a pK_a value of 9.2. At a lower pH than 7, boron is present in its non-dissociated form (boric acid) and at a pH greater than 10.5, it is present in the dissociated borate form. The exact percentage of boric acid and borate in any aqueous system is basically dependent on pH. The borate monovalent anion $B(OH)_4^-$ dominates at higher pH while non-ionized boric acid $B(OH)_3$ at lower pH. The dissociation of boric acid in water can be described as follows (Kabay et al., 2010).

$$H_3BO_3 \leftrightarrow H^+ + H_2BO_3^- \qquad pKa = 9.14$$
$$H_2BO_3^- \leftrightarrow H^+ + HBO_3^{2-} \qquad pKa = 12.74$$
$$HBO_3^{2-} \leftrightarrow H^+ + BO_3^{3-} \qquad pKa = 13.8$$
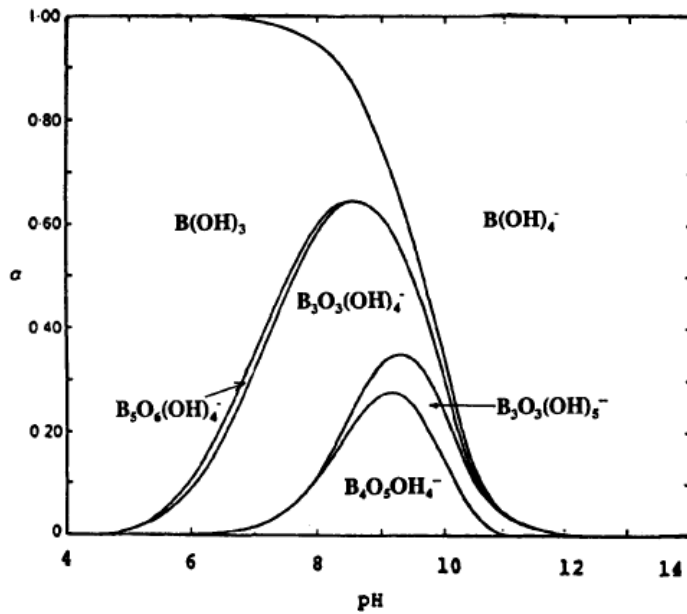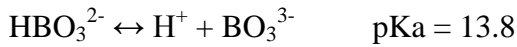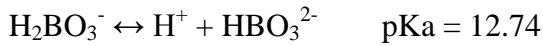
Figure 1.1. Distribution of polyborate species as a function of pH, 0.40M boric acid (Abu Ali et al., 2005).

Its concentration is usually expressed as "total boron", which includes all species and is expressed in terms of the molecular weight of the boron atom (Redondo et al., 2003). In Figure 1.1, distribution of boron species as a function of pH is given. At pH values lower than 9.24, the dominant species is boric acid in molecular form. Increase in pH provides higher concentration for dissociated species while lowering the boric acid concentration (Redondo et al., 2003).

Boron also enters to the environment from human activities such as, agricultural use, mainly from the use of borate-containing fertilizers and herbicides burning of domestic waste, crop residues and wood fuel, as boron is present in many plants being necessary for their growth power generation using fossil fuels such as coal and oil waste from borate mining and processing, including the manufacture of glass products. The use of glass products does not release boron, however, as the boron is tightly bound within the glass itself, the use of borates and perborates in the home and industry leaching from treated wood or paper and disposal of sewage and sewage sludge (Redondo et al., 2003).

The essential role of boron in plants was first described in the 20s of the XX century (Takano et al., 2008). Boron is a micronutrient essential for growing fruits and vegetables (Melnyk et al., 2005). This is the element of special attention as its deciency and excess are harmful for many plants, and the gap between both these levels is very narrow (Nadav, 1999; Sarp, 2006; Badruk et al., 1999).

Boron plays an important role in the normal growth and functioning of plants while its deficiency inhibits growth of meristematic tissue, disrupts normal cell formation and delays enzymatic reactions. The visible effects can be seen in the interruption of root and leaf growth leaf thickening, bark cracking, poor budding, excessive branching an eduction of germination (Nadav, 1999; Kabay et al., 2004a; Brown and Hu, 1997). When boron amount is higher than required, there are signs of toxic effects: yellow tips of leaves, defoliation, spots on fruits, decay and fall of unripe fruit (Nadav, 1999; Kabay et al., 2006).

Boron can run on almost all cultivations, but its concentration in irrigation water should not exceed 0.34 mg B/L depending on the crop type and soil characteristic. In agricultural production, boron toxicity is more difficult to manage than boron deficiency which can be avoided by proper fertilization (Takano et al., 2008). Different plants can tolerate boron on a different level. Some plants are more and some less sensitive to the excess of boron compounds (Tu et al,, 2010; Nable et al., 1997).

1.1.1. Effects of boron on animal and humans

According to the medical and biological research, boron compounds are among the second group of toxic substances. Since 1981 there have been many studies on the different species of animals that showed the effect of boron

deciency on the composition and functioning of many parts of an animal's body. This element has a positive effect on the metabolism of several other nutrients such as calcium, copper or nitrogen. It was noted that boron deficiency reduced absorption of calcium, magnesium and phosphorus (Sarp, 2006). Boron is also an important element in the humans' diet, but its function is not so unequivocal as for plants and its essence of action is not fully understood. The mammalian organisms need boron only in very small amounts. World Health Organization has defined 1-13 mg/day dose of boron as safe and adequate for a healthy individual (Şimşek et al., 2003).

Boron is a mineral that is delivered naturally in the food supplies. It is found in fresh and dried fruit, as well as in vegetables, nuts and in wine (Şimşek et al., 2003). Mammalians do not display any effect on boron deciency and the organisms need only the amounts that come from food (Melnik et al., 2008).

Relatively for long time, boron compounds were not treated in terms of toxic hazards. In 1993, the European Union initiated the first attempts to determine the risk caused by boron to the environment and to human health. In the same year the World Health Organization (WHO) identified this element on a list of drinking water standards and determined the permissible boron level at 0.3 mg/L. At that time, however, it was not known any technology that allowed to achieve such level of boron content. Due to this, WHO raised the value to 0.5 mg/L in 1998 (Sarp, 2006; Wyness et al., 2003; Kabay et al., 2006). Lately, the Drinking-Water Quality Committee, at its meeting on 9-13 November 2009, recommended raising the Boron Guideline Value to 2.4 mg/L in accordance with the latest data from the UK and USA on dietary intakes (Tu et al., 2011). The revised Guideline Value was incorporated into the Guidelines for Drinking-Water Quality, 4th Edition and was published in 2011 (WHO, 2011). The WHO guideline was formulated on the basis of human health consideration only. It was not related to irrigation water where old standards should stil be applied.

The content of boron in drinking water, irrigation as well as in the wastewater is adjusted through out the world. However, the recommended level of boron varies in different countries and regions. Hilal et al. (2011) summarized the maximum B concentrations in drinking water from any regions in the world. In the European Union including UK, as well as in South Korea and Japan, the maximum amount of boron in potable water is kept at the 1.0 mg/L level. The USA has no federal regulations, and the permissible level depends on the state

(e.g. State of Minnesota 0.6 mg/L, State of Florida 0.63 mg/L, State of California 1.0 mg/L). In New Zealand, the value is 1.4 mg/L. In Israel, the maximum boron concentration is 1.5 mg/L. Canada (5mg/L) and Australia (4 mg/L) have set the maximum boron concentration over the WHO guideline. Only Saudi Arabia is the country complying with the guidelines (Hilal et al., 2011; Melnyl et al., 2005).

Boron is widely distributed in surface and ground waters, occurring naturally or from anthropogenic contamination, mainly in the form of boric acid or borate salts. Water contamination by boron is one of the widespread environmental problems, since even a few parts per million present in irrigation water can cause stunting of plant growth (Sabarudin et al., 2005).

1.1.2. Boron separation methods

Taking into account the increasing concentration of boron in surface waters and the need for treatment of seawater, which contains large amounts of this element, the current research focuses on the development of effective technologies for the removal of boron. Unfortunately, there is no simple and economic method for this task. The great difficulty in selecting of such method is the fact that boron appears in water in several numbers of chemical compounds and its concentration varies from place to place (Melnyk et al., 2005). The methods commonly used in water purication as sedimentation, coagulation or adsorption on clays are not effective in the case of boron compounds. It is not an effective water treatment by biological or chemical compounds as they remove only small amounts of boron or they do not remove it at all (Melnyk et al., 2005; Kabay et al., 2006). The processes of evaporation, crystallization or solvent extraction, suited only for solutions with high concentrations, are more useful in the production of boric acid than in the process of removing its traces from water (Sahin, 2002).

The methods for boron removal can be classified as follows:
Electrocoagulation
Co-precipitation
Solvent extraction
Adsorption
Membrane processes
Ion exchange
Hybrid processes

1.1.2.1. Electrocoagulation

Yılmaz et al. (2008) used electrocoagulation method for removal of boron from geothermal water. Current density (CD), pH of solution and temperature of solution were selected as operational parameters. The results showed that boron removal efficiency increased from pH 4.0 to 8.0 and decreased at pH 10.0. Boron removal efficiency reached to 95% with increasing current density from 1.5 to 6.0 mA/cm^2, but energy consumption also increased in this interval. At higher temperatures of solution, such as 313 and 333K, boron removal efficiency increased. At optimum conditions, boron removal efficiency in geothermal water reached up to 95%. Elsewhere, boron removal from boron-containing solution by electrocoagulation and chemical coagulation methods was compared by Yılmaz et al. (2007). Boron removal obtained was higher with electrocoagulation process. At optimum conditions (e.g. pH 8.0 and aluminum dose of 7.45 g/L), boron removal efficiencies for electrocoagulation and chemical coagulation were 94.0% and 24.0%, respectively.

Sayiner et al. (2008) studied boron removal from wastewater by electrocoagulation. Aluminum and iron were used in the reactor as materials for cathode and anode. For optimal operation conditions determination, different values of current density (CD), initial concentrations and time was discussed.

1.1.2.2. Co-precipitation

Co-precipitation method using metal hydroxide is an inefficient and environmentally ineffective process due to low removal rate, requirement of a large amount of metalhydroxide, disposal of large amount of unrecyclable wastes (Itakura et al., 2005). Aydın et al. (2013) studied boron removal from the solution through the chemical precipitant method by using $Mg(OH)_2$. They found that the efficiency depends on temperature and the amount of the precipitant.

Yilmaz et al. (2012) investigated boron removal by chemical precipitation from aqueous solutions containing boron using $Ca(OH)_2$. pH, initial boron concentration, amount of $Ca(OH)_2$, stirring speed and solution temperature were selected as operational parameters in a batch system. The highest boron removal efficiency was reached at pH 1.0 and at a stirring speed of 150 rpm. Increasing initial boron concentration and amount of calcium hydroxide increased boron removal efficiency. Also, increasing solution temperature improved importantly

boron removal. When the optimum operational conditions were selected, over 96% of boron removal efficiency was reached by this method.

1.1.2.3. Solvent extraction

Boron extraction mechanism has been classified into three groups: (a) physical extraction, (b) extraction by forming nonionic ester complex, (c) extraction by forming borate salt complex. The extractants belonging to groups (b) and (c) are suitable for boron extraction from acidic and alkaline solutions, respectively (Matsumoto et al., 1997).

Ayers et al. (1981) tested petroleum ether solutions of 2-ethyl-l,3-hexanediol (EHD) and 2-chloro-4-(l,l,3,3-tetramethylbutyl)-6-methylol-phenol (CTMP), employed both singly and in admixture for solvent extraction of boron.

Hosgoren et al. (1997) tested 1,2-dihidroxy-4-oxadodecane (DHD) for solvent extraction of boron from aqueous solutions.

Bicak et al. (2003) tested N,N-Bis(2,3-dihydroxypropyl) octadecylamine (BPO) in 2-ethyl hexanol for liquid-liquid extraction of boric acid from aqueous solutions.

Fortuny et al. (2012) prepared boron extractants from ionic liquids derived from Cyanex 272 and from Aliquat 336, Cyphos IL 101 and Cyphos IL 167.

1.1.2.4. Adsorption

Okay et al. (1985) studied the removal of boron from the drainage waters of the Bigadic boron mines of Turkey by using cellulose, magnesium oxide as adsorbents. Experimental results show that the adsorption method using magnesium oxide is effective in removing boron from the drainage waters. Cellulose as an adsorbent had a minimum efficiency on boron removal.

Morisada et al. (2011) performed a study to investigate the adsorption removal of boron in solutions at various pHs and temperatures by using the tannin gel (TG) and the amine-modified tannin gel (ATG). Both the tannin gels can adsorb boron in aqueous solutions effectively in the range of pH above 7.

Some hydrous oxides of tetravalent metals ($CeO_2.nH_2O$, $ZrO_2.nH_2O$, $HfO_2.NH_2O$) or pentavalent metals ($Ta_2O_5.NH_2O$) showed good adsorptivity for boron. On the other hand, hydrous oxide of trivalent metal did not show a high boron adsorptivity (except for the double oxide of aluminium and iron) although they are known as anion exchangers (Ooiet al., 1996).

1.1.2.5. Ion exchange

Ion exchange (IX) processes are used to remove undesirable ions such as arsenic and boron. The exchange medium consists of a solid phase of naturally occurring minerals or a synthetic resin having a mobile ion attached to an immobile functional acidic or basic groups. In ion exchange process, the mobile ions are exchanged with solute ions having a stronger affinity for the functional group. Once the resins become "saturated" and can not bind the boron, it must be regenerated (regeneration occurs either on a time cycle or on demand). This requires a process of essentially "stripping" the resin from the removed ions and getting them back to a state where they can once again be exchanged (Bick and Oron, 2005).

Among several methods of boron removal, the use of boron selective chelating ion exchange resins seems to have still the greatest importance (Sabarudin et al., 2005; Recepoglu and Beker et al., 1991). It was shown that chelating resins containing ligands having three or more hydroxyl groups, located in the cis position, the so-called 'vis-diols', show a high selectivity to boron while these groups are not reactive to ordinary metals and other elements. Selective sorption of these resins is due to reactions that are characteristic for boron. Molecules of polyoxide compounds tend to bond through the formation of boric acid esters of boron or borate anion complexes with a proton as a counterion (Badruk et al., 1999; Melnyk et al., 2005; Kabay et al., 2004; Bicak et al., 2001). The obtained results suggest that the presence of tertiary amine group is critical for boron chelating. It captures proton freed during complexing of borate by hydroxyl functionalities (Bicak et al., 2001; Li et al., 2011). According to these findings, the studies on construction of B-selective resins has been launched (Bicak et al., 2001; Senkal and Bicak et al., 2003). Most synthesized resins were formed by modication with the N-methyl-D-glucamine (NMDG) of copolymer of styrene and divinylbenzene (see Figure 1.2).
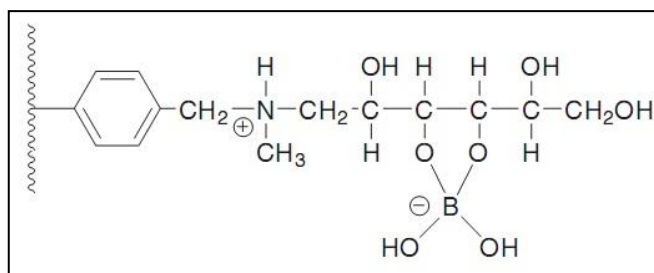
Figure 1.2. Chelating resins with NMDG groups, used to remove boron from aqueous solutions (Marston et al., 2005).

The functional groups of these resins capture boron through a covalent attachment and form a coordination complex as is shown in Figure 1.3 (Bicak et al., 2000).
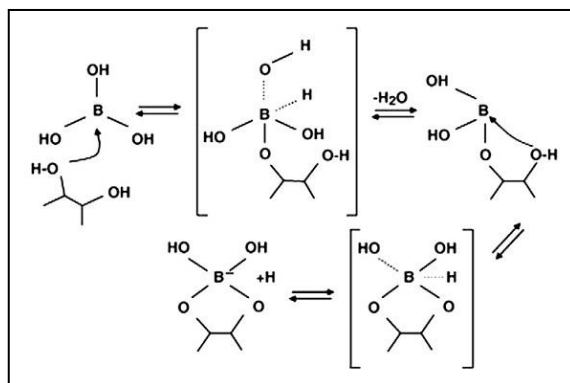
Figure 1.3. Binding mechanism of boron by NMDG type chelating resin (Marston et al., 2005).

The N-methyl-D-glucamine-type chelating resins and fibers are the most extensively studied and reported in the literature. The development of new boron selective chelating resins and fibers with a large capacity, high selectivity, and high sorption rate received great interest for boron removal and recovery from natural waters and wastewaters (Kabay et al., 2004).

On the market, the following boron selective ion exchange resins are available Amberlite IRS 743 (Rohm & Haas Corporation), BSR1 (Dow Chem), Purolite S-108 (Purolite International), Diaion CRB03 and Diaion CRB05 (Mitsubishi Corporation, Japan). These resins are able to remove boron selectively with an efficiency of 93-98%, even from highly mineralized solutions (Melnyk et al., 2005).

There have been efforts to improve the ability of boron selective resins, since polystyrene based resins with N-methyl-D-glucamine function emerged as

boron specic resins in the mid 1960s (Bicak et al., 2005). As the performance of the resins depends on its polymeric support and functional groups, it has been of interest to develop new polymeric support or functional groups.

Bicak et al. prepared terpolymers of glycidyl methacrylate (GMA)-methyl methacrylate (MMA)-divinyl benzene (DVB) and used the terpolymers as a support for boron specific resins possessing N-methyl-D-glucamine as functional groups. From sorption and elution tests, it was found that the resin showed good stability in terms of particle disintegration for long term uses and better performance of regeneration in comparison to common polymeric boron sorbents (Bicak et al., 2001).

Parschova et al. compared the performance of each sorbent possessing N-methyl-D-glucamine functional groups with different polymeric supports, polypropylene-styrene, polypropylene-GMA, viscose-GMA and commercially used polystyrene-DVB (Purolite D-4123), respectively. The breakthrough capacity of the resins synthesised was much lower than the commercial BSR under the conditions investigated. However, viscose GMA based sorbent showed much faster sorption kinetics and was easy to regenerate even with diluted (0.1 mol/L) hydrochloric acid solution (Parschova et al., 2007).

The comparative results were obtained using different N-methyl-D-glucamine type resins and column performances of these resins for boron removal from geothermal wastewater were investigated by Kabay et al. (2004b). It was determined from the data of batch-mode tests that, for the boron selective resins, Diaion CRB01, Diaion CRB02 and Purolite S108, to remove more than 90% of boron, 3 g resin/L wastewater was required (Kabay et al., 2004b). In another study, a column mode removal of boron from geothermal wastewaters using Diaion CRB02, N-methyl-D-glucamine-type chelating resin for 10 sorption-washing-elution-washing regeneration-washing cycles was also studied in Kizildere geothermal field, Denizli. Column-mode recovery of boron from acidic eluate solution was performed using Diaion WA 30, a weak base anion exchange resin (Kabay et al., 2004a).

Yilmaz-Ipek et al. (2010) performed the batch and column mode tests to evaluate the efficiency of boron removal from geothermal water containing 10-11 mg B/L using Lewatit MK 51 which is a macroporous weak base anion exchange resin with polyhydroxyl groups showing a very high selectivity and capacity for

boron. The optimum resin amount for boron removal from geothermal water was determined as 4.0 g resin/L-geothermal water.

1.1.2.6. Membrane processes

Removal of boron can be achieved by some membrane processes, such as, electrodialysis (ED), nanofiltration (NF) and reverse osmosis (RO).

Reports on boric acid transport in electrodialysis (ED) are the most widely found in the existing literature (Melnik et al., 1999; Turek et al., 2007). However, the effectiveness of boric acid removal or the boron transport in feed waters with pH<9 by ED is poor (Melnik et al., 1999; Banasiak et al., 2009). The maximum degree of boron removal reported was 87%. Turek et al. reported that it is only possible to remove less than 12.4% of boron from the waters of low salinity at pH<9. However, when the pH of the solution was brought up to above 11.2 the effectiveness of boron removal increased up to 85% (Turek et al., 2005; Turek et al., 2008). Kabay et al. (2008) reported that at a pH of 9.0, only 20% of boron can be removed by ED, while at higher pH, the effectiveness of boron removal by ED can be much higher. In addition, Banasiak and Schafer et al. (2009) reported that at pH<9, a maximum of 40% of boron can be removed from water of moderate salinity (5 g/L of NaCl). It was reported that as the pH of boron-containing water is increased to just above a pH of 9, a significant increase in the rate of boron transport in ED is observed (Melnik et al., 1999; Melnik et al., 2007; Yazicigil et al., 2006).

According to Glueckstern and Priel (2003), currently available RO membranes for seawater desalination have the ability to remove boron (boric acid and borate ions) from 85 to 90% at standard test conditions by manufacturers. However, this corresponds to around 78-80% of boron rejection at normal operation conditions of SWRO systems (Glueckstern and Priel, 2003).

Prats et al. (2000) reported the rejection of boric acid by RO in the region of 40-60% at pH ranges of 5.5-9.5 while borate ion removal under the same conditions is more than 95%. Therefore, the overall boron removal by RO is dependent on the boric acid/borate ion ratio. Using a RO membrane for feed water with a high proportion of boric acid will lead to unsatisfactory levels of boron in the permeate water (Prats et al., 2000).

Koseoglu et al. investigated boron removal from seawater using two commercial high rejection SWRO membranes. The membranes used were the Toray^{TM} UTC-80-AB and Filmtec^{TM} SW30HR membranes. The boron rejection was much higher at pH of 10.5 (>98%) for both of the membranes, than those obtained at original seawater pH of 8.2 (about 85–90%). Permeate boron concentrations less than 0.1 mg/L were easily achieved at pH 10.5 by both membranes, which was provided by electrostatic repulsion and size exclusion mechanisms with dominant dissociated boron species (Koseoglu et al., 2008).

Sarp et al. studied the removal of boron efficiency from model and natural seawater using different types of nanofiltration (NF) and RO membranes and effect of ionic strength on boron removal. Boron removal efficiencies of NF membranes decreased by increasing ionic strength of the solution and they showed better removal efficiencies with 5 mg/L of boron solution. Boron removal efficiencies of RO membranes increased by increasing ionic strength (Sarp et al., 2008).

1.1.2.7. Boron separation by hybrid methods

Recently, a new type of separation process that integrates the sorption process with membrane separation of the binding agents, presents the possibility of an effective and inexpensive process, which can be successfully applied either to water treatment or recovery of any component. A combination of the advanced binding agents with their separation on membranes reveals many advantages compared with conventionally used fixed-bed systems. The main advantage of this separation method is the high efficiency and lower costs of the process compared to classical sorption in a fixed bed. The sorbents can be used as very fine particles with increase sorption surface area. Consequently, sorbates show higher uptakes and the rate of the process increase. Moreover, synergetic effects that appear on the membrane surface may cause the high intensification of the process (Koltuniewicz and Bazak, 2000; 2001a; 2001b).

In a sorption-membrane filtration hybrid system, as shown in Figure 1.4., at first, specific complexing agent (C) binds the selected component (B) and this complex (BC) is separated from water (W) by an appropriate semi-permeable membrane. In this stage, the pure water (W) is a main product whereas the complex (BC) passes to the second stage of separation. Splitting of the complex BC onto the free sorbent (C) and pure component (B) and their separation on

membrane is carried out in the second stage of the process. This provides sorbent regeneration and recovery (Kabay et al., 2006).
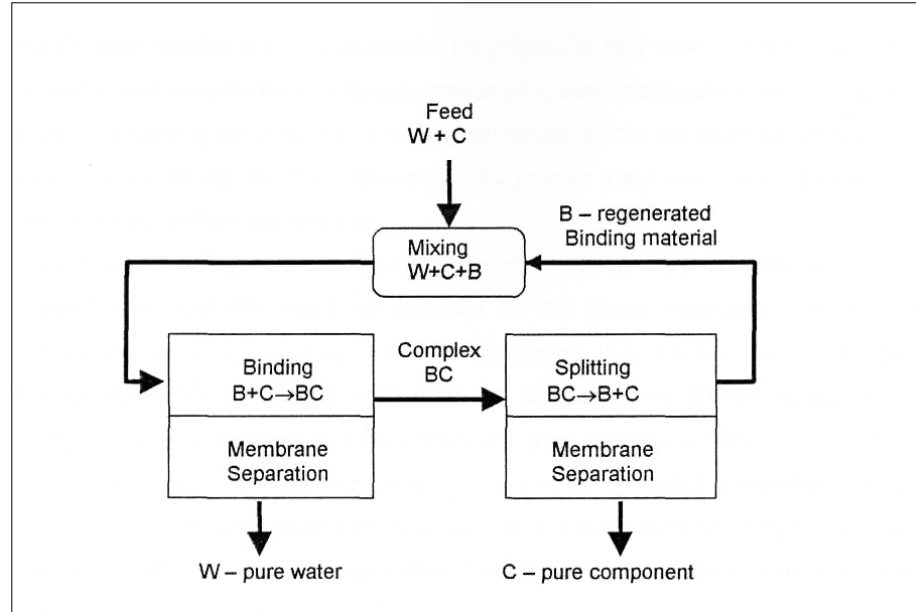
Figure 1.4. Flow sheet of a sorption–membrane filtration hybrid system (Kabay et al., 2006).

When a fixed-bed system is compared with a sorption-membrane filtration hybrid system, it is obviously seen that we can not use the powder form adsorbents in fixed bed columns because of the pressure drop. Higher pressure drop means higher pumping costs of the fluid through the sorbent which is economically not feasible. The pressure drop is very sensitive to particle size (dp) according to Darcy law (Eq. (1.1)) (Koltuniewicz et al., 2004):

$$\Delta P = \mu_0 \frac{\mu h}{K} \tag{1.1}$$

where μ is viscosity (Pa s), h is the height of the layer (m), and μ_0 (m/s) is superficial velocity referred to the cross-section of the sorbent layer. The permeability of the layer formed with particles of various shapes is dependent on a specific surface area, a (m^2/m^3), the porosity, ε, and tortuosity, τ of the capillaries shaped between the sorbent particles (Eq. (1.2)) (Koltuniewicz et al., 2004):

$$K = \frac{\varepsilon^3}{2a^2(1-\varepsilon)^2\tau} \tag{1.2}$$

If all particles have spherical shape, the permeability of the layer depends on their diameter dp according to Carman–Kozeny equation (Eq. (1.3)) (Koltuniewicz et al., 2004):

$$K = \frac{\varepsilon^3 d_p^2}{72\tau(1-\varepsilon)^2} \qquad (1.3)$$

From the equations of (1.1) and (1.3), it is seen that as the particle size decreases, the pressure drop increases for a fixed bed system. The same equation (1.3) describes the pressure drop caused by the cake layer on a membrane. As, the thickness of the cake (if there is) is much lower than the height of a fixed bed, the pressure drop and energy lost should be substantially smaller for the membrane case (Koltuniewicz et al., 2004).

Also, it is possible to prevent cake formation entirely by keeping the permeate flux under the critical flux value according to the critical flux theory. Then, the sorbent may be only concentrated (but not settled) on the membrane surface in the form of the suspension, which flows tangentially to the membrane surface (Figure 1.5.). In this case, during the permeate flow through the membrane, the pressure drop is independent of particle size but is dependent on the membrane resistance (Equation 1.4) (Koltuniewicz et al., 2004):

$$\Delta P = J\mu R_m \qquad (1.4)$$
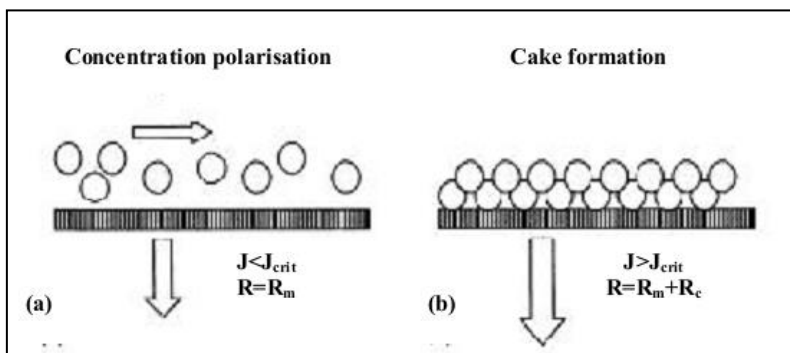
Figure 1.5. Comparison of the sorbent layers at membrane surface depending on the flux: (a) below the critical flux and (b) above the critical flux (Koltuniewicz et al., 2004).

It is also possible to avoid cake formation on membrane surface by several methods such as; pulsative flow and turbulence promoters, back-pulsing and

backflushing, skimming, gas sparking, and many others (Koltuniewicz et al., 2004).

Kabay et al. investigated the suitability and performance of the adsorption-membrane filtration (AMF) hybrid process technology for boron removal from seawater and/or RO first stage permeate (Kabay et al., 2008).

Kabay et al. investigated the efficiency of ion exchange-membrane hybrid process for boron removal and compared it to the conventionally used ion exchange process. Commercially available chelating ion-exchange resins containing N-methyl glucamine groups were used to determine the effect of particle size of chelating resins on their kinetic performance using both processes. (Kabay et al., 2006). In another study of boron removal from geothermal water by ion exchange-microfiltration hybrid process, the effect of various parameters such as resin particle size, flow rate and resin concentration on boron removal was investigated (Kabay et al., 2009).

1.2. Lithium

Lithium is present in the Earth's crust to the extent of about 0.006 w% (Habashi, 1997). It is the 27th most abundant element in nature. The major lithium minerals with commercial value are classified into three major groups:

Silicates (spodumene-$LiAlSi_2O_6$, petalite- $LiAlSi_4O_{10}$)

Micas (lepidolite-$K[Li,Al]_3[Al,Si]_4O_{10}[F,OH]_2$

Phosphates (mainly amblygonite-$[Li,Na]Al[F,OH]PO_4$

Lithium is also found in natural brines (Salar de Atacama—Chile, Salar de Hombre Muerto and Salar de Rincon—Argentina and Searles Lake and Clayton Valley in the USA) and lakes (Great Salt Lake, USA; Zabuye Lake, Tibet; Dachaidan, Qinghai—China and Dead Sea, Israel) (Habashi, 1997). The lithium content of these brines varies from 20 mg/L in the Dead Sea to 1500 mg/L in Salar de Atacama (Habashi, 1997; Moore, 2007). Geochemically, lithium is a highly mobile element, therefore, the environmental and occupational health and safety risks related to lithium in brines are higher.

Lithium is used in many items, such as high-performance grease, heat-resistant ceramics, flux for welding, batteries, and pharmaceuticals. It is also required for use in a nuclear fusion furnace. Lithium-ion batteries have been commercialized since 1991, initially concerning mobile devices such as cell phones and laptops (Nagura, 1990). Interest on this technology has considerably increased and generated a lot of research in order to improve the performances of those batteries (Brodd, 2002).

A small proportion of lithium production (less than 1% of the total) is used in medicine. Lithium occurs naturally in biological tissues and hence is incorporated into food stuffs. It occurs widely in drinking water, usually at low concentrations. Natural waters that contain higher concentrations of lithium and other metals frequently are designated, as 'mineral waters', with supposed medicinal properties (Chitrakar et al., 2001).

1.2.1. Lithium separation methods

Several methods such as adsorption, ion exchange, solvent extraction, coprecipitation have been investigated for the extraction of lithium from seawater, brine, and geothermal water. The adsorption method is suitable for recovery of lithium from seawater because certain inorganic ion-exchange materials show extremely high selectivity for lithium ions only. In the past 20 years, several studies have been done on the recovery of lithium from seawater using different types of inorganic adsorbents (Chitrakar et al., 2001).

Of these methods, the ion-exchange process employing resins is not favoured because of its low selectivity for the extremely low concentration of lithium in seawater in the presence of large amounts of other salts. However, some inorganic ion exchangers exhibit an extremely high selectivity for certain elements or groups of elements (Abe and Chitrakar, 1987).

Certain inorganic adsorbents with extremely high selectivity for lithium ions are called lithium ion-sieves. Due to the noticeable properties of low toxicity, low cost, high chemical stability and high lithium adsorption capacity, the lithium ion-sieves are suitable for recovery of lithium from salt lake brine and seawater. Among the inorganic adsorbents, spinel-type hydrous manganese oxides are interesting materials because of their extremely high affinity toward lithium ions only. Examples such as λ-MnO_2, $MnO_2.0.31H_2O$ and $MnO_2.0.5H_2O$ which are

obtained from $LiMn_2O_4$, $Li_{1.33}Mn_{1.67}O_4$, $Li_{1.6}Mn_{1.6}O_4$, respectively, have been used to adsorb Li^+ from lithium solutions, and shown satisfying adsorption performances (Ma et al., 2011).

For the past several years, many studies have been done to develop lithium manganese oxides with less capacity losses at high temperatures (Premanand et al., 2002; Striebel et al., 2002; Tucker et al, 2002; Hwang et al., 2002). However, a lithium ion battery using lithium manganese oxide as a positive electrode has a disadvantage that it deteriorates badly at high temperatures. This has been attributed to the severe capacity loss of a carbon negative electrode on the deposition of Mn ions dissolved out of a lithium manganese oxide (Tsunekawa et al., 2002). However, a little work on the Mn dissolution in each charged state was found among the published literatures (Xia et al., 1997; Lee et al., 2000; Yamane et al., 2001; Yamane et al., 2002; Saitoh et al., 2003) . Further research on the Mn dissolution in lithium manganese oxide should lead to better materials as the positive electrode.

The spinel-type manganese oxide MnO_2. 0.31 H_2O derived from $Li_{1.33}Mn_{1.67}O_4$ is suitable as a lithium selective adsorbent, because it has a high chemical stability against lithium insertion-extraction in the aqueous phase as well as selective lithium uptake (Miyai et al., 1994).

Chitrakar et al. developed a new type of lithium selective manganese oxide, MnO_2. $0.5H_2O$ ($H_{1.6}Mn_{1.6}O_4$) derived from $Li_{1.6}Mn_{1.6}O_4$. First, the ion-exchange capacity was markedly larger than that of the other manganese oxides, because the theoretical exchange capacity reaches 10.5 mmol/g on the basis of the chemical composition. Second, the chemical stability is sufficiently high, because it contains only tetravalent manganese (Chitrakar et al., 2001).

1.3. Arsenic

Arsenic (atomic number 33) is ubiquitous and ranks 20th in natural abundance, comprising about 0.00005 % of the Earth's crust, 14th in the seawater, and 12th in the human body (Mandal and Suzuki, 2002).

Thermodynamic predictions provide a useful understanding of the equilibrium chemistry of inorganic arsenic species in water as seen in Figure 1.6. Arsenic is perhaps unique among the heavy metalloids and oxyanion-forming

elements (e.g., As, Se, Sb, Mo, V, Cr, U, Re) in its sensitivity to mobilization at the pH values typically found in ground waters (pH 6.5-8.5) and under both oxidizing and reducing conditions. Arsenic can occur in the environment in several oxidation states (at the valences of 3, 0, 3, and 5), but in natural waters, it is mostly found in inorganic form as oxyanions of trivalent arsenite (As(III)) or pentavalent arsenate (As(V)) (Ioannis and Zouboulis 2004). The mobility of As(III) was commonly considered to be greater than that of As(V), which has recently been successfully challenged. It remains true that iron oxyhydroxide phases probably play a key and complex role in controlling the mobility and fate of arsenic in groundwater. Redox potential (Eh) and pH are the most important factors controlling arsenic speciation. Under oxidizing conditions, $H_2AsO_4^{1-}$ is dominantat low pHs (between pH 2.2 and 6.9), while at higher pHs, $HAsO_4^{2-}$ becomes dominant. At extremely acidic and alkaline conditions, arsenic may be present as H_3AsO_4 and AsO_4^{3-}, respectively. Under reducing conditions at pH less than 9.2, the uncharged arsenite species H_3AsO_3 will predominate (Smedley and Kinniburgh, 2002).
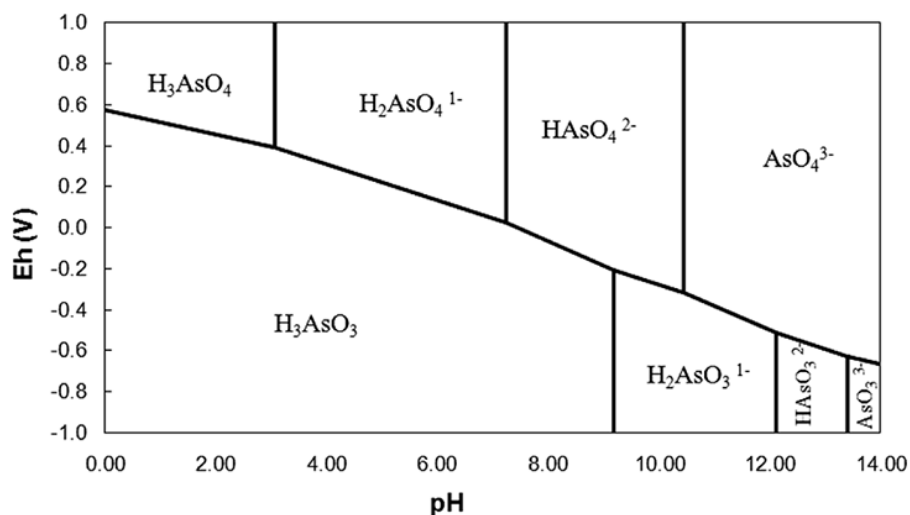
Figure 1.6. Equilibrium chemistry of inorganic arsenic aqueous species in the system As-O_2-H_2O at 25°C and 1 bar total pressure (Smedley and Kinniburgh, 2002).

Several forms of arsenic undergo acid-base equilibrium; thus, different major and minor species are present depending on the pH. As(V) dissociates sequentially in water as follows:

$$H_3AsO_4 \leftrightarrow H^+ + H_2AsO_4^- \quad pK_{a1} = 2.1$$

$$H_2AsO_4^- \leftrightarrow H^+ + HAsO_4^{2-} \qquad pK_{a2} = 6.7$$

$$HAsO_4^{2-} \leftrightarrow H^+ + AsO_4^{3-} \qquad pK_{a3} = 11.2$$
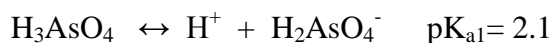
Arsenic occurrence in the environment, its toxicity, health hazards, and the techniques used for speciation analysis are well known and have been reviewed (Bodek et al., 1998; Penrose, 1974; Jain and Ali, 2000; Matschullat, 2000; Bissen and Frimmel, 2003a). Long term ingestion of high concentrations of inorganic arsenic from drinking water, or by other ways, can cause skin, liver, lung, kidney, or bladder cancer and can also lead to skin hyperk-eratosis, pigmentation changes, neurological disorders, muscular weakness, loss of appetite, and nausea by bioaccumulation (Smith et al., 1992).

Arsenic in natural waters is a world wide problem. Arsenic pollution has been reported recently in the USA, China, Chile, Bangladesh, Taiwan, Mexico, Argentina, Poland, Canada, Hungary, New Zealand, Japan and India. The largest population at risk among the 21 countries with known groundwater arsenic contamination is in Bangladesh, followed by West Bengal in India (Burkel and Stoll, 1999; Cebrian et al., 1983; Dhar et al., 1997; Karim, 2000; Mondal et al., 2006; Borgono and Greiber, 1971).

The World Health Organization (WHO) and the Environmental Protection Agency (EPA) have strictly reduced the maximum contaminant level recommended from 50 μg/L to 10 μg/L to minimise the risk to humans (WHO, 2004).

1.3.1. Methods of arsenic removal from water

Arsenic contamination of water sources is estimated to affect over 144 million people around the world, spurring the development of numerous water treatment technologies to limit negative health impacts associated with exposure to arsenic contaminated water including skin lesions and cancers (Dhar et al., 1997; Chakraborti et al., 2010; Ng et al., 2003; Smith et al., 2000). Conventionally, there are several methods for arsenic removal. These methods include coagulation and flocculation, precipitation, adsorption and ion exchange, membrane filtration. Alternative methods like ozone oxidation, bioremediation and electrochemical treatments are also used in the removal of arsenic.

Precipitation/coprecipitation process causes dissolved arsenic to form low-solubility solid minerals. Adsorption process for arsenic removal is realized through arsenic species on special solid adsorbents, such as activated carbon (Dambies et al., 2002). Ion exchange process uses synthetic resins to remove dissolved ions from water. Membrane separation process, including microltration, reverse osmosis, electrodialysis, ultraltration, and nanoltration, has also been proved to be effective for arsenic removal from water (Feenstra et al., 2007). Biological process has attracted attention recently in this area (Johnston and Heijnen, 2001). Among the possible treatment processes, adsorption is considered to be less expensive than membrane separation, easier and safer to handle as compared with the contaminated sludge produced by precipitation, and more versatile than ion exchange.

1.3.1.1. Oxidation and reduction

Oxidation is a previously required step to transform As (III) species in more easily removable As (V) species. Simple direct aeration is slow (Bissen and Frimmel, 2003b), but a number of chemicals, including gaseous chlorine, hypochlorite, ozone, permanganate, hydrogen peroxide, manganese oxides and Fenton's reagent (H_2O_2/Fe^{2+}) can be employed to accelerate oxidation. Chlorine is a rapid and effective oxidant, but it may react with organic matter, producing toxic and carcinogenic trihalomethanes as by-products. Potassium permanganate effectively oxidizes arsenite, and it may be a widely available inexpensive reagent suitable for developing countries. Ultraviolet radiation alone or with suitable light absorbers such as TiO_2 can be also convenient options for As (III) oxidation (Pirnie, 2000).

1.3.1.2. Coagulation-flocculation

In arsenic removal processes, coagulation and flocculation are among the most common method employed.

Coagulation is the destabilization of colloids by neutralizing the forces that keep them apart. Cationic coagulants provide positive electrical charges to reduce the negative charge (zeta potential) of the colloids. As a result, the particles collide to form larger particles. Rapid mixing is required to disperse the coagulant throughout the liquid. Flocculation is the action of polymers to form bridges

between the larger mass particles or flocs and bind the particles into large agglomerates or clumps (Thomas et al., 2007).

Coagulation process is traditionally realized by adding ferric or aluminum ions (Hering et al.,1996). In this process, fine particles in water first aggregate because added ferric or aluminum ions strongly reduce the absolute values of zeta potentials of the particles. Then, arsenic ions (arsenate or arsenite) precipitate with the ferric or aluminum ions on the coagulates, and thus concentrate in the coagulates. After that, the coagulates are separated from water through filtration, eliminating arsenic from the water. Besides iron and aluminum compounds, manganese, calcium and magnesium compounds are also of effective coagulants for eliminating arsenic from water (Song et al., 2006).

Iron coagulants are more effective than aluminum, titanium, and zirconium ones (Shen and Am, 1973; Scott et al., 1995; Lakshmanan et al., 2008). Karcher et al. (1999) and Guo et al. (2000) also reported the the uses of ferric chloride and lime-polyferric sulfate as the coagulants. Han et al. used ferric chloride and ferric sulphate as flocculants in arsenic removal.

The coagulation is much more effective for the removal of As (V) than As (III). In the case when only As (III) is present, oxidation to convert As (III) to As (V) is needed prior to coagulation. The effective pH for arsenic removal was reported to be 5–7 with aluminum ions, and 5–8 for ferric ions (Sorg and Longsdon, 1978).

1.3.1.3. Adsorption

Adsorption systems use the affinity of different material to bind the pollutants from an aqueous phase to the surface of a solid phase. Advantages of adsorption processes over other techniques are: its low running cost, the absence of electrical supply and its low maintenance requirements. Combined with their capacity to remove arsenic to very low level and their high removal capacity, adsorbent materials are reliable media in treating arsenic. The extended review of arsenic adsorbents by Mohan and Pittman et al. (2007) shows the considerable interest within the scientic community to develop low cost, high capacity adsorbents for arsenic removal.

Natural adsorbents, such as laterite soil, natural red earth, red mud, natural iron ores, plant biomass, sea nodule, and ferralite contain components which can effectively adsorb and remove arsenic from water media. Developed natural adsorbents are effective but sometimes a high adsorbent dose is required and removal efciency is low (Maji et al., 2007; Maji et al., 2007). Synthetic adsorbents developed and applied to remove arsenic from aqueous media include iron-oxide-coated cement, coconut husk carbon, red mud sludge, iron-oxide-coated sponge, ferric ions, hardened paste of Portland cement, and hydrous zirconium oxide (Manju et al., 1998; Kundu et al., 2005).

Activated carbon is also commonly used as the material in arsenic treatment (Daus Wennrich and Weiss et al., 2004; Huang and Fu et al., 1984). Eguez and Cho et al. (1987) measured the adsorption of As (III) and As (V) using activated carbon at various values. Zhu et al. supported nano zero-valent iron onto activated carbon (NZVI/AC) by impregnating carbon with ferrous sulfate followed by chemical reduction with $NaBH_4$ and to test its performance for arsenic removal from water. Activated carbon was used as the supporting material due to its excellent properties in mechanical strength and pore structures.

Iron oxides also have been widely used as sorbents to remove contaminants from wastewater and liquid hazardous wastes compared to activated carbon (Choong et al., 2007). Arades et al. (2013) investigated the suitability of various natural iron oxide minerals for the removal of arsenic from water. A study was conducted to evaluate hematite, magnetite, goethite and iron rich laterite soil as arsenic adsorbents. Adsorption tests showed that iron rich laterite was most effective for arsenic removal, followed by goethite, magnetite and hematite (Aredes et al., 2013).

Deliyanni et al. (2000 and 2003) synthesized a novel adsorbent, akaganéite-type β-FeO(OH) in the laboratory by precipitation from aqueous solution of Fe(III) chloride and ammonium carbonate for arsenic removal. Advantage of this sorbent, which found to be nanostructured, was its high surface area and narrow pore size distribution.

Kumar Maji et al. (2008) studied on removal of arsenic from real-life groundwater using laterite soil as an adsorbent. Laterite soil is a red-colored clay-rich soil found in the tropics and subtropics. Under optimized conditions, the laterite soil could remove up to 98% of total arsenic.

1.3.1.4. Membrane processes

From the possible membrane processes, microfiltration (MF) or ultrafiltration (UF), which use low-pressure membranes (large nominal pore sizes, 10-30 psi) are not completely adequate for arsenic removal because the arsenic species are very small and can pass through the membranes. The RO membrane rejects especially polyvalent ions, being suitable for arsenic oxyanions. The process is efficient over an extended pH range (3-11) (Clifford, 1999).

In electrodialysis (ED), ions are transported from a lesser to a higher concentrated solution through ion permeable membranes under the influence of a direct electrical current. The efficiency of the technique is similar to that of RO, mainly in treating water with high total dissolved solids (TDS). Electrodialysis with reversion of polarity of the electrodes (EDR) is an improvement of ED with minimization of scaling (Ravenscroft et al., 2009). The electrodialys is units made up of cation and anion exchange resins are more effective in removing As(V) than As(III) (Kartinen and Christopher et al., 1995).

The membrane technology is very little used when the objective is to remove only the arsenic, and when this element is the only one contaminant in the raw water. The membranes are justified when the total dissolved solids due to the presence of sulphates, nitrates, carbonates etc., are important and require a treatment. In practice, the in-line coagulation used before a membrane treatment (MF or UF) provides very good performances. Impact of chemical pretreatment on the performance of membrane systems (i.e., membrane reversible fouling, chemical cleaning frequency), the compatibility of these chemicals with membrane materials, the optimum conditions for chemical pre-treatment, and overall cost and benefits of chemical pre-treatment to MF and UF membrane systems (Farahbakhsh et al., 2004).

Recent advances in membrane technology in arsenic removal include electro-ultrafiltration (EUF). EUF is found to possess good potential in treating arsenic from water. Weng et al. (2005) demonstrated removal of arsenic and humic substances from water using electro-ultrafiltration (EUF) membrane after applying voltage to the EUF cell. These membranes showed 71% rejection for As-III at pH 10 and >90% rejection for As-V at pH 6 (Weng et al., 2005).

Ergican et al. (2005) reported that As (V) was removed from water with cationic surfactant micelles using polyethersulfone (PES) UF membrane. With the addition of 10 mM cationic surfactant (cetylpyridiniumchloride, CPC) to the feed water, the arsenic removal effciency was signicantly increased, ranging between 78.1 and 100%.

Sato et al. (2002) also investigated arsenic removal by pressure driven membrane process such as nanofiltration (NF) for arsenic removal. In their studies, both As(V) and As(III) removal by NF membranes were not affected by source water chemical compositions. NF membranes could remove over 95% of As(V). Furthermore, more than 75% of As(III), which is toxic form of arsenic, could be removed without any chemical additives (Sato et al., 2002).

Kang et al. (2000) had studied the effect of pH on removing of arsenic using reverse osmosis (RO). They found that the removal of arsenic compound is almost proportional to the removal efficiency of NaCl. The removal of As(V) is much higher than As(III) over the pH range 3–10. The effect of solution pH on the removal of arsenic using RO membranes was strongly affected by the solution pH, especially for the case of As(III).

1.3.1.5. Ion-exchange

Synthetic ionic exchange resins can be applied for arsenic removal. Quaternary amine groups, $-N^+(CH_3)_3$, are the preferred functional groups. As(V) removal is efficient, producing effluents with less than 1 μg/L of arsenic, while As(III), is not removed, and a pre-oxidation step is necessary (Pirnie, 2000; Ravenscroft et al., 2009).

Commonly, ion exchange resins are pretreated with hydrochloric acid to establish chloride ions at the surface, which are easily displaced by arsenic. Arsenate removal is relatively independent of pH and influent concentration. $HAsO_4^{2-}$ has adsorption ability higher that of $H_2AsO_4^{2-}$. Competing anions, especially sulfate, TDS, selenium, fluoride, and nitrate, interfere strongly and can affect run length. Suspended solids, SS, and precipitated iron can cause clogging (Kartinen and Martin, 1995).

Strong-base anion-exchanger resin removes arsenic from water according to the following reactions:

$$R\!-\!Cl + H_2AsO_4^- \leftrightarrow R\!-\!H_2AsO_4 + Cl^-$$

$$2R\!-\!C1 + HAsO_4^{2-} \leftrightarrow R_2\!-\!HAsO_4 + 2Cl^-$$
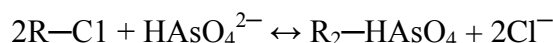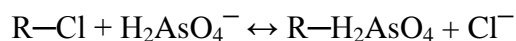
As the selectivity of such resin to divalent anions is higher than its selectivity to monovalent anions, the efficiency of the process at high pH, under which the proportion of divalent arsenic anions in the water is greater, may be expected to be higher too. Regeneration is carried out with excess of chloride ions according to the following reaction (Korngold et al., 2001):

$$R_2HAsO_4 + Cl^- \leftrightarrow RCl + H_2AsO_4^-$$
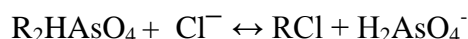
Ficklin (1983) separated As(III) and As(V) with a strong anion-exchange resin. Samples were acidified with 1% (v/v) of concentrated HCl. As(III) passed through the resin, As(V) was retained (Ficklin, 1983). Russeva et al. (2003) used a chromatographic column filled with inert support modified with the organotin reagent $(C_8H_{17})_2SnCl_2$ for the separation of As(III) and As(V). As(V) was quantitatively retained, while As(III) was not retained (Russeva et al., 1993). Dominguez et al. (2003) synthesized anion exchange fibers from a vinylbenzyl chloride precursor for arsenate removal.

Iesan et al. (2004) used strong base anion resins to remove arsenic present in drinking water by conducting column studies. It was compared with Purolite A-300E (styrenic, Type II, gel, dimethyl hydroxyethylammonium functional groups); Purolite A-520E (styrenic, Type I, macroporous, trimethyl ammonium functional groups); Purolite A-530E (styrenic, Type I, macroporous, biquat with mixed amine functionality); Purolite A-555 (styrenic, Type I/III, macroporous, quaternary amonium functional groups); Sybron A 554 (styrenic, Type II, gel, dimethyl hydroxyethylammonium functional groups); Purolite A-250 (styrenic, Type II, opaque gel, dimethyl hydroxyethylammonium functional groups). The studies were conducted as a function of pH, and less than 10 ppb was achieved from an initial concentration of 200 ppb for As(V) with Purolite A-250 resin, a strong base anion (SBA) type II at a pH of 7.5 - 8.0, range typically encountered in drinking water supplies. A sulfate-selective resin, Purolite A-250 tends to be superior to nitrate-selective resins (Purolite A-520E and Imac HP555) for arsenic removal.

1.4. Aim of this study

In this study, it was aimed to investigate the removal of boron from geothermal water by ion exchange resin and composite fiber with batch-mode and column mode sorption-desorption tests. EDI method was applied for boron separation from RO permeate of geothermal water. Also, sorption-membrane filtration hybrid system using λ-MnO_2 a lithium selective adsorbent and ZW-1 hallow fiber UF membrane was employed for lithium removal from geothermal water. Besides, P(VbNMDG) and P(ClVBTA) ion exchange resins were synthesized at University of Conception in Chile. These resins were used for As(V) removal from water.

2. EXPERIMENTAL

2.1. Materials

2.1.1. Ion exchange resins and fiber

In this study, N-methyl-D-glucamine type boron selective resin, Amberlite PWA 10, supplied by Rohm&Haas and a boron selective composite fiber, supplied by Mr. A. Katakai, JAERI, Takasaki, Japan, were used for boron removal from geothermal water samples.

Boron selective resin, Amberlite PWA-10, has functional groups of N-methyl-D-glucamine (Figure 2.1), which form chelating complexes with boric acid and borates. The characteristics of boron selective chelating resin, Amberlite PWA10, were given in Table 2.1. The boron selective composite fiber is a polyethylene coated polypropylene fiber with N-methyl-D-glucamine functional groups (Figure 2.2).
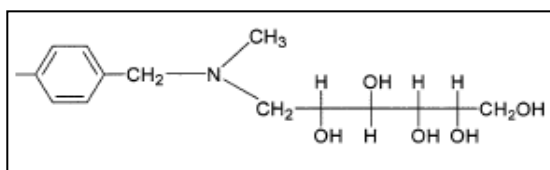
Figure 2.1. Structure of N-methyl-D-glucamine type boron selective resin (Dambies et al., 2004).

Table 2.1. Chemical and physical characteristics of Amberlite PWA 10 (www.dow.com).

Matrix	Macroporous polystyrene
Physical form	Opaque beige beads
Shipping weight (g/dm^3)	700
Moisture holding capacity (%)	48-54
Total exchange capacity (eq/L)	≥ 0.7
Particle size: screen grading (mm)	0.3-1.2
Particle size: fines content (mm)	<0.300
Operating temperature (^{o}C), max	45
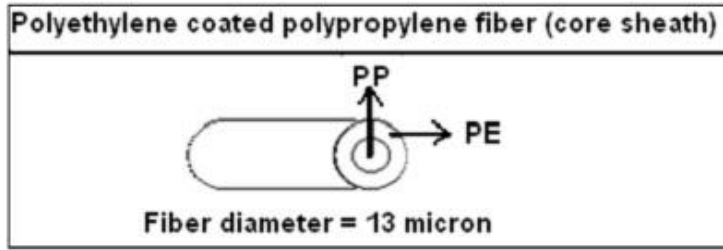
Figure 2.2. Structure of composite fiber.

Purolite CT 175 and Purolite A 500 ion exchange resins (Purolite, Italy) were used in EDI tests for boron removal. The properties of ion exchange resins are listed in Table 2.2.

Table 2.2. Chemical and physical characteristics of ion exchange resins (www.purolite.com).

	Purolite CT 175	**Purolite A 500**
Polymer structure	Macroporous polystyrene crosslinked with divinylbenzene	Macroporous polystyrene crosslinked with divinylbenzene
Functional group	Sulfonic Acid	Type 1 Quaternary Ammonium
Capacity (eq/L)	1.8 (H^+ form)	1.15 (Cl^- Form)
Moisture retention (%)	50-57 (H^+ form)	53-58 (Cl^- Form)
Temperature limit (ºC)	125 (H^+ form)	65 (OH^- Form)

2.1.2. Ion exchange membranes

The properties of ion exchange membranes (Asahi Glass (Japan) and ASTOM Corporation (Japan)) used in the EDI tests were listed in Table 2.3.

Table 2. 3. Chemical and physical characteristics of ion exchange membranes (http://www.astom-corp.jp/en/en-main2-neosepta.html, http://www.selemion.com/SEL3_4.pdf).

Grade	Neosepta AMX	Neosepta CMX
Type	Strongly basic anion exchange	Strongly acidic cation exchange
Characteristic	High mechanical strengths (Cl^- form)	High mechanical strength (Na^+ form)
Electric resistance (Ω-cm^2)	2.0 ~3.5	1.8 ~3.8
Burst strength (kgf/cm^2)	$\geq$0.30	$\geq$0.40
Thickness (mm)	0.12 ~ 0.18	0.14~0.20

Cation and anion exchange membranes were pre-conditioned before used in experiments. For this purpose, ion exchange membranes were firstly contacted with 1.0 M NaCl for 24 h and then washed with deonized water. Secondly, ion exchange membranes were contacted with 0.1 M NaCl for 24 h and then washed with deionized water. After that they were stored in pure water at dark.

2.1.3. Lithium adsorbent

A novel λ-type manganese dioxide (λ-MnO$_2$) adsorbent has been developed for selectively recovering Li$^+$ from seawater. This adsorbent can be prepared from spinel-type lithium di-manganese tetra-oxide (LiMn$_2$O$_4$) using ion exchange of Li$^+$ by hydrogen ion (Yoshizuka et al., 2002). In the LiMn$_2$O$_4$ spinel, the O atoms have a cubic close packing or face-centered close packing structure, and contrary to expectations based on ionic radius, the Mn atoms are in octahedral sites (16d) and the Li in the tetrahedral sites (8a) as shown in Figure 2.3 (Zhang et al., 2010).
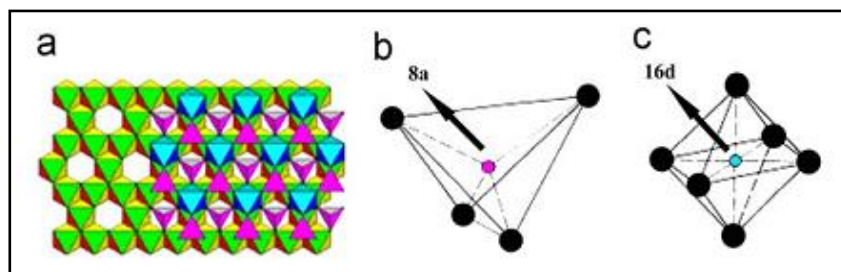
Figure 2.3. LiMn$_2$O$_4$ spinel structure with crystal face perpendicular to the page layout (a). Li atoms are in the red tetrahedral 8a sites (b) and the Mn in the blue octahedral 16d sites (c). (Zhang et al., 2010).

Before using the LiMn$_2$O$_4$ adsorbent, it was converted to H$^+$ form. For this, 5 g of adsorbent was contacted with 1 L of 1.0 M HCl , by shaking at 30°C, for 24 h (5 times). After acid washing, adsorbent was washed with deionized water until pH 4-5 and then the adsorbent was shaked with 1 L NH$_4$$^+$ / NH$_3$ buffer solution (pH = 8.12) at 30°C, for 24 h. After then, adsorbent was filtrated using 5 μm membrane filter and were subjected to air drying and vacuum drying until a constant mass is obtained as shown in Figure 2.4 (Yoshizuka, et al., 2002).
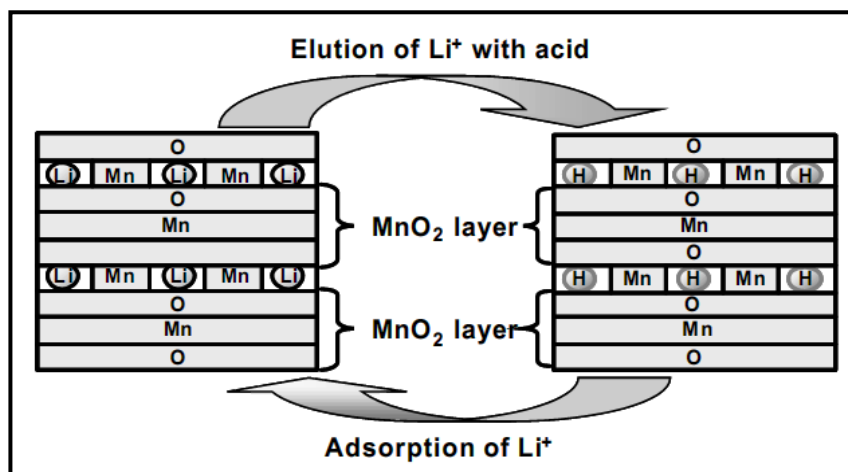
Figure 2.4. Schematic diagram of adsorption and elution mechanism of Li$^+$ in λ-MnO$_2$ adsorbent. (Yoshizuka, et al., 2002).

2.1.4. Chemicals

- Curcumine (C$_{12}$H$_{20}$O$_6$, Acros Organics)
- Azomethine-H monosodium salt hydrate (C$_{17}$H$_{12}$NNaO$_8$S$_2$, Merck)
- Ascorbic acid (99%, Acros Organics)
- Ethylenediamine tetraacetic acid disodium salt dehydrate (EDTA) (Analar, analytical grade)
- Ammonium acetate (CH$_3$COONH$_4$, Merck)
- Acetic acid (CH$_3$COOH, 99-100%, Carlo Erba)
- Sulfuric acid (H$_2$SO$_4$, 96%, Carlo Erba)
- Boric acid (H$_3$BO$_3$, 99.8%, Merck)
- Sodium hydroxide (NaOH, J.T. Baker)
- Lithium carbonate (Li$_2$CO$_3$, 99.9%, Merck)
- Sodium arsenate heptahydrate (Na$_2$HAsO$_4$.7H$_2$O, Aldrich)

For the synthesis of arsenic selective resins, the monomer N-(4-vinylbenzyl)-N-methyl-D-glucamine (VbNMDG) was synthesised using the precursors 4-vinylbenzyl chloride (VBC, Aldrich) and N-methyl-D-glucamine

(NMDG, Aldrich) as received. The reagent N,N-methylene-bis-acrylamide (MBA, 98% Aldrich) and ammonium persulphate (Aldrich) were used as cross-linker and initiator reagents, respectively. For the synthesis of ClVBTA, (4-vinylbenzyl) trimethylammonium chloride (Aldrich) and potassium persulphate (Aldrich) were used. Hydrochloric acid (37%), potassium iodide (Merck) and ascorbic acid (Merck) were used for analysis of arsenic.

2.1.5. Polymers for arsenic removal

Structures of P(VbNMDG) and P(ClVBTA) resins synthesized at Concepcion University were given in Figure 2.5.
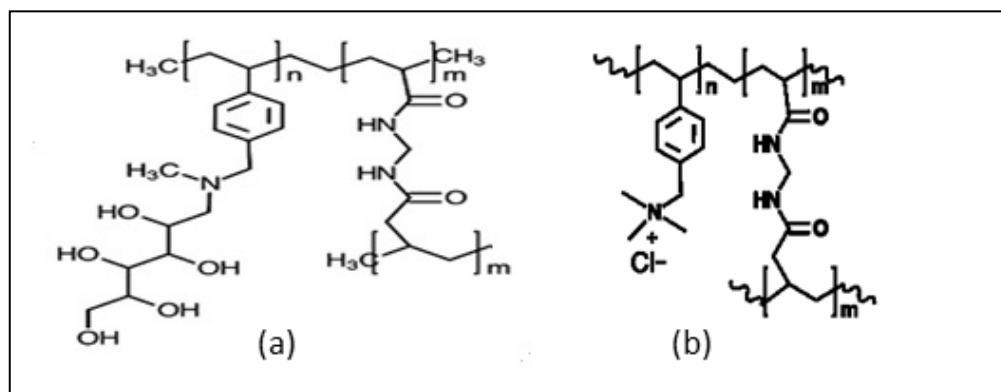
Figure 2.5. Structure of ion exchange resins a) P(VbNMDG) b) P(ClVBTA).

2.1.5.1. Synthesis of N-(4-vinyl benzyl)-N-methyl-D-glucamine resin (P(VbNMDG))

The reaction of N-methyl-D-glucamine and 4-vinyl benzyl chloride was carried out in a three-neck round-bottom flask using a moler ratio of 1:1. Reagent grade N-methyl-D-glucamine (44 mmol) was dissolved in 150 mL of 2:1 volume solvent mixture of dioxane and deionized water. The solution was added to the reactor and heated for 20 min, until NMDG was completely dissolved. Subsequently, 3.20 mL (44 mmol) of 4-vinyl benzylchloride was dissolved in 20 mL of dioxane and was subsequently added slowly to the reactor. The reaction was maintained under reflux with constant stirring for 5 h, and a yellowish solution was obtained. In order to remove unreacted VBC, the final solution was washed with ethylether twice. The VbNMDG monomer, which was dissolved in a dioxane/water solvent, was transferred to the reactor and added to N,N-

methylene-bis-acrylamide (15%). After crosslinking reagent was dissolved, ammonium persulfate (1%) as initiator was added. The mixture was degassed with a nitrogen gas for 10 min. The reaction was stirred for overnight under a a nitrogen atmosphere at 70ºC (Figure 2.6).

Resin was washed with distilled water and subsequently dried in an oven at 50ºC. Finally, dry resin was sieved, and a particle-size fraction in the range of 180 -250 μm was chosen for all sorption experiments.
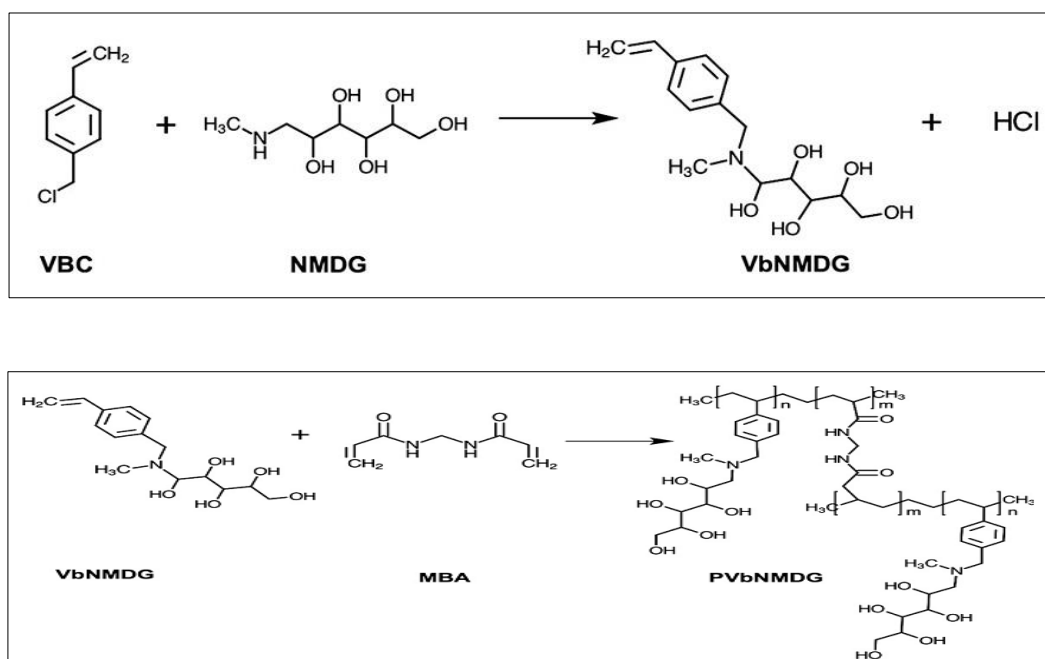
Figure 2.6. Scheme of reactions for the monomer (VbNMDG) and resin (PVbNMDG).

2.1.5.2. Synthesis of (4-vinylbenzyl) trimethylammonium resin (P(ClVBTA))

A 8 g of (4-vinylbenzyl) trimethylammonium chloride and N,N-methylene-bis-acrylamide (15%) were dissolved in water. After crosslinking reagent was dissolved, potassium persulfate (1%) as initiator was added. The mixture was degassed with a nitrogen gas for 10 min. The reaction mixture was stirred overnight under a nitrogen atmosphere at 70ºC (Figure 2.7).

Resin was washed with distilled water and subsequently dried in an oven at 50ºC. Finally, dry resin was sieved, and a particle-size fraction in the range of 180 -250 μm was chosen for all sorption experiments.
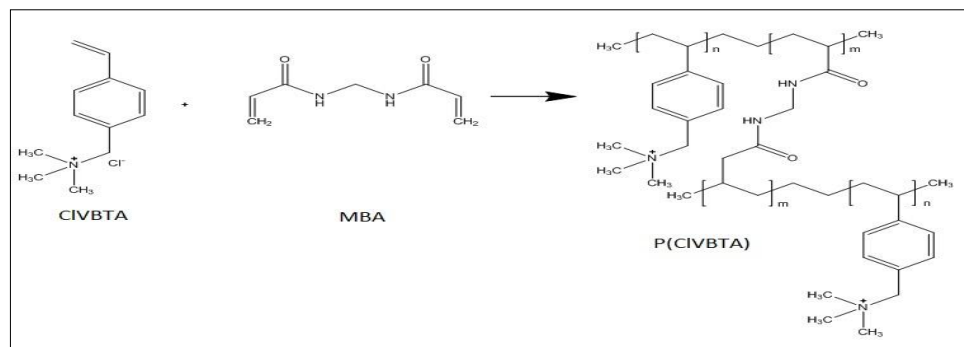
Figure 2.7. Scheme of reactions for the PClVBTA resin.

2.1.5.3. Material characterization

The characterizations of polymers P(VbNMDG) and P(ClVBTA) were carried out by Fourier transformed infrared spectroscopy (FTIR) on a Perkin Elmer 1760-X spectrometer from 4000 to 400 cm^{-1} using KBr pellets.

2.1.6. Geothermal water

Geothermal water provided by the Izmir Geothermal Co. was used in experiments. The chemical composition of geothermal water was shown in Table 2.4.

Table 2.4. Chemical composition of geothermal water (Sampling time 25.07.2011).

Cations	Concentration (mg/L)	Anions	Concentration (mg/L)
*Na^+	365.00	■Cl^-	195.21
*K^+	35.20	■SO_4^{2-}	165.49
*Ca^{2+}	45.00	□HCO_3^-	503.5
*Mg^{2+}	13.49	□CO_3^{2-}	0.090
*Li^+	1.28		
pH		7.25	
EC (mS/cm)		2150	
TDS (mg/L)		1075	
Salinity (‰)		1.03	
Turbidity (NTU)		3.19	
▲B (mg/L)		10.44 (Azomethine Method)	

* **AAS**   ■ **IC**   □ **Titrimetric**   ▲ **Spectrophotometric**

2.2. Equipments

2.2.1. Equipments used in batch-mode sorption studies

Shaker: Selecta (Figure 2.8)

Figure 2.8. Selecta – Unitronic OR shaker.

2.2.2. Equipments used in kinetic sudies

Magnetic stirer: Ikamag[®] EDA 9 magnetic stirer (Figure 2.9)
Syringe: SET Inject
Filter: Millipore Millex-FH 0.45 μm filter
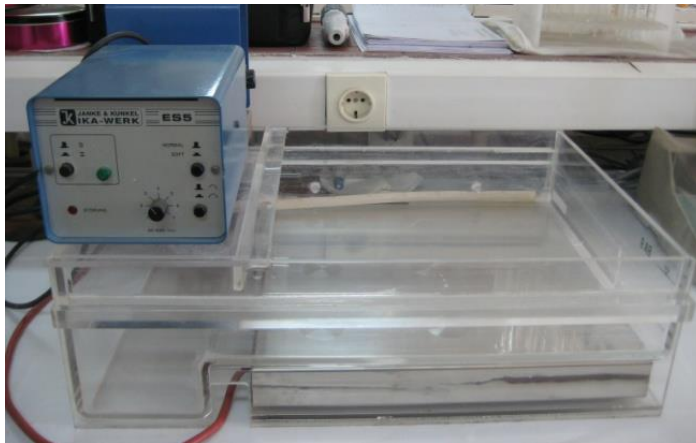
Figure 2.9. Ikamag® EDA 9 magnetic stirer.

2.2.3. Equipments used in column-mode sorption studies

Fraction collector: IWAKI ASAHI TECHNO GLASS Fraction Collector FRC-2100 (Figure 2.10)
Peristaltic pump: ISMATEC (Figure 2.11)
Glass column: ID= 0.7 cm

Figure 2.10. Fraction collector: IWAKI ASAHI TECHNO GLASS Fraction Collector FRC-2100.

Figure 2.11. Peristaltic pump (ISMATEC).

Figure 2.12. Experimental set-up of column-mode studies.

2.2.4. Equipments used in submerged sorption-membrane filtration hybrid method

ZeeWeed®-1 (ZW-1) Module:

In the studies of submerged sorption-membrane filtration hybrid system, an ultrafiltration module, ZeeWeed®-1 (ZW-1), supplied by General Electrics, Israel was used (Figure 2.13). The module has a nominal pore size of 0.04 μm, an effective membrane surface area of 0.047 m^2, a length of 17.5 cm and a diameter of 5.8 cm. Characteristics of ultrafiltration membrane module ZeeWeed®-1 (ZW-1) were given in Table 2.5. Air was supplied to membrane module by the air compressor at a flow rate of 4 L/min to eliminate the accumulation of adsorbent particles on the membrane surface.

Table 2.5. Characteristics of ultrafiltration membrane module ZeeWeed®-1 (ZW-1).

General Type	Supported, non-ionic, hydrophilic
Effective membrane surface area	0.047 m^2
Nominal pore diameter	0.04 μm
Hold up volume	10 Ml
Maximum permeation pressure	0.6 bar
Operating transmembrane pressure	0.07-0.55 bar
Permeate flow range	5-25 mL/min
Maximum scouring air flow	1.8 m^3/h
Maximum operating temperature	40ºC
pH range	5 – 9

Figure 2.13. ZeeWeed®-1 (ZW-1) hollow fiber ultrafiltration membrane module.

Peristaltic Pumps: Masterflex® (Type: L/STM, Economy drive, Easy-Load II) Eyela (Micro Tube Pump MP-3)

Tubings: Masterflex®

Magnetic stirrer: Heating Magnetic Stirrer**,** Velp scientifica

Compressor: Aras air compressor

Figure 2.14. Experimental set-up of submerged sorption-membrane filtration hybrid method using lithium adsorbent.

2.2.5. Equipments used in synthesis of ion exchange resins

- **Polymerization reactor:** Schlenk polymerization tube
- **Heater:** IKA C-MAG HS 7 (Figure 2.15)
- **Oven:** Equilab Memmert

Figure 2.15. Polymerization system.

2.2.6. Equipments used in characterization of ion exchange resins

Fourier transformed infrared spectroscopy (FTIR): Perkin Elmer 1760-X spectrometer.

2.2.7. Analysis of boron

Spectrophotometer: JASCO V-530 UV/VIS Spectrophotometer (Figure 2.16).

Figure 2.16. Spectrophotometer: JASCO V-530 UV/VIS Spectrophotometer.

2.2.8. Analysis of lithium

Atomic absorption spectrophotometer: VARIAN Spectra AA atomic adsorption spectrophotometer (Figure 2.17).

Figure 2.17. VARIAN Spectra AA atomic adsorption spectrophotometer.

2.2.9. Analysis of arsenic

Flow injection atomic spectroscopy: FIAS-100 flow injection for atomic spectroscopy (Figure 2.18).
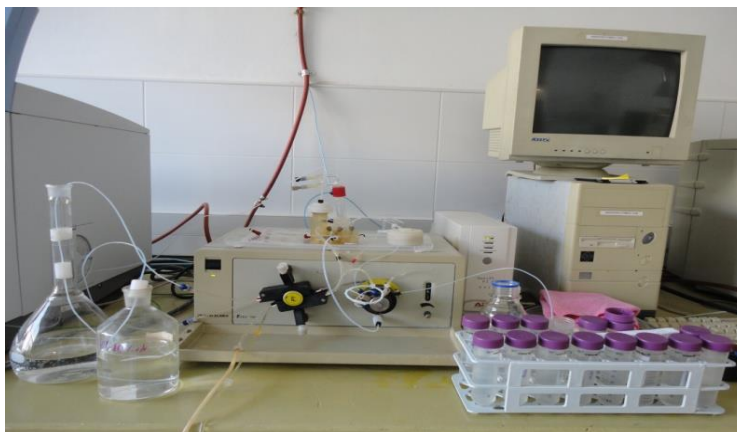
Figure 2.18. FIAS-100 flow injection for atomic spectroscopy.

2.3. Batch-Mode Sorption Tests

2.3.1. Batch-mode sorption with composite fiber

2.3.1.1. Effect of fiber amount on boron removal from geothermal water

Optimum fiber amount for boron removal from geothermal water was determined by using boron selective composite fiber. In these studies, various dry fiber amounts (0.005, 0.01, 0.02, 0.05, 0.06, 0.07 and 0.1 g) were contacted with 25 mL of İzmir geothermal water by shaking in a shaker at 30ºC for 24 hours.

2.3.1.2. Kinetic tests

Kinetic tests were performed with 400 mL of Izmir geothermal water using boron selective composite fiber. The fiber concentration used in these tests was 2 g fiber/L geothermal water. The test was performed at 30ºC for 24 hours by using a water bath with a mechanical stirrer. The stirring rate was adjusted to 250 rpm. Supernatant samples of 3 mL were collected at a defined time interval of 0, 5, 10, 15, 20, 30, 45, 60, 120, 180, 240, 360, 480 minutes and 24 hours and boron concentrations were measured.

2.3.1.3. Cycle studies

Cycle studies including sorption-washing-eluted-washing-regeneration-washing cycles for 10 times were carried out using boron selective composite fiber. In sorption step, optimum amount of composite fiber that was determined in batch-mode studies, were contacted with 25 mL of Izmir geothermal water at 30ºC for 24 hours. In the first washing step, composite fiber was washed with deionized water. Washed composite fiber was contacted twice with 20 mL of H_2SO_4 solution at different concentrations (0.1, 0.5, 1 and 2 M H_2SO_4) in a shaker during 2 hours for elution at 30ºC. In this washing step, composite fiber was washed with deionized water until pH 6-7. Following the elution and washing stage, composite fiber was contacted with 20 mL of 4% NaOH solution in a shaker for 2 hours. After regeneration, the composite fiber was washed with deionized water until neutralization.

2.3.2. Batch-mode sorption with Amberlite PWA-10

2.3.2.1. Effect of resin amount on boron removal from geothermal water

To determine the optimum resin amount for boron removal from geothermal water, boron selective resin, Amberlite PWA-10, at a particle size range of 0.500-0.710 mm was used. In these studies, various amounts of boron selective resin (0.005, 0.01, 0.02, 0.05, 0.06, 0.07 and 0.1 g) were contacted with 25 mL of geothermal water by shaking in a shaker at 30ºC for 24 hours.

2.3.2.2. Kinetic tests

Kinetic studies were performed with 400 mL of Izmir geothermal water using boron selective resin, Amberlite PWA-10, at a particle size range of 0.500-0.710 mm. The resin concentrations used in these tests were 2 g resin/L geothermal water and 2.8 g resin/L geothermal water. All of the tests were performed at 30ºC for 24 hours by using a water bath with a mechanical stirrer. The stirring rate was adjusted to 250 rpm. Supernatant samples of 3 mL were collected at a defined time interval of 0, 5, 10, 15, 20, 30, 45, 60, 120, 180, 240, 360, 480 minutes and 24 hours and boron concentrations were monitored.

2.3.2.3. Cycle studies

Cycle studies including ten sorption-washing-eluted-washing-regeneration-washing cycles were carried out using boron selective ion exchange resin Amberlite PWA-10. In sorption step, optimum amount of resin that was determined in batch-mode studies, were contacted with 25 mL of geothermal water at 30ºC for 24 hours. In the first washing step, boron selective resin was washed with deionized water. Washed resin was contacted twice with 20 mL of H_2SO_4 solution in different concentrations (0.1, 0.5, 1 and 2 M H_2SO_4) in a shaker during 2 hours for elution at 30ºC. In this washing step, resin was washed with deionized water until pH 6-7. Following the elution and washing stage, resin was contacted with 20 mL of 4% NaOH solution in a shaker for 2 hours. After regeneration, the resin was washed with deionized water until neutralization.

2.4. Column-Mode Sorption Tests

To investigate the column performances of the boron selective resins, Amberlite PWA-10 at a particle size range of 0.355-0.500 mm, Diaion CRB02 at a particle size range of 0.250-0.355 mm and 0.355-0.500 mm, and boron selective composite fiber, for boron removal from geothermal water, column-mode sorption and elution tests were performed.

In column-mode studies a glass column with an internal diameter of 0.7 cm was used. A 0.5 mL of wet-settled volume of the resin was packed into the column. Geothermal water was delivered down-flow to the column at a flow rate of SV (Space velocity) 15 h^{-1} for Amberlite PWA-10 (at a particle size range of 0.355-0.500 mm) and Diaion CRB02 (at a particle size range of 0.250-0.355 mm and 0.355-0.500 mm) and SV 10,15 and 25 h^{-1} for composite fiber. Each successive 5 mL (10 BV) fractions of the effluent were collected using a fraction collector. The fractions were analyzed using a spectrophotometer to obtain the breakthrough curves. After the sorption step, resin packed into the column was washed with deionized water. The boron loaded adsorbent was eluted with 5% H_2SO_4 at SV 5 h^{-1} and then washed with deionized water. The column elution profiles were obtained by analysis of each successive 2 mL (4 BV) fractions of eluates.

To examine the effect of eluting agent concentration on elution performance, Diaion CRB02 resin at a particle size range of 0.355-0.500 mm, was

eluted with 10% H_2SO_4. Geothermal water passed through the column down-flow at a space velocity of 10, 15 and 25 h^{-1} for composite fiber.

2.5. EDI Tests

Removal of boron from RO permeate of geothermal water was carried out with an EDI cell consisting of a three compartment cell with DSA (Dimensionally Stable Anode) and stainless steel cathode electrodes, three separate liquid lines. The voltage was controlled with a voltmeter. The current was monitored with a current meter through this power supply. The cathode and anode compartments of the cell are separated from the central compartment with the Neosepta-AMX and Neosepta-CMX membranes. Central compartment was filled with the Purolite CT 175 and A500 (at a particle size range of 0.355-0.500 mm) and Amberlie PWA-10 (at a particle size range of 0.500-0.710 mm) resins (total volume of resin was 5 mL). The effective areas of the membranes inside the cell are 10.2 cm^2 (3.4 cm x 3 cm). Also, model solution which includes same boron concentration in RO permeate was prepared and used for EDI tests.

2.6. Ion Exchange-Membrane Filtration Hybrid System Tests

In this study, the removal of lithium from 10 mg/L of lithium spiked geothermal water with ion exchange-membrane filtration hybrid system was performed using different amounts of granulated and powder lithium adsorbents.

Totally 1200 mL geothermal water was used as feed solution. The granulated and the powder lithium adsorbent with four different concentrations (3, 2, 1 g/L adsorbents) were used for removal of lithium from geothermal water. A 1.2 g of granulated adsorbent was used for 1 g/L adsorbent concentration while 2.4 g of granulated adsorbent was used for 2 g/L adsorbent concentration and 3.6 g granulated adsorbent for 3 g/L adsorbent concentration. Also, same amount of powder adsorbent was used for a comparative study.

During the experiments using granulated adsorbent with all concentrations of adsorbents, fresh adsorbent suspension was delivered into the main tank at a constant flow rate of 3 mL/min. With the experiments using powder adsorbent with 2 and 1 g/L concentrations, the flow rate of fresh suspension was also 3 mL/min. The experiment performed with 3 g/L of powder adsorbent concentration, flow rate of fresh suspension was set as 6 mL/min.

2.7. Arsenic Removal

2.7.1. Effect of pH on the sorption of As(V)

Batch sorption tests were performed to evaluate the arsenate retention by P(VbNMDG) and P(ClVBTA) resins. The effect of pH on retention was studied to obtain a correlation between arsenic speciation and sorption performance of resins P(VbNMDG) and P(ClVBTA) at a particle size range of 180-250 μm. Arsenic aqueous solutions were adjusted to a pH of 3-9 using dilute HNO_3 and NaOH solutions. In these studies, various amounts of P(VbNMDG) (10, 20, 30, 40 and 50 mg) and P(ClVBTA) (2, 3, 4, 5 and 10 mg) were contacted with 10 mL As(V) solution (10 mg/L) by shaking in a shaker at 30ºC, a stirring rate of 140 rpm for 24 hours. After contact, resins were filtered and washed and then the solution was transferred to volumetric flask of 50 mL.

To investigate the sorption performances of these resins for arsenic, they were used by changing the polymer:polymer ratio in moles. Different P(VbNMDG):P(ClVBTA) mole ratios such as 25:75, 50:50 and 75:25 were employed in a way that the total amount of resin is 50 mg. These experiments were performed by contacting 50 mg resin with 10 mL As(V) solution (10 mg/L) at 30ºC, a stirring rate of 140 rpm for 24 hours. After contact, resins were filtered and washed and then the solution was transferred to volumetric flask of 50 mL.

2.7.2. Kinetic studies

To evaluate the effect of time on sorption, kinetic experiments were performed with 10 mL As(V) solution (10 mg/L) at 3-9 pH and molar ratio of P(VbNMDG):P(ClVBTA) is 25:75 (50 mg). The experiments were performed at 30ºC and a stirring rate of 140 rpm. The contact tubes were withdrawn from the shaker at different time intervals (0, 1, 3, 5, 10, 15, 30, 60, 120 and 1440 min). After that resins were filtered and washed and then the solution was transferred to volumetric flask of 50 mL. The experimental data were evaluated using pseudo-first-order and pseudo-second-order kinetic models.

2.7.3. Equilibrium studies

The equilibrium experiments (isotherms) were carried out using a range of arsenic concentrations (5-400 mg/L) and mole ratio of P(VbNMDG):P(ClVBTA)

was 25:75 (50 mg). These experiments were carried out at 30ºC for 24 h at a pH of 3-9. The experimental data were evaluated using Langmuir and Freundlich isotherm models to evaluate the sorption process.

2.7.4. Elution studies

In order to study the arsenate elution process, different acid solutions were used. In sorption step, mole ratio of P(VbNMDG): P(ClVBTA) was 25:75. A 50 mg of resin mixture was contacted with 10 mL As(V) solution (10 mg/L) by shaking in a shaker at 30ºC, a stirring rate of 140 rpm for 24 hours. After sorption step, the resins were contacted with 4 M 10 mL HCl, HNO_3 and $HClO_4$ in a shaker during 4 hours at 30ºC for elution. After elution step, the solutions were analysed.

2.8. Boron Analyses

Boron analyses were performed spectrophotometrically by a JASCO V-530 UV/VIS spectrophotometer using Azomethine-H and Curcumine methods.

2.8.1. Azomethine-H method

This method was employed for the samples obtained from all batch sorption tests except kinetic tests.

Reagents:

Azomethine-H solution: 0.5000 g azomethine-H and 1.000 g of ascorbic acid are dissolved in 50.0 mL pure water and immediately transferred to a plastic bottle freshly at each analysis day.

Buffer solution: This solution is prepared by dissolving 50.0 g of ammonium acetate in 100.0 mL pure water and by adding to this solution 25.0 mL of glacial acetic acid and 1.4000 g of EDTA di-sodium salt.

Procedure of Azomethine-H method:

10 mL of sample, 2.5 mL of Azomethine-H solution, and 2.5 mL of buffer solution are added into a plastic bottle.

This mixture is kept at room temperature and in the dark without shaking. After 1 h, the absorbance of the sample is read at 415 nm using a spectrophotometer.

The concentrations of prepared standard solutions for calibration curve were 0.1, 0.5, 1.0 and 2.0 mg B/ L. The absorbance values of standard boron solutions at 415 nm were given in Table 2.6. An example of calibration curve for Azomethine-H method was given in Figure 2.19.

Table 2. 6. Concentrations of standard boron solutions and their absorbances at 415 nm for calibration curve in Azomethine-H Analysis.

Boron Concentration (mg/L)	Absorbance at 415 nm
0.1	0.0522
0.5	0.2201
1.0	0.4495
2.0	0.8894
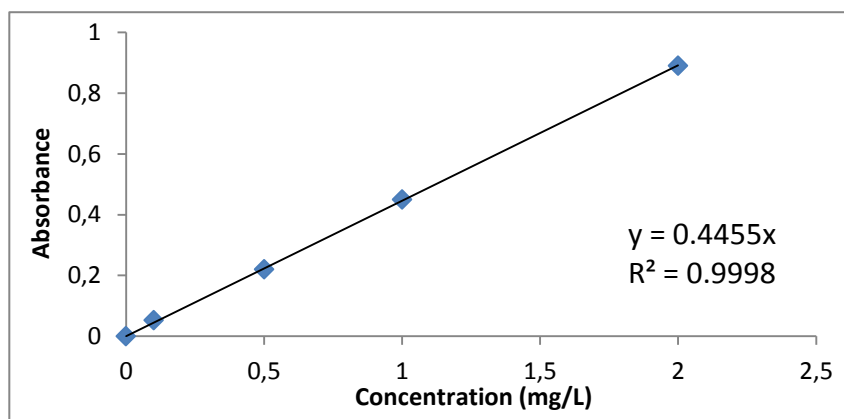
Figure 2.19. Calibration curve obtained at 415 nm using Azomethine-H method.

2.8.2. Curcumine method

This method was employed for kinetic tests and column-mode studies.

Reagents:

Curcumine Solution (0.1%): The solution is prepared by dissolving 0.1000 g curcumine in 100.0 mL of glacial acetic acid in polyethylene bottle wrapped with aluminum foil on the day of use.

H₂SO₄: CH₃COOH (1:1) Solution: Equal volumes of the two acids are mixed.

Sodium Acetate Buffer Solution: 200.0 g sodium acetate is dissolved in 250.0 mL of glacial acetic acid and diluted to 1.0 L with deionized water.

Procedure of Curcumine method:

0.5 mL sample, 3.0 mL 0.1 % Curcumine solution, and 3.0 mL H_2SO_4:CH_3COOH (1:1) solution are added into a plastic bottle.

This mixture is shaken at 30°C and at a certain stirring rate.

After 1 h, 10.0 mL of CH_3COONa buffer solution is added and samples are left to cool. The absorbance of the sample is measured at λ_{max}= 543 nm with a spectrophotometer.

For Curcumine analysis, standart boron solutions of 0.025, 0.05, 0.1, 0.25, 0.5, 1, 1.5 and 2 mg/L were used for the calibration curve (Figure 2.20). The adsorbance values of standart boron solutions at 543 nm were given in Table 2.7.

Table 2.7. Concentrations of standard boron solutions and their absorbances at 543 nm for calibration curve in Curcumine Analysis.

Boron Concentration (mg/L)	Absorbance at 543 nm
0.025	0.0102
0.05	0.0229
0.10	0.0436
0.25	0.1068
0.50	0.2020
1.00	0.3838
1.50	0.5687
2.00	0.7553
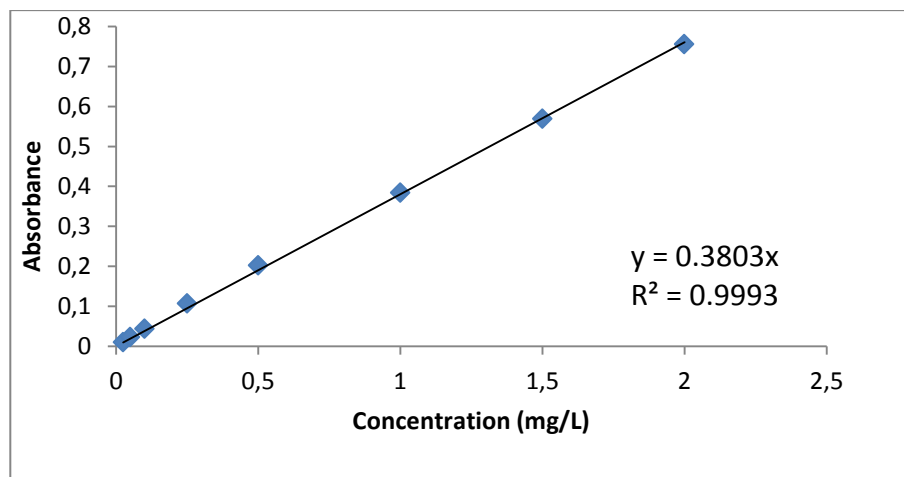
Figure 2.20. Calibration curve obtained at 543 nm using Curcumine method.

2.9. Lithium Analyses

Standard lithium solutions were prepared from a 100 mg Li/L stock lithium solution, which was prepared by dissolving 5.3280 g lithium carbonate (Li_2CO_3) in 1 L pure water.

Lithium analyses of batch-mode and ion exchange-membrane filtration hybrid system tests were carried out by using an atomic absorption spectrophotometer (VARIAN Spectra AA) with acetylene-air mixture. The calibration curve and absorbance data of standart lithium solutions were given in Table 2.8.

Table 2.8. Concentrations of standard lithium solutions and their absorbances for calibration curve

Lithium Concentration (mg/L)	A
1.0	0.066
2.5	0.174
5.0	0.316
10	0.620
15	0.980
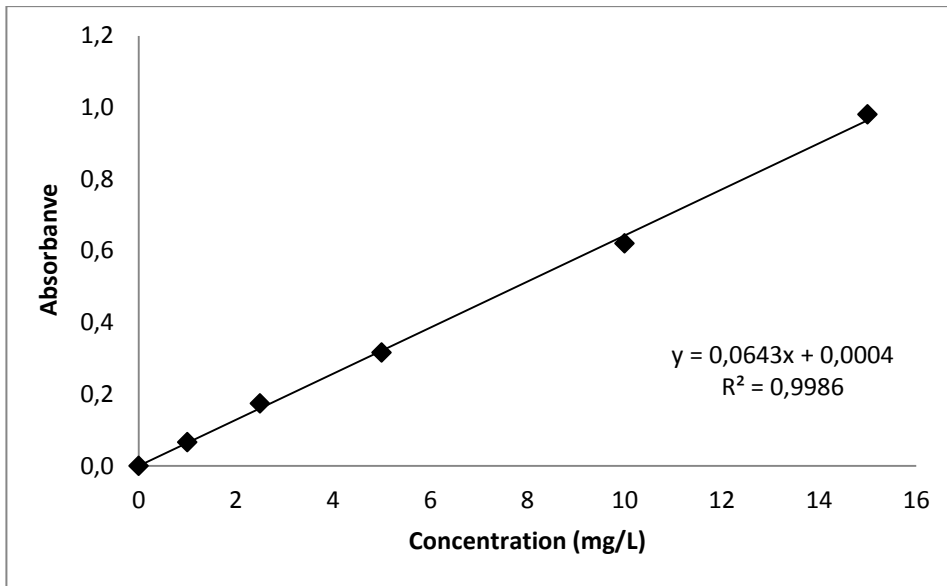
Figure 2. 21. Calibration curve of lithium analysis using atomic absorption spectrophotometer.

2.10. Arsenic Analyses

Arsenic analyses were performed with a FIAS-100 flow injection for atomic spectroscopy by oxidation method.

Procedure of method:

52.4 mL sample, 8.0 mL 50 % (V/V) HCl, 4.0 mL 20 % (w/V) KI, and 0.4 mL 10 % (w/V) ascorbic acid are added into a plastic tube and volume of 40 mL with water.

This mixture is shaken at a certain stirring rate.

After, the absorbance of the sample is read using a FIAS-100 flow injection for atomic spectroscopy.

The concentrations of prepared standard solutions from sodium arsenate heptahydrate for calibration curve were 2, 4, 6, 8, 10, 20, 30, 50, 60, 70, 80, 100 µg As(V)/L. The absorbance values of standard arsenic solutions were given in Table 2.9. An example of calibration curve was given in Figure 2.22.

Table 2. 9. Concentrations of standard arsenic solutions and their absorbances for calibration curve.

Arsenic Concentration (µg/L)	Absorbance
2	0.023
4	0.033
5	0.036
6	0.045
8	0.053
10	0.066
20	0.135
30	0.174
50	0.320
60	0.347
70	0.430
80	0.444
100	0.514
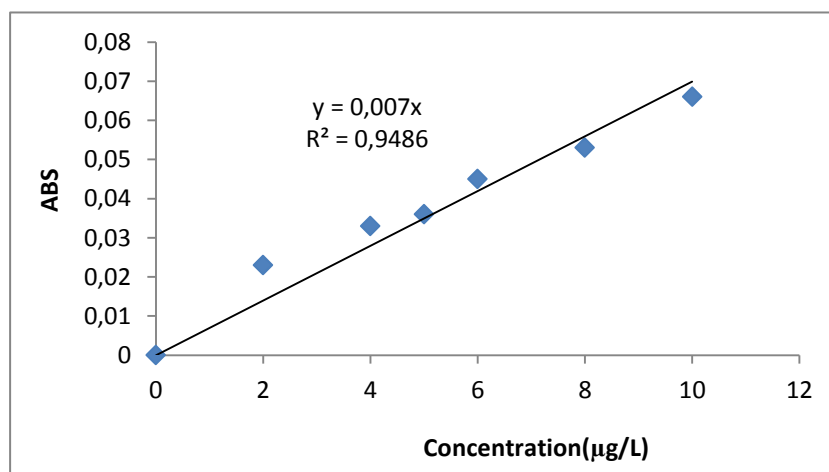
(a)
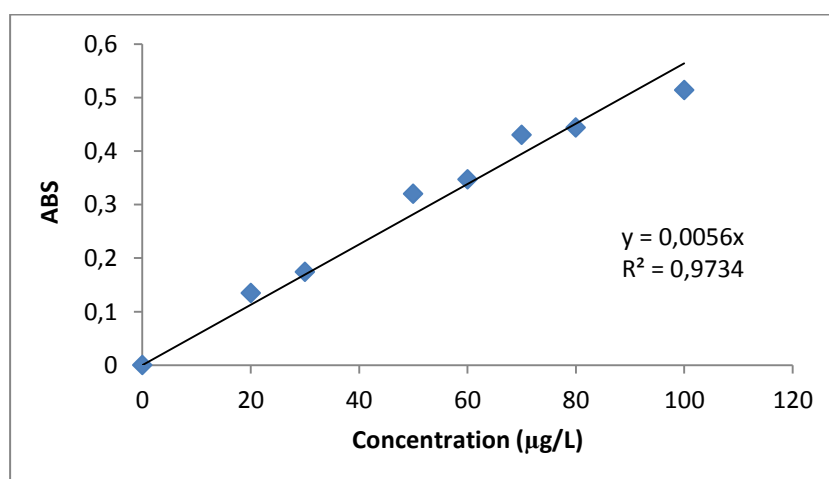
(b)

Figure 2.22. (a) Calibration curve obtained using FIAS-100(Conc. 2-10µg/L), (b) Calibration curve obtained using FIAS-100(Conc. 20-100µg/L).

3. MATHEMATICAL MODELLING

The kinetic data, obtained from batch-mode kinetic tests performed by using Amberlite PWA10 resin for boron removal and λ-MnO$_2$ adsorbent for lithium removal from geothermal water, were evaluated using conventional kinetic modeling and diffusional and reaction models equations (Ozacar and Sengil, 2004; Badruk et al., 1999).

3.1. Conventional Kinetic Modeling

A simple kinetic of sorption is the pseudo first-order equation in the form:

$$\frac{dq_t}{dt} = k_1(q_e - q_t) \qquad (3.1)$$

Integrating Equation 3.1 and applying the boundary conditions $q_t = 0$ at $t = 0$ and $q_t = q_t$ at $t = t$, gives:

$$log(q_e - q_t) = log q_e - \frac{k_1}{2.303}t \qquad (3.2)$$

where q_e and q_t are the amounts of species sorbed at equilibrium and at time t (mg/g), respectively, and k_1 is the rate constant of pseudo first-order sorption, (min^{-1}) (Ozacar and Sengil, 2004).

On the other hand, a pseudo second-order equation based on sorption equilibrium capacity may be expressed in the form:

$$\frac{dq_t}{dt} = k_2(q_e - q_t)^2 \qquad (3.3)$$

After define integration by applying initial conditions, Equation 3.3 becomes:

$$\frac{1}{(q_e - q_t)} = \frac{1}{q_e} + k_2t \qquad (3.4)$$

Equation 3.4 can be rearranged to obtain a linear form:

$$\frac{t}{q_t} = \frac{1}{k_2 q_e^2} + \frac{1}{q_e}t \tag{3.5}$$

where k_2 is the rate constant of pseudo second-order sorption (g/mg min) (Ozacar and Sengil, 2004).

3.2. Diffusional and Reaction Models

The models for process dynamics include both the diffusional steps (bulk solution, a film layer at the external surface of the particle, pores) and the exchange reaction on the active sites. Since the resistance in bulk solution is easily controlled and negligible, three resistances, such as film diffusion, particle diffusion, and chemical reaction, usually determine the overall rate of the ion-exchange process. The kinetic study data were evaluated by using two approaches. The first one is based on Fick's first law of integration of material balance for infinite solution volume (ISV). The second method uses the unreacted core model (UCM) in which ion exchange is treated as a heterogeneous reaction. According to UCM, reaction first occurs at the outer skin of the particle, then within a zone moving into the particle through the unreacted core. Kinetic models developed for spherical particles to specify the rate-determining steps were given in Table (3.1) (Badruk et al., 1999).

Table 3.1. Diffusional and reaction models (Badruk et al., 1999).

Model	Equation	Rate-determining step
ISV	$F(X)=-\ln(1-X)=K_{1i}t$ where $K_{1i}=3DC/r_o\delta C_r$	Film diffusion
ISV	$F(X)=-\ln(1-X^2)=kt$ where $k=D_r\pi^2/r_o^2$	Particle diffusion
UCM	$F(X)=X=(3C_{Ao}K_{mA}/a_{ro}C_{so})t$	Liquid film
UCM	$F(X)=3-3(1-X)^{2/3}-2X=(6D_{eR}C_{Ao}/a_{ro}^2C_{so})t$	Reacted layer
UCM	$F(X)=1-(1-X)^{1/3}=(k_sC_{A0}/a_{ro}C_{so})t$	Chemical reaction

3.3. Adsorption Isotherms

Equilibrium sorption isotherms are one of the most important studies to design adsorption processes. Moreover, isotherms provide useful information on the interaction between the adsorbate and the adsorbent. Experimental results were fitted to the isotherm models of Langmuir and Freundlich. The Langmuir isotherm is valid for monolayer sorption onto a surface containing a finite number of identical sites and is commonly applied for adsorption on a completely homogeneous surface with negligible interaction between adsorbed molecules. On the other hand, the Freundlich isotherm describes the exponential distribution of active centers of a heterogeneous adsorbent surface. The linear equations that describe the models are as follows:

The Langmuir isotherm;

$$\frac{C_e}{Q_e} = \frac{1}{Q_{max}b} + \frac{C_e}{Q_{max}} \tag{3.6}$$

The Freundlich isotherm;

$$\log(q_e) = \log(k_F) + \frac{1}{n}\log(C_e) \tag{3.7}$$

where q_e represents the As(V) adsorbed on the resin (mg As/g), Ce is the equilibrium concentration of As(V) (mg/L), k_L is the Langmuir equilibrium constant (L/mg), Q is the monolayer capacity, K_f is the adsorption capacity and n is a dimensionless parameter associated with the intensity of adsorption.

4. RESULTS AND DISCUSSION

4.1. Boron Removal from Geothermal Water

In these studies, boron removal from geothermal water was performed by using ion exchange resin, Amberlite PWA-10 (at a particle size range of 0.500-0.710 mm) with N-methyl-D-glucamine functional groups and boron selective composite fiber. The functional groups of N-methy-D-glucamine form chelating with boric acid and borates. Figure 4.1 shows ion exchange mechanism of boric acid with cis-diol active sites of N-methyl-D-glucamine.
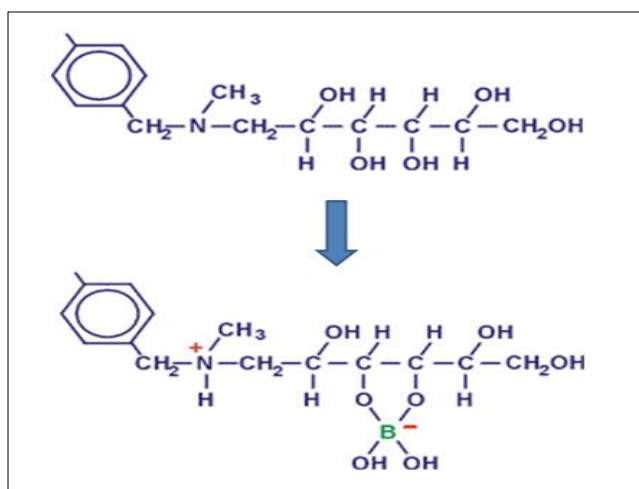
Figure 4.1. Binding mechanism of boron by N-methyl-D-glucamine groups type chelating resin (Rohm and Haas Product Data Sheet IE-724EDS, 2006.)

4.1.1. Batch-mode sorption studies

4.1.1.1. Effect of adsorbent amount on boron removal from geothermal water

The optimum adsorbent amounts for boron removal from geothermal water were determined by accepting the optimum adsorbent amount as the required amount of adsorbent which is necessary to lower the concentration of boron in the geothermal water below 1.0 mg/L. As shown in Figure 4.2 for the boron selective chelating resin Amberlite PWA-10, at the particle size range of 0.500-0.710 mm, the optimum resin amount was determined as 2.8 g resin/L geothermal water. Optimum fiber amount of boron selective composite fiber was found to be 2 g fiber/L geothermal water.
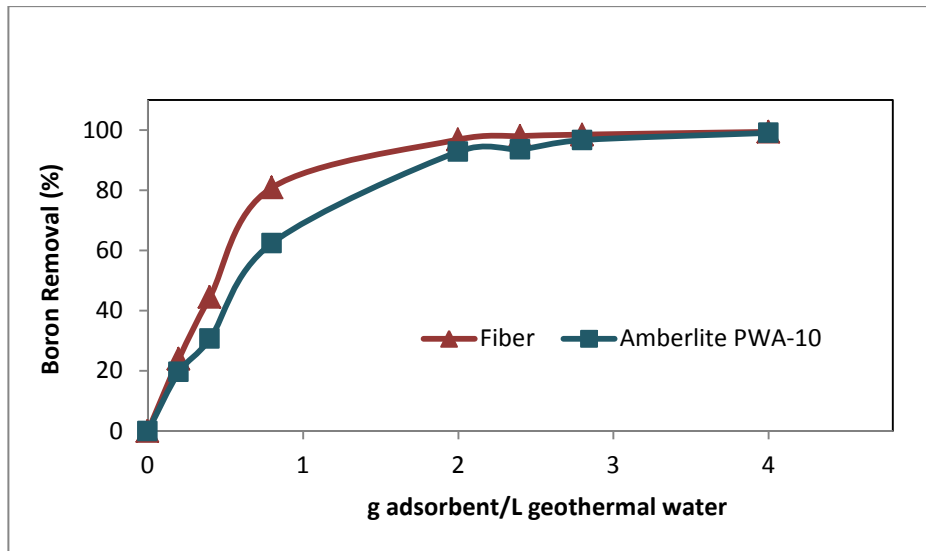
Figure 4.2. Effect of resin/fiber amount on boron removal from geothermal water by boron selective resin (0.500-0.710 mm) and fiber.

4.1.1.2. Kinetic studies and mathematical modelling

In these experiments, Amberlite PWA-10 (at particle size ranges of 0.500-0.710 mm) and boron selective composite fiber were contacted with 400 mL of geothermal water separetely. The experiments were performed at 25ºC with adsorbent concentrations of 2.8 g resin/L geothermal water and 2 g fiber/L geothermal water. The graphs of boron concentration versus time and the ratio of boron concentration at any time to initial boron concentration of geothermal water versus time were given in Figures 4.3 (a) and 4.3 (b), respectively. As seen in Figure 4.3, boron removal with composite fiber was faster than that with Amberlite PWA-10 at a particle size of 0.500-0.710 mm.

The boron concentration of the geothermal water was reduced below 1.0 mg B/L after 120 minutes by composite fiber. But for Amberlite PWA-10 at a particle size of 0.500-0.710 mm, after 180 minutes, the boron concentration of the geothermal water was reduced below 1.0 mg B/L. The measured boron concentrations of the geothermal water were 0.86 mg/L and 0.79 mg/L for the experiments performed by using 2.0 g fiber/L and 2.8 g resin/L, respectively.

Furthermore, for better comparison in sorption kinetics behaviors of resin and fiber, kinetic tests were studied using 2.0 g of Amberlite PWA-10 resin at a particle size range of 0.500-0.710 mm. As seen in Figure 4.4, boron removal with composite fiber was faster than with Amberlite PWA-10 used at the same amount.
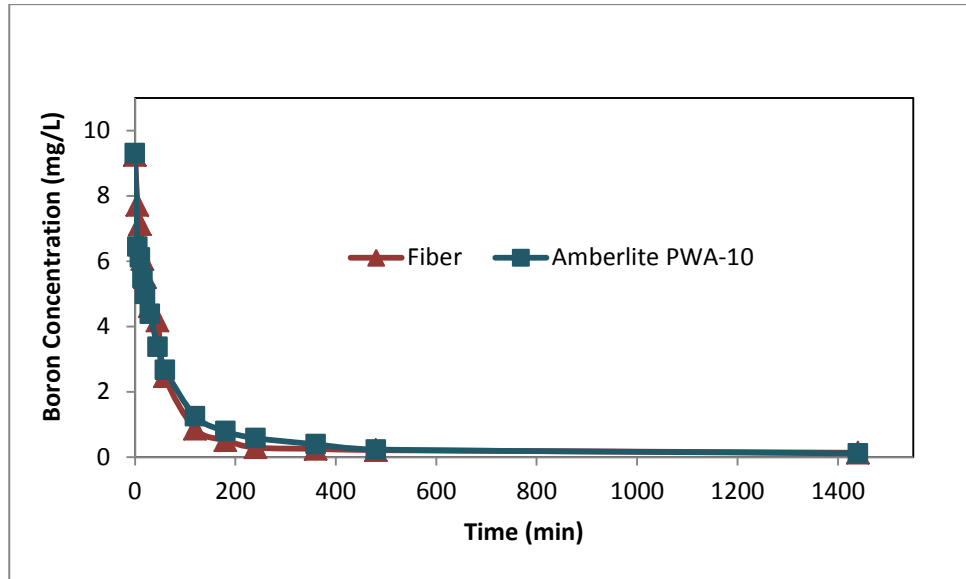
(a)
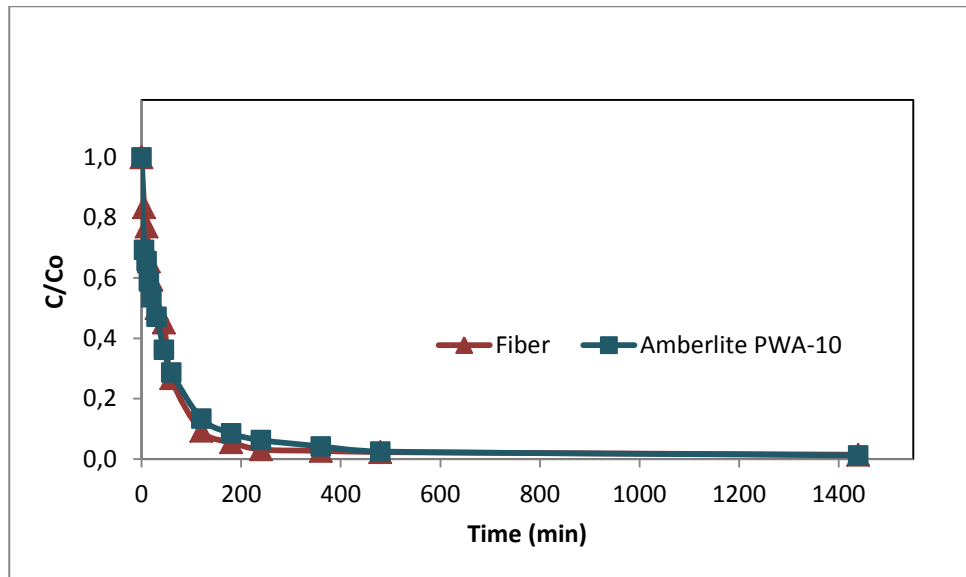
(b)

Figure 4.3. Effect of adsorbent concentration on boron sorption kinetics. (a) boron concentration versus time, (b) ratio of boron concentration at any time to initial boron concentration of geothermal water. (2.0 g fiber /L and 2.8 g Amberlite PWA-10/L).
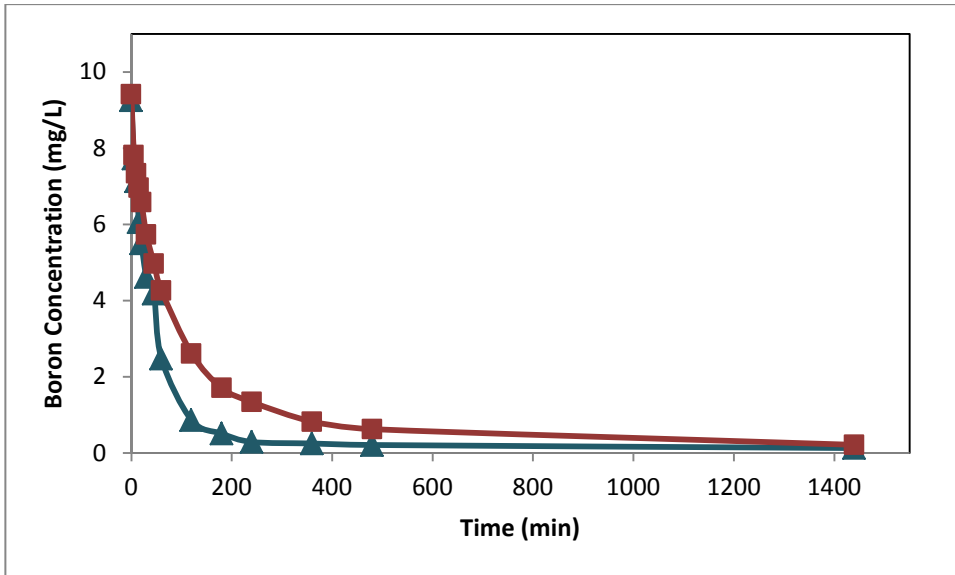
(a)
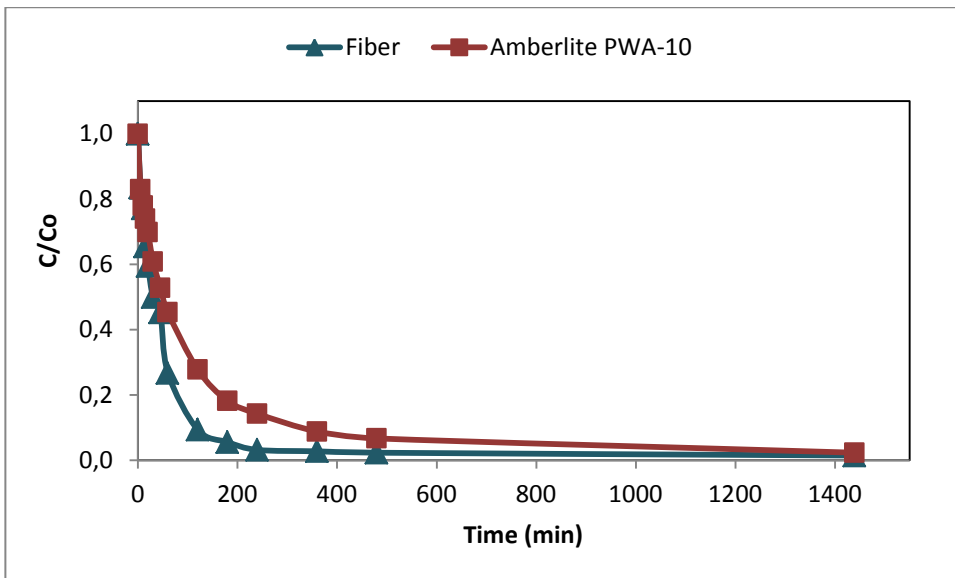
(b)

Figure 4.4. Effect of adsorbent concentration on boron sorption kinetics. (a) boron concentration versus time, (b) ratio of boron concentration at any time to initial boron concentration of geothermal water. (2 g fiber/L and 2g Amberlite PWA-10/L)

The kinetic data obtained were evaluated with pseudo-first-order and pseudo-second-order kinetics models as explained in Section 3.1. The graphs of $\log(q_e-q_t)$ versus t and t/q_t versus t were plotted for first-order and second-order kinetic models to determine the correlation coefficients (Figures 4.5 - 4.10).
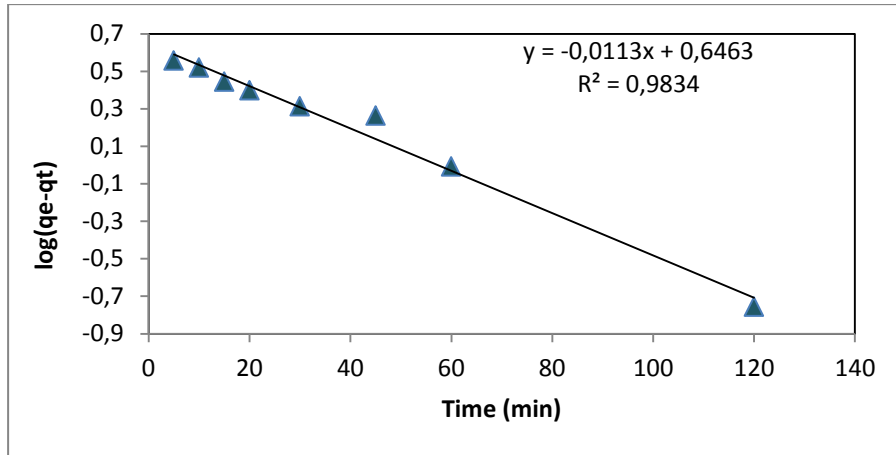
Figure 4.5. Evaluation of kinetic data using pseudo-first-order model (fiber concentration: 2.0 g/L).
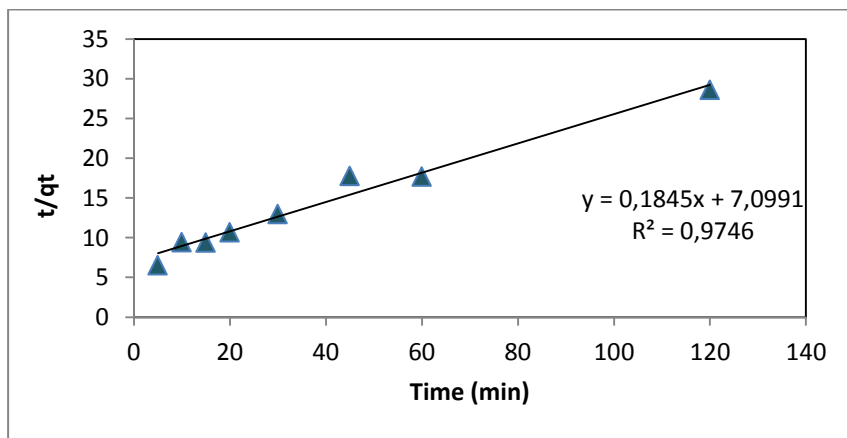
Figure 4.6. Evaluation of kinetic data using pseudo-second-order kinetic model (fiber concentration: 2.0 g/L).
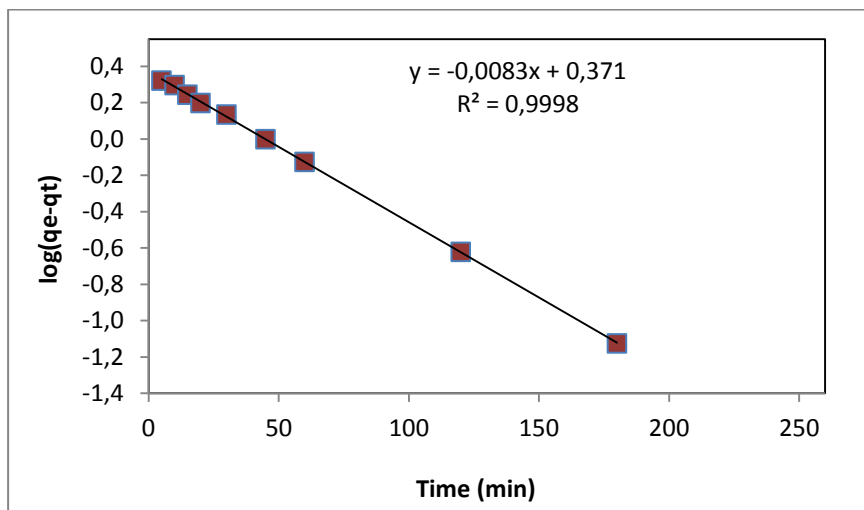
Figure 4.7. Evaluation of kinetic data using pseudo-first-order model (resin concentration: 2.8 g/L).
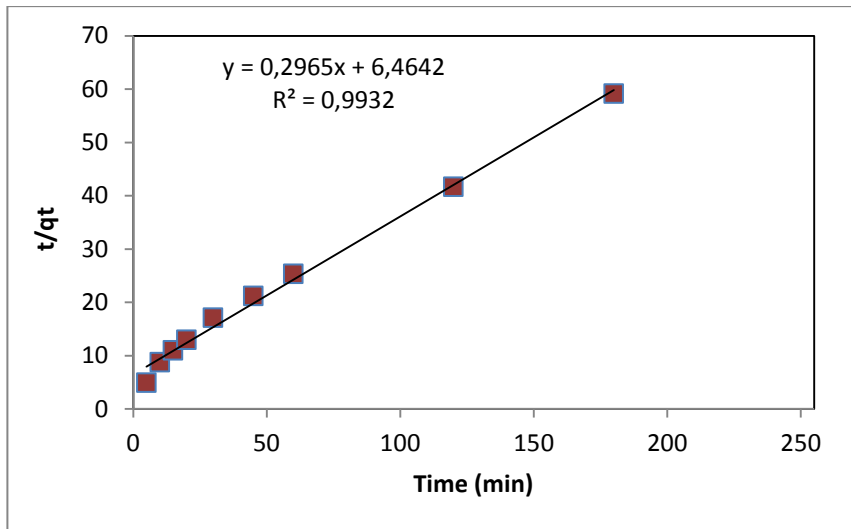
Figure 4.8. Evaluation of kinetic data using pseudo-second-order kinetic model (resin concentration: 2.8 g/L).
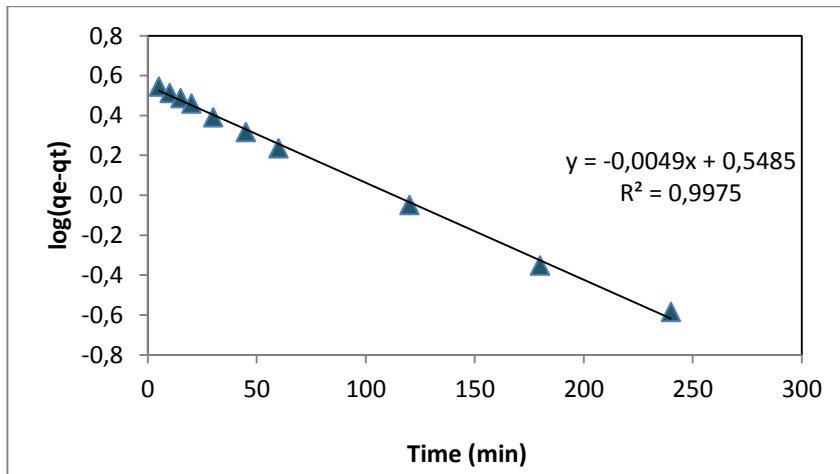
Figure 4.9. Evaluation of kinetic data using pseudo-first-order model (resin concentration: 2.0 g/L).
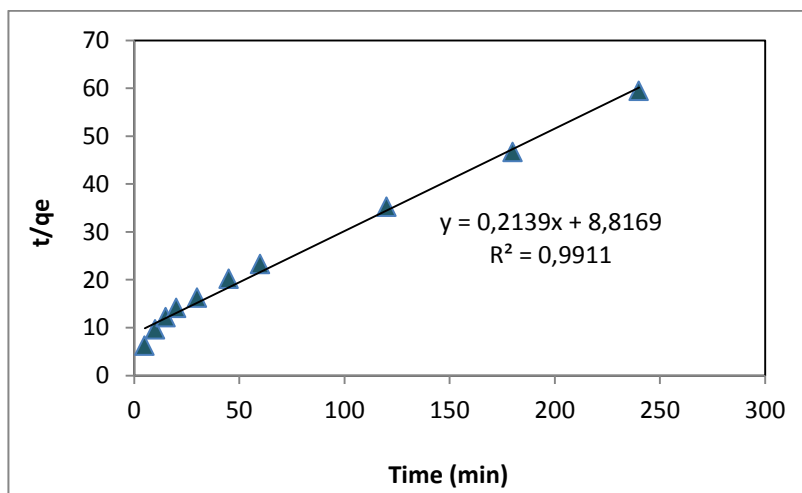
Figure 4.10. Evaluation of kinetic data using pseudo-second-order kinetic model (resin concentration: 2.0 g/L).

When the linear correlation coefficients were compared, it was seen that sorption kinetics for composite fiber and Amberlite PWA-10 resin agreed well with pseudo-first-order mechanism (Table 4.1).

Table 4.1. Evaluation of sorption kinetic data obtained using conventional kinetic modeling for adsorbents.

Sorbent	R^2 (First Order Kinetics)	R^2 (Second Order Kinetics)
Composite Fiber (2 g/L)	**0.9834**	0.9746
Amberlite PWA-10 (2.8 g/L)	**0.9998**	0.9932
Amberlite PWA-10 (2 g/L)	**0.9975**	0.9911

The kinetic studies were also evaluated with diffusional and reaction models as explained in Section 3.2. The maximum correlation coefficients for the linear models show that the rate is film diffusion controlled according to ISV models and reacted layer controlled according to UCM models for the study done with composite fiber. For Amberlite PWA-10, the rate is particle diffusion controlled according to ISV models and reacted layer controlled according to UCM models for both of the studies done with 2.0 g resin/L and 2.8 g resin/L concentrations, as they have greater linear correlation coefficients. Table 4.2 shows the linear correlation coefficients obtained from the plots of F(X) function versus time shown in Figures 4.11-4.16.
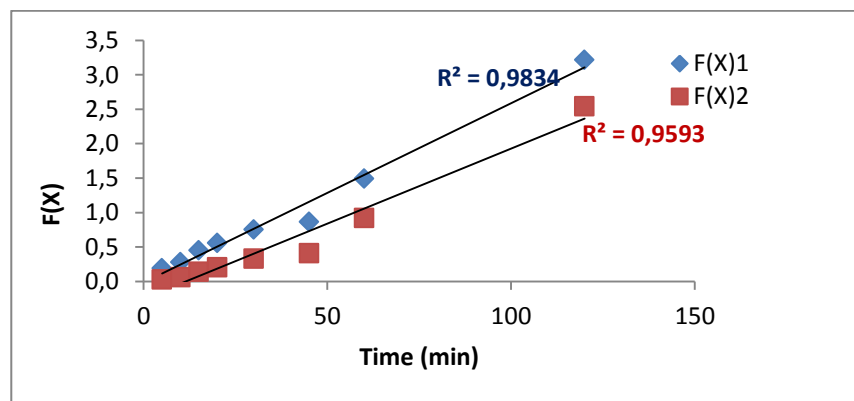
Figure 4.11. Evaluation of kinetic data using infinite solution volume model (ISV) (fiber concentration: 2 g/L).
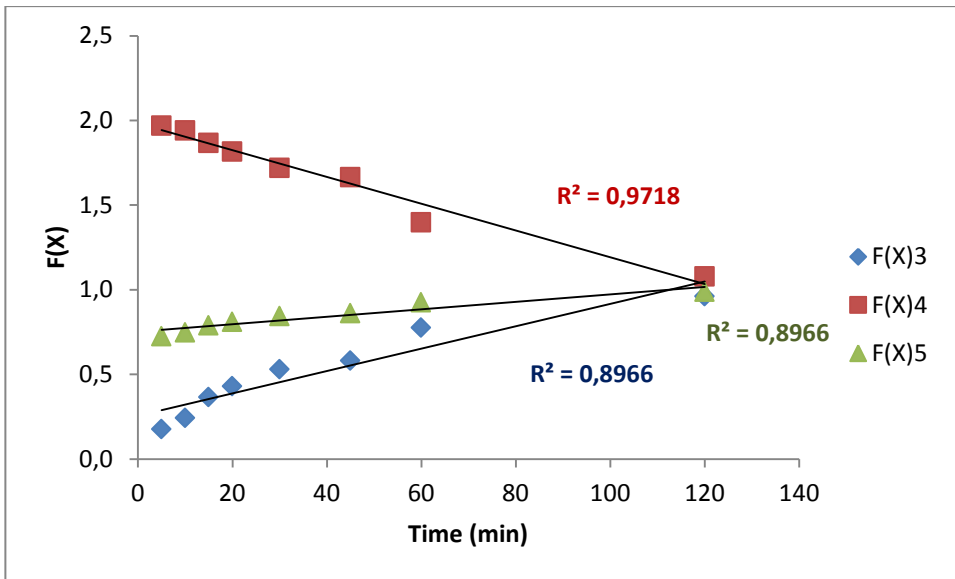
Figure 4.12. Evaluation of kinetic data using unreacted core model (UCM) (fiber concentration: 2 g/L).
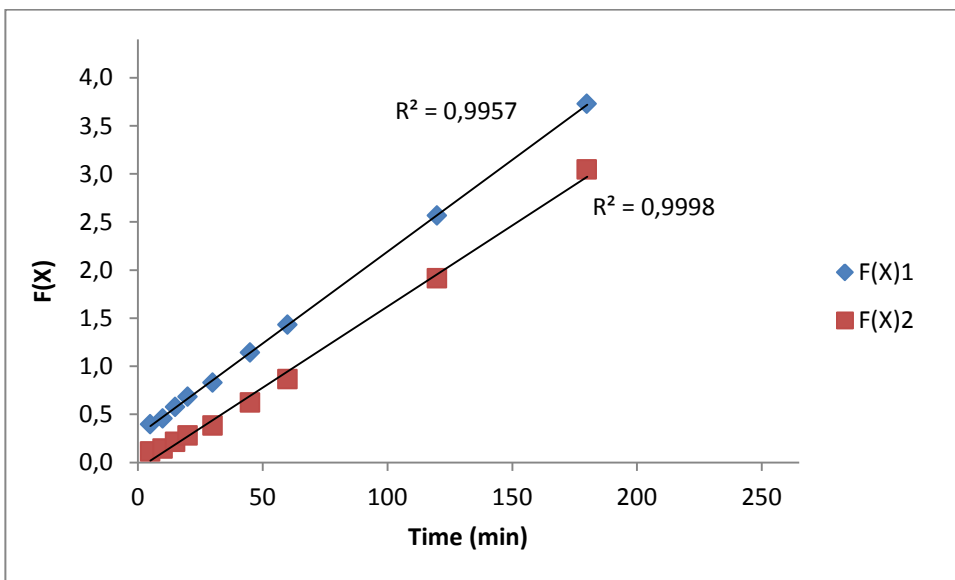
Figure 4.13. Evaluation of kinetic data using infinite solution volume model (ISV) (resin concentration: 2.8 g/L).
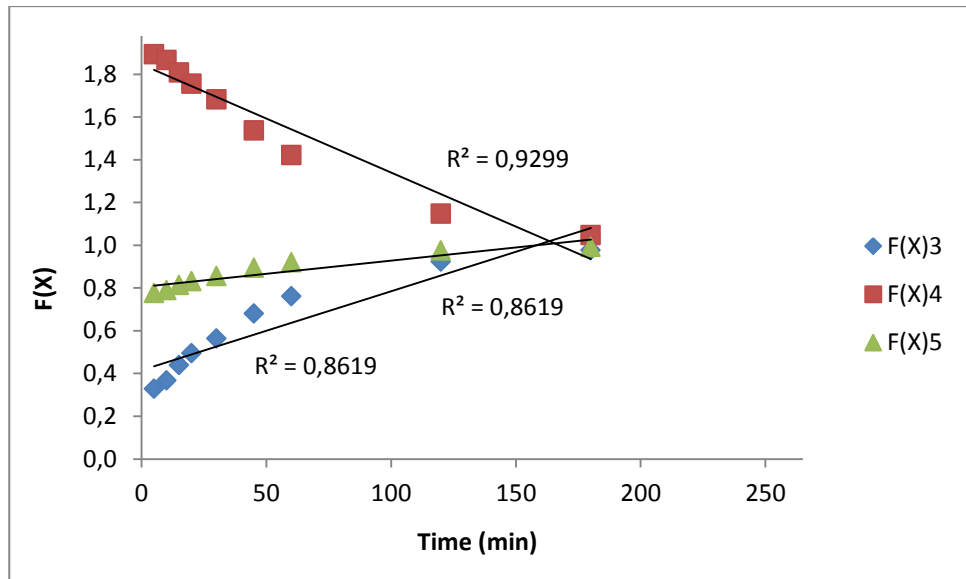
Figure 4.14. Evaluation of kinetic data using unreacted core model (UCM) (resin concentration: 2.8 g/L).
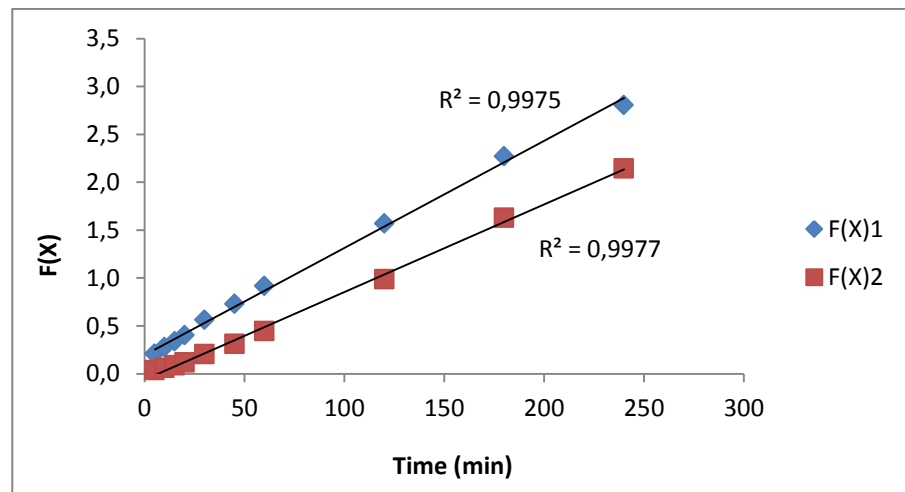
Figure 4.15. Evaluation of kinetic data using infinite solution volume model (ISV) (resin concentration: 2.0 g/L).
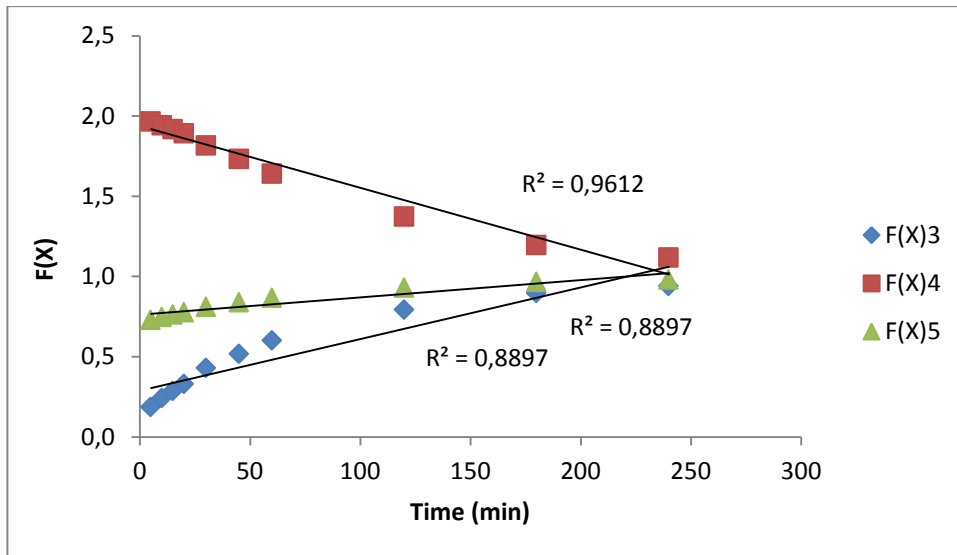
Figure 4.16. Evaluation of kinetic data using unreacted core model (UCM) (resin concentration: 2.0 g/L).

Table 4.2. Evaluation of sorption kinetic data obtained using diffusional and reaction models for composite fiber and Amberlite PWA-10.

	R^2				
	ISV			**UCM**	
ADSORBENT	**-ln(1-X)**	**-ln(1-X^2)**	**X**	**3-3(1-X)$^{2/3}$-2X**	**1-(1-X)$^{1/3}$**
Composite Fiber (2.0 g/L)	**0.9834**	0.9593	0.8966	**0.9718**	0.8966
Amberlite PWA-10 (2.8 g/L)	0.9957	**0.9998**	0.8619	**0.9299**	0.8619
Amberlite PWA-10 (2.0 g/L)	0.9975	**0.9977**	0.8897	**0.9612**	0.8897

4.1.1.3. Cycle studies

Cycle studies, were performed to detect the recycle and sustainability performance for both composite fiber and Amberlite PWA-10 resin. The experiments were performed using 0.05 g fiber/25 mL-geothermal water and 0.07 g resin/25 mL-geothermal water by shaking in a shaker at 30ºC for 24 h. In sorption stages, as seen in Figures 4.17 and 4.18, during ten cycles the capacity of both adsorbents did not change significantly. As seen in Figures 4.19 and 4.20, the elution study was performed with different concentration of H_2SO_4 solution. The concentration of H_2SO_4 that is used to elute boron did not influence the adsorption, elution efficiency of boron significantly for both fiber and resin.
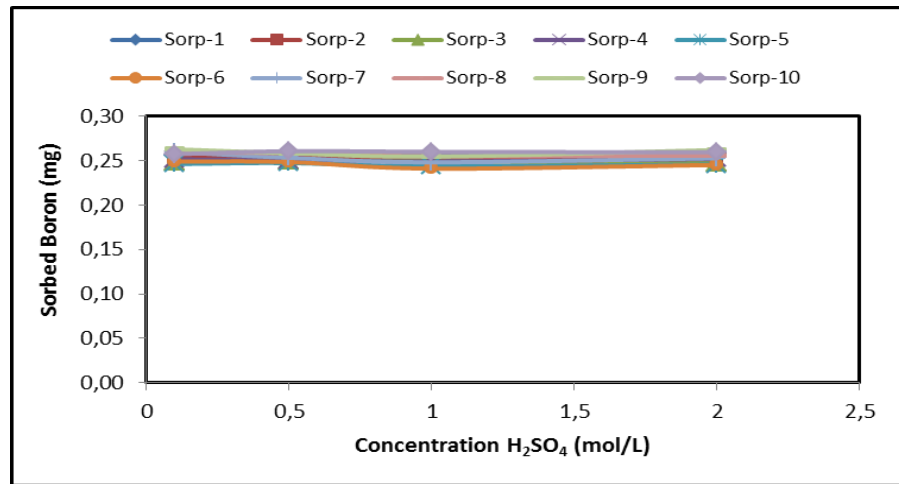
Figure 4.17. Sorption profile of boron using Amberlite PWA-10 for cycle studies.
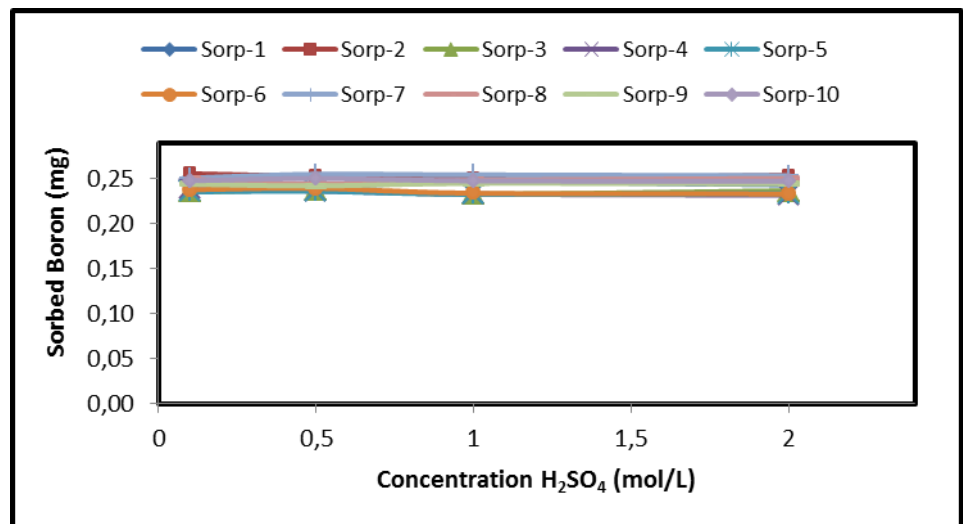
Figure 4.18. Sorption profile of boron using composite fiber for cycle studies.
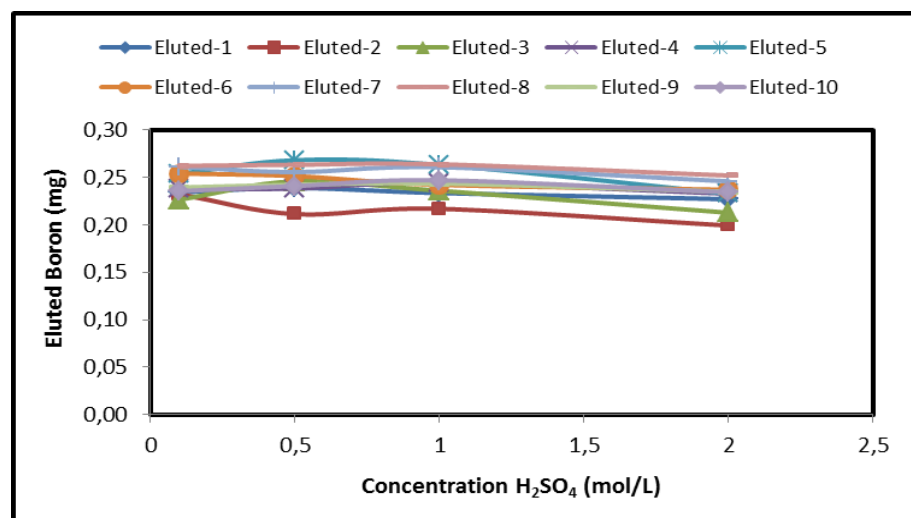
Figure 4.19. Elution profile of boron using Amberlite PWA-10 for cycle studies.
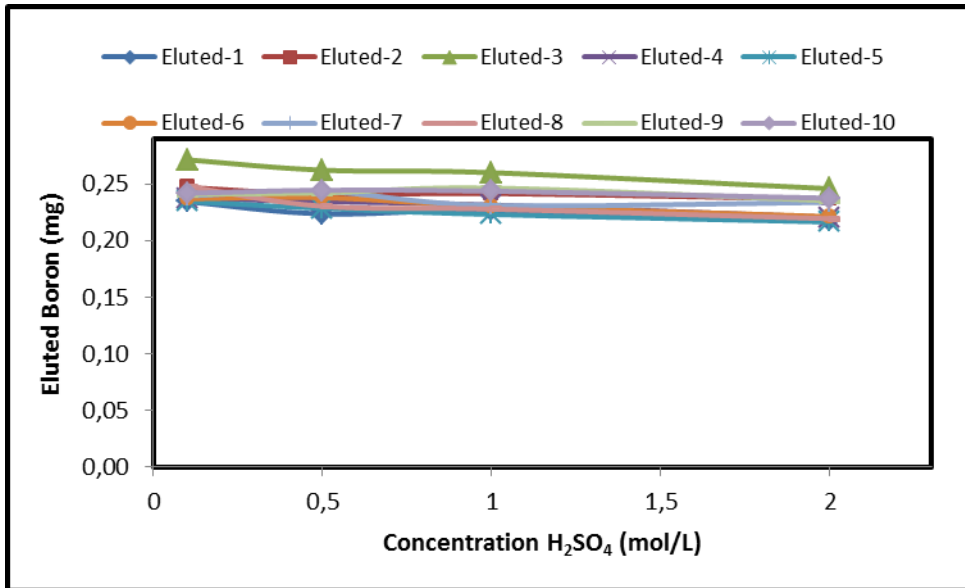
Figure 4.20. Elution profile of boron using composite fiber for cycle studies.

As seen in Figures 4.21 and 4.23, sorption profiles of boron using Amberlite PWA10 resin and composite fiber adsorbent were carried out for ten cycles. During ten cycles, the capacity of both adsorbents remained constant. Elution profiles of boron were also obtained, as seen in Figures 4.22 and 4.24. The scattering data in elution profiles are due to uncompleted elution of boron in some cycles.
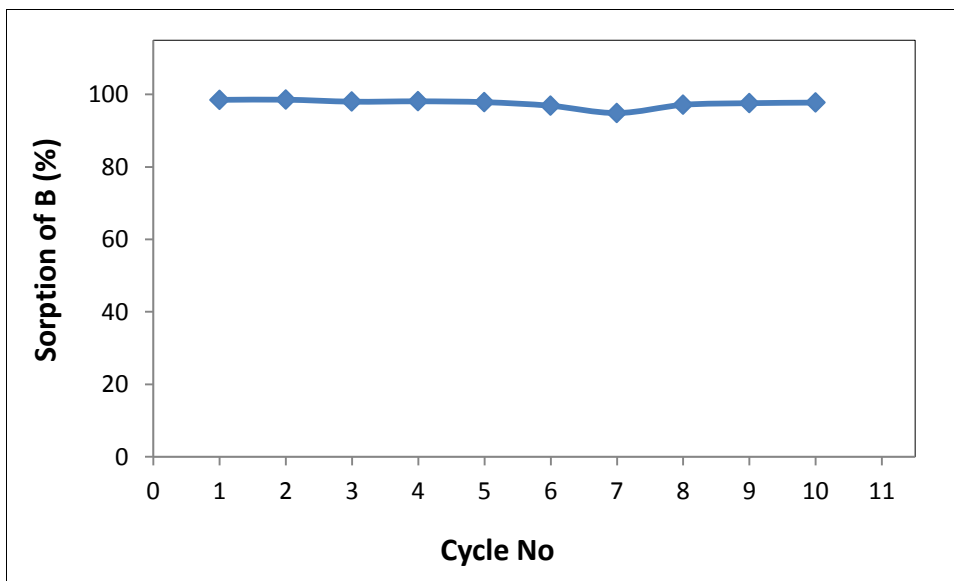
Figure 4.21. Sorption profile of boron using Amberlite PWA-10 during ten cycles.
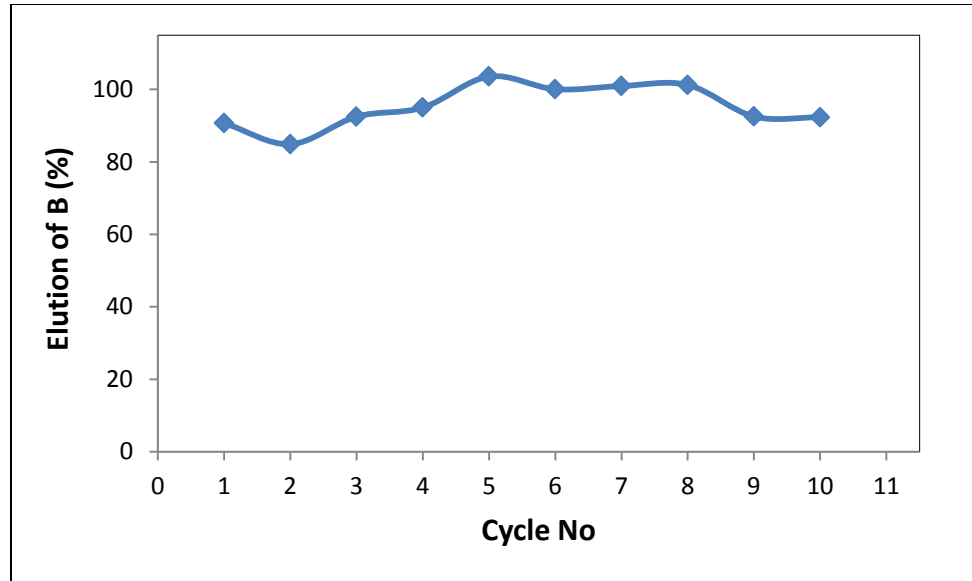
Figure 4.22. Elution profile of boron using Amberlite PWA-10 during ten cycles.
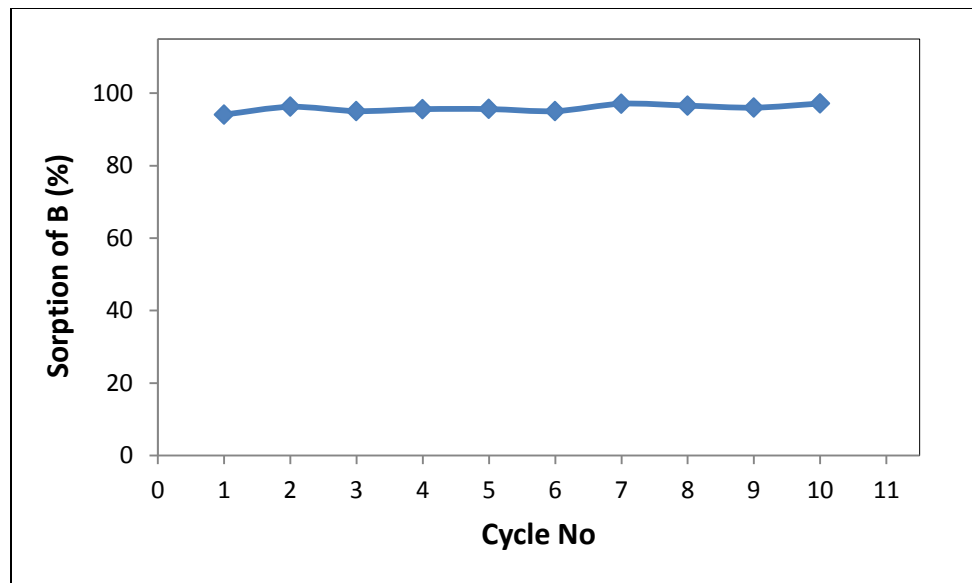
Figure 4.23. Sorption profile of boron using composite fiber during ten cycles.
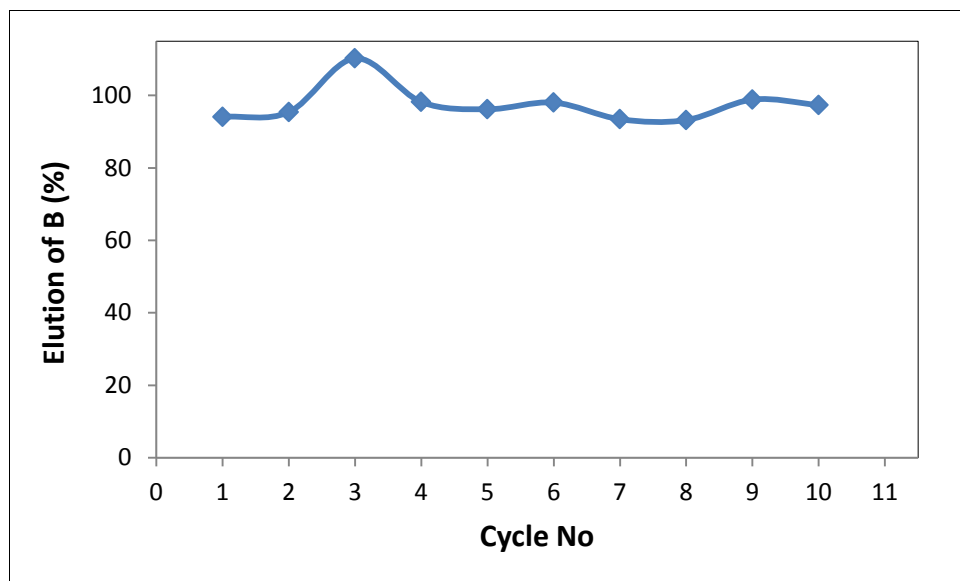
Figure 4.24. Elution profile of boron using composite fiber during ten cycles.

4.1.2. Column-mode sorption studies

The chelating resin Amberlite PWA-10 (at a particle size range of 0.355-0.500 mm), Diaion CRB02 (at a particle size range of 0.250-0.355 mm and 0.355-0.500 mm) and boron selective composite fiber were used in small-scall column tests for boron removal from geothermal water. The effect of SV on the column performances for the composite fiber was also studied. Space velocity values of 10, 15 and 25 h^{-1} were tested with composite fiber. In the column-mode study of Amberlite PWA-10, Diaion CRB02, space velocity was adjusted to 15 h^{-1}. All of the elution stages were performed at SV 5 h^{-1} with 5% H$_2$SO$_4$ solution.

The breakthrough profiles of the column-mode studies of composite fiber at SV 10,15 and 25 h^{-1} were given in Figure 4.25 and their elution profiles were shown in Figure 4.26.
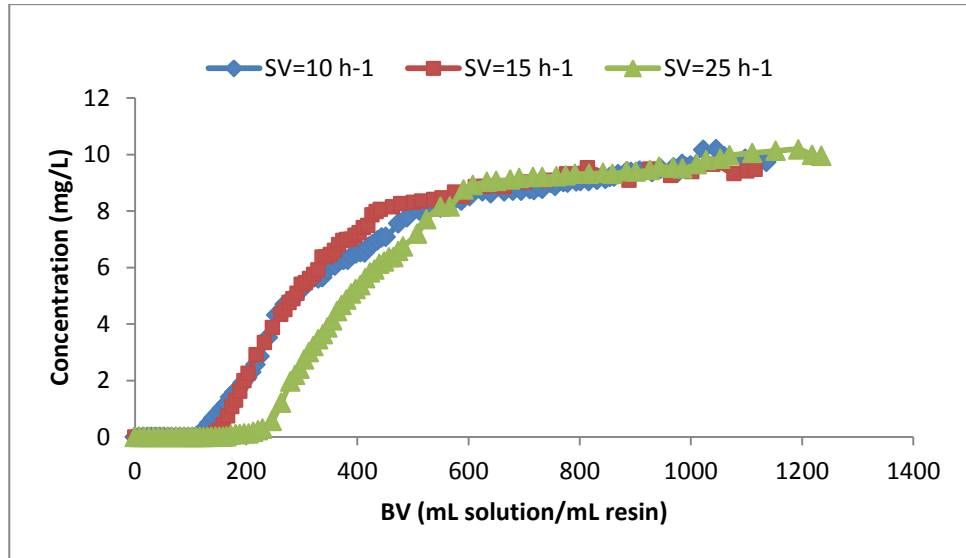
Figure 4.25. Breakthrough profiles of B by composite fiber at SV 10,15 and 25 h^{-1}.
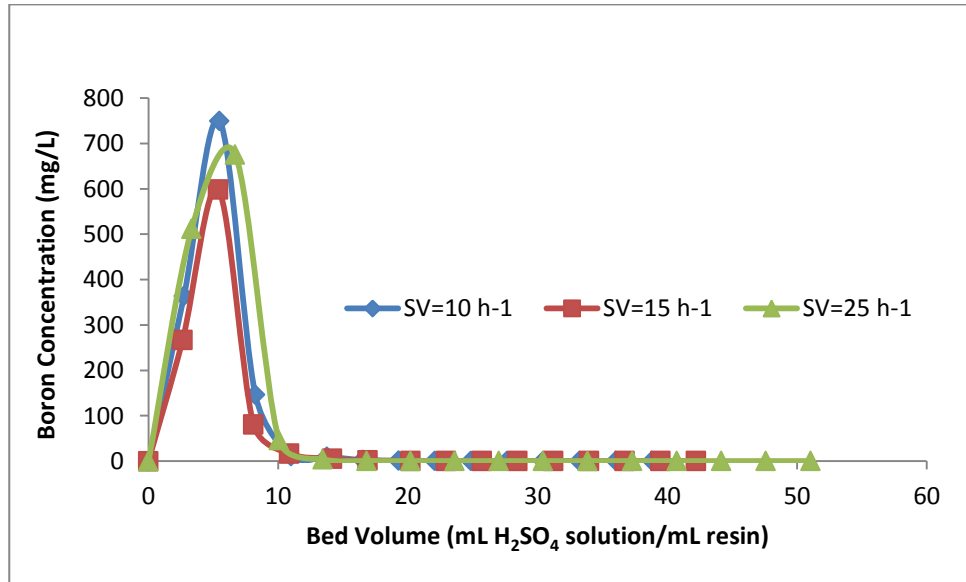
Figure 4.26. Elution profiles of B by composite fiber at SV 10,15 and 25 h^{-1}.

The breakthrough capacities, total capacities, elution efficiencies and column utilizations of the column-mode tests were given in Table 4.3. Breakthrough capacities were calculated by accepting the breakthrough point as the one just before the concentration of 0.5 mg B/L. The breakthrough capacities were calculated as 1.35, 1.53 and 2.31 mg B/mL at SV 10,15 and 25 h^{-1}, respectively. It seems that breakthrough capacities increased to some extent with increase in SV. When the comparison was made considering the column utilization, it was calculated as %35, %44 and %52 at SV 10, 15 and 25 h^{-1}, respectively.

Table 4. 3. Results of column-mode studies performed with geothermal water for composite fiber.

SV (h^{-1})	Breakthrough capacity (mg B/mL resin)	Total capacity (mg B/mL resin)	Elution efficiency (%)	Column utilization (%)
10	1.35	3.86	91	35
15	1.53	3.45	83	44
25	2.31	4.45	93	52

Space velocity value of 15 h^{-1} was employed for Amberlite PWA-10 with a particle size range of 0.355-0.500 mm. The loaded resin was eluted with 5% H_2SO_4 solution. The breakthrough profiles of the column-mode studies of composite fiber and Amberlite PWA-10 at SV 15 h^{-1} were given in Figure 4.27 and their elution profiles were shown in Figure 4.28.
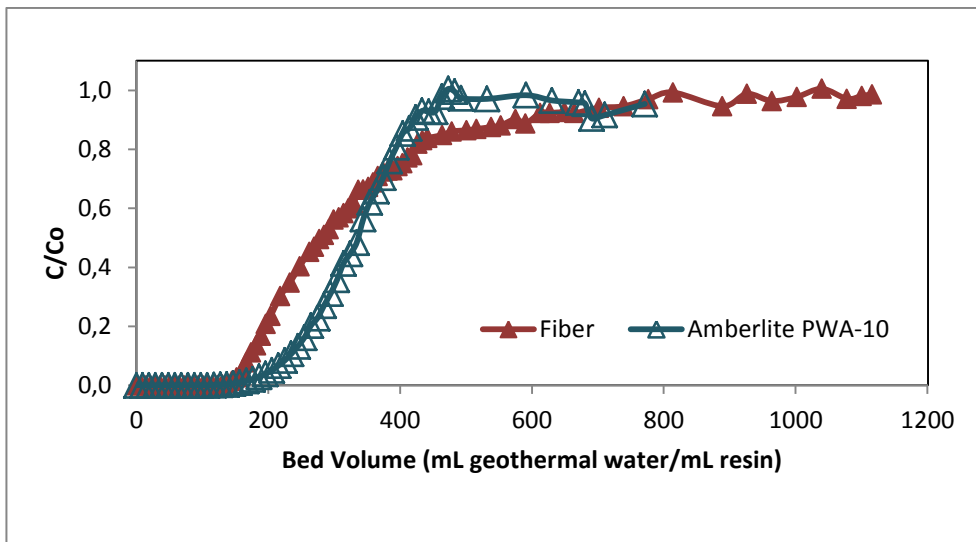
Figure 4.27. Breakthrough profiles of B by composite fiber and Amberlite PWA-10 (SV:15h^{-1}).
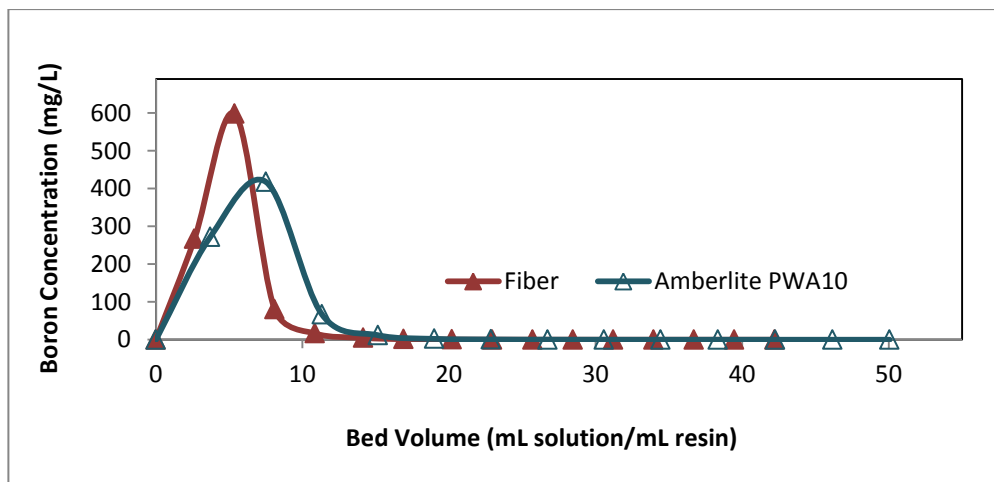
Figure 4.28. Elution profiles of B by composite fiber and Amberlite PWA-10 (SV:15h^{-1}).

As seen from Table 4.4, Amberlite PWA-10 had a breakthrough capacity of 2.04 mg B/mL resin and a total capacity of 3.52 mg B/mL at SV:15h^{-1}, while composite fiber had a breakthrough capacity of 1.53 mg B/mL fiber and a total capacity of 3.45 mg B/mL at the same SV. Total capacities of composite fiber and Amberlite PWA-10 were close to each other. But the breakthrough capacity of Amberlite PWA-10 was higher than the one of composite fiber. Experiments with Amberlite PWA-10 show that the column utilization is better than that with composite fiber at SV:15h^{-1}. When the space velocity of composite fiber was increased to 25 h^{-1}, the breakthrough and total capacity values were obtained higher than for both values of the Amberlite PWA-10.

Table 4. 4. Results of column-mode studies performed with İzmir geothermal water for composite fiber and Amberlite PWA-10.

Adsorbent	Breakthrough capacity (mg B/mL resin)	Total capacity (mg B/mL resin)	Elution efficiency (%)	Column utilization (%)
Composite Fiber (SV: 15h^{-1})	1.53	3.45	83	44
Amberlite PWA-10 (SV: 15h^{-1})	2.04	3.52	85	58
Composite Fiber (SV: 25h^{-1})	2.31	4.45	93	52

The effect of particle size of the resin on the column performances for the Diaion CRB02 was also studied. Sorption of boron from geothermal water was carried out at SV 15 h^{-1}. The breakthrough profiles of the column-mode studies of Diaion CRB02 at SV 15 h^{-1} were given in Figure 4.29 and their elution profiles were shown in Figure 4.30.
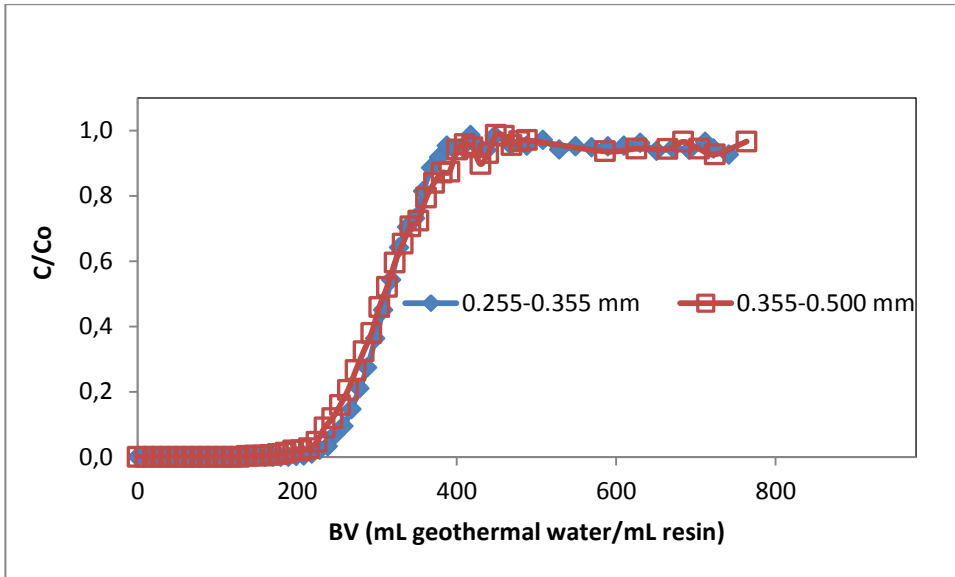
Figure 4.29. Breakthrough profiles of B by Diaion CRB02 at a particle size range of 0.250-0.355 mm and 0.355-0.500 mm.
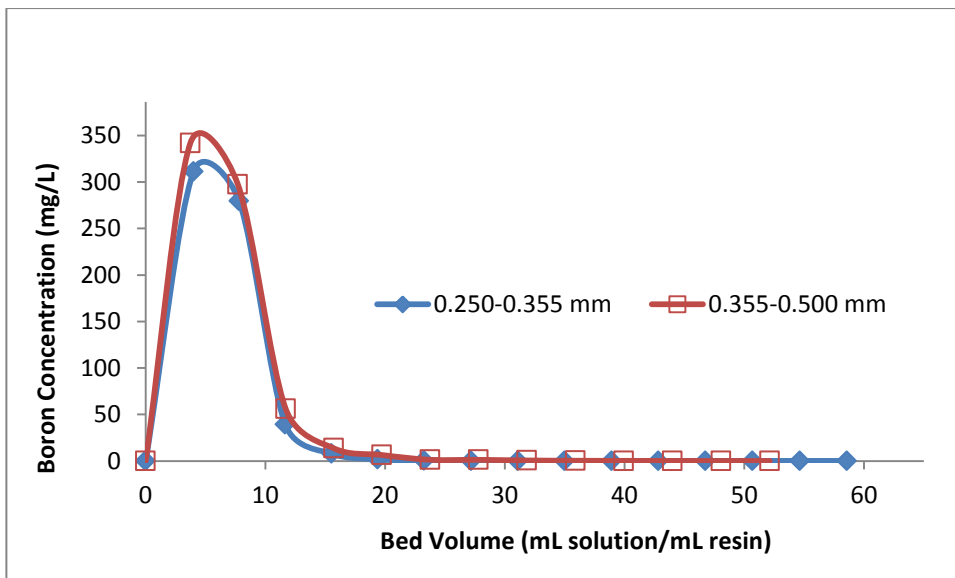
Figure 4.30. Elution profiles of B by Diaion CRB02 at a particle size range of 0.250-0.355 mm and 0.355-0.500 mm.

As seen from Table 4.5, Diaion CRB02 had a breakthrough capacity of 2.46 mg B/mL resin at a particle size range of 0.250-0.355 mm and 2.28 mg B/mL resin at a particle size range of 0.355-0.500 mm. The breakthrough capacity of resin with a particle size range of 0.250-0.355 mm was higher than that with a particle size range of 0.355-0.500 mm. The column utilizations of Diaion CRB02 were 77% and 72% for the resins with a particle size range of 0.250-0.355 and 0.355-0.500 mm, respectively.

Table 4.5. Results of column-mode studies performed with Diaion CRB02 at different particle size range (SV:15h^{-1}).

Particle size range (mm)	Breakthrough capacity (mg B/mL resin)	Total capacity (mg B/mL resin)	Elution efficiency (%)	Column utilization (%)
0.250-0.355	2.46	3.21	78	77
0.355-0.500	2.28	3.16	88	72

The effect of eluting agent concentration on the elution performance of boron from Diaion CRB02 (at a particle size range of 0.355-0.500 mm) was also studied. Boron loaded onto the resin Diaion CRB02 was eluted with 1.0 M H$_2$SO$_4$ solution. Figure 4.31 shows the breakthrough profiles and their elution profiles obtained with 0.5 and 1 M H$_2$SO$_4$.
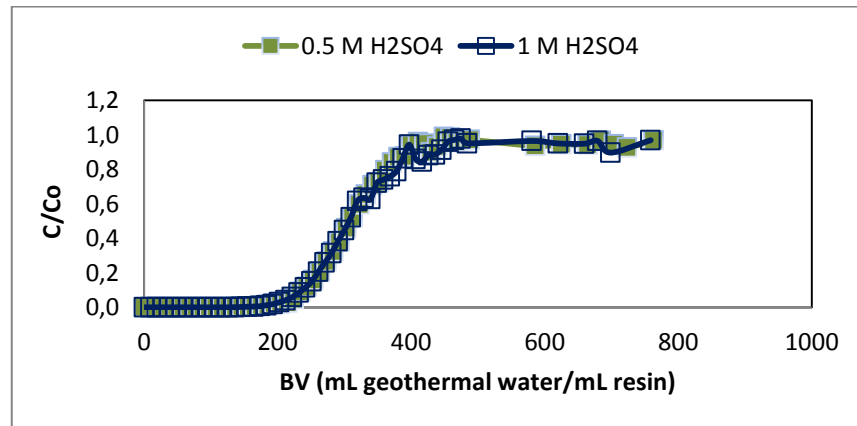
(a)
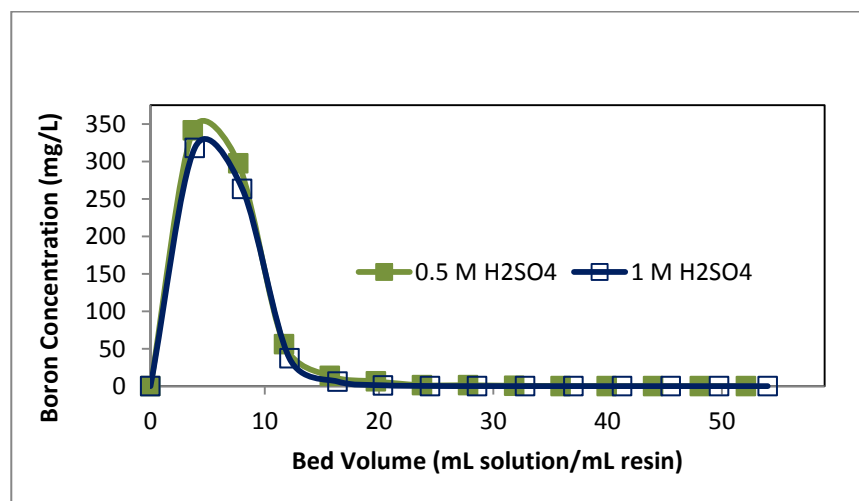
(b)

Figure 4.31. (a) Comparison of breakthrough profiles of B by Diaion CRB02 at a particle size range of 0.355-0.500 mm. (b) Comparison of eluting agent concentration for elution of B by Diaion CRB02 at a particle size range of 0.355-0.500 mm.

As seen from Table 4.6, elution efficiency of boron from Diaion CRB02 resin was higher when the acid concentration is lower.

Table 4.6. Results of column-mode studies performed with Diaion CRB02 at different eluting agent concentration.

Acid Concentration	Breakthrough capacity (mg B/mL resin)	Total capacity (mg B/mL resin)	Elution efficiency (%)	Column utilization (%)
0.5 M H_2SO_4	2.28	3.16	88	72
1 M H_2SO_4	2.14	3.16	80	68

4.1.3. EDI tests

In this experiment, RO permeate of geothermal water was used as a feed solution. Purolite CT 175, Purolite A500 (at a particle size range of 0.355-0.500 mm) and Amberlie PWA-10 (at a particle size range of 0.500-0.710 mm) resins were used. The solution containing 5.0 mg B/L was passed through the ion-exchange bed in the central compartment with the Purolite CT 175 and A500 (at a particle size range of 0.355-0.500 mm) in layered bed.

Na_2SO_4 solution (500 µS/cm conductivity) was circulated through the electrode compartments with a flow rate of 2.5 L/h. Flow rate of permeate was 1 L/h. A voltage of 25 V was applied to system.

The graphs of boron concentration versus time and the ratio of boron concentration at any time to initial boron concentration of RO permeate with Amberlite PWA-10 and Purolite CT 175 and A500 resins versus time were given in Figures 4.32 (a) and 4.32 (b), respectively. During the first 15 minutes, the boron concentration in the stream of central compartment with Amberlite PWA-10 was decreased from 3.98 mg B/L to 1.85 mg B/L. When the resins Purolite CT 175 and A500 were used, boron concentraiton was decreased from 4.00 mg B/L to 3.69 mg/L. At the end of 3 h, boron concentration was reduced below 0.69 mg B/L and 1.42 mg B/L for the experiments performed by using Amberlite PWA-10 and Purolite CT 175 and A500, respectively.
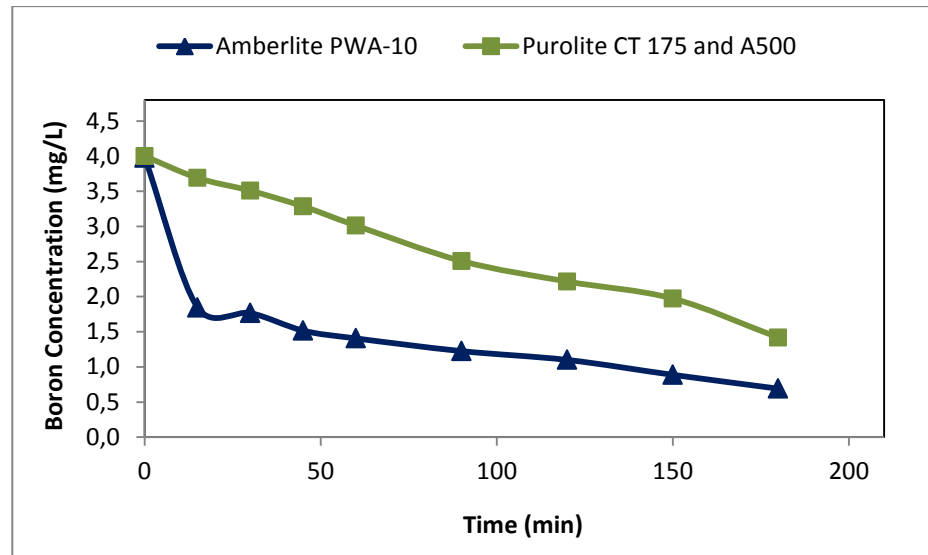
(a)
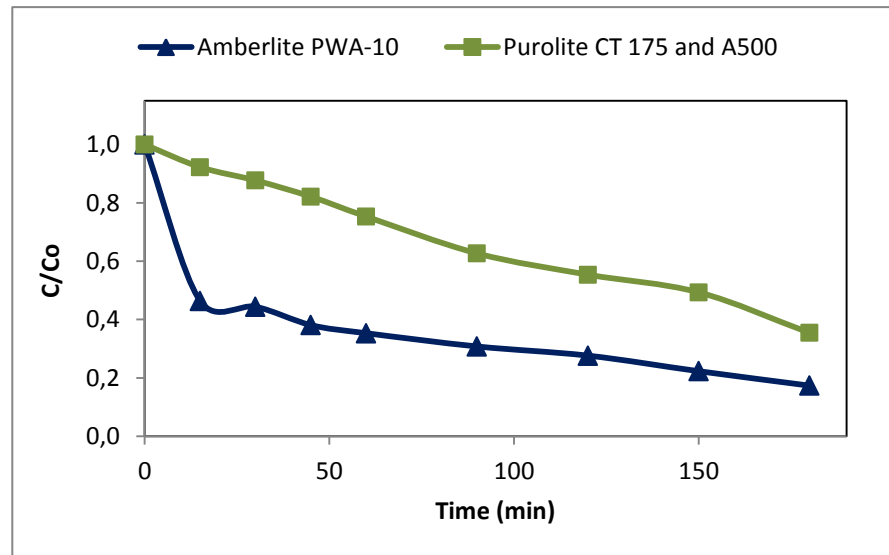
(b)

Figure 4.32. Comparison of boron concentrations in the stream of central compartment with respect to time (a) boron concentration versus time, (b) ratio of boron concentration at any time to initial boron concentration of RO permeate.

Boron concentration in the anode compartment is lower when Amberlite PWA-10 is in the central compartment than that of the system containing Purolite CT 175-A500 resins as seen in Figure 4.33. Boron concentration was reduced below 0.064 mg B/L and 0.308 mg B/L for the experiments performed by using Amberlite PWA-10 and Purolite CT 175-A500, respectively. On the other hand,

because of the complexation with boron, it is difficult to separate boron from boron selective resin Amberlite PWA-10.
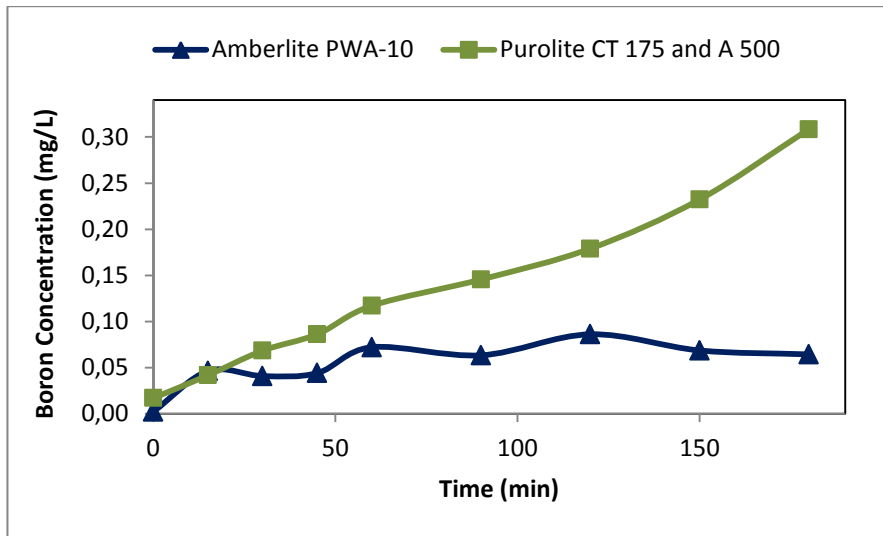
Figure 4.33. Boron concentration in the anode compartment versus time with Amberlite PWA-10 and Purolite CT 175-A500.

The graphs of boron concentration versus time and the ratio of boron concentration at any time to initial boron concentration of RO permeate and model solution (containing 5.0 mg B/L) with Purolite CT 175 and A500 resins versus time were given in Figures 4.34 (a) and 4.34 (b), respectively. The measured boron concentrations after 180 minutes were 0.96 mg/L and 1.42 mg/L for the experiments performed by using model solution and RO permeate of geothermal water, respectively. Boron concentration was obtained lower in model solution than RO permeate of geothermal water. This was resulted from the other co-existing ions in the RO permeate.
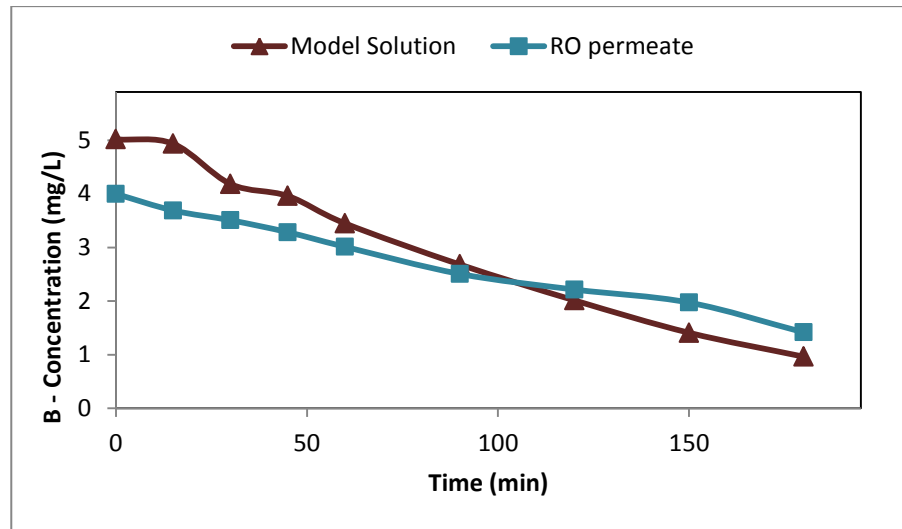
(a)
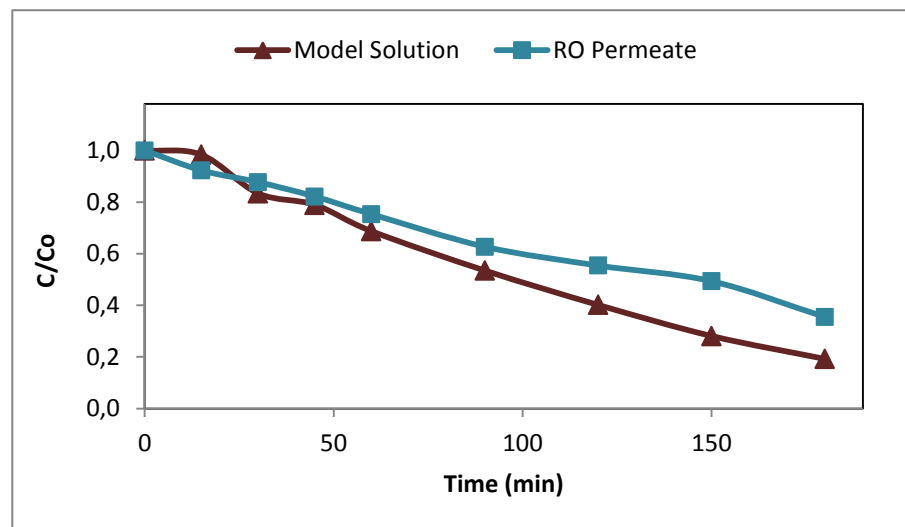
(b)

Figure 4.34. Comparison of boron concentrations in central compartment with respect to time (a) boron concentration versus time, (b) ratio of boron concentration at any time to initial boron concentration of RO permeate and model solution containing 5.0 mg B/L.

4.1.4. Separation of lithium by ion exchange-membrane filtration hybrid system

4.1.4.1. Effect of adsorbent concentration on lithium removal

To determine the effect of lithium adsorbent concentration on lithium removal from geothermal water, granulated and powder λ-manganese oxide (λ-MnO_2) adsorbents were used for ion exchange-membrane filtration filtration tests. The concentration of lithium in the geothermal water is at a level of 1.28 mg Li/L-

geothermal water. These tests were done by spiking standard lithium solution with geothermal water in a way that geothermal water contains 10 mg Li/L.

The operational parameters in the hybrid system for granulated and powder adsorbents were summarized in Table 4.7.

Table 4.7. Parameters applied for the hybrid system using granulated and powder adsorbent for Li removal from geothermal water.

Adsorbent concentration (X), g/L	Adsorbent type	Rate of replacement of saturated and fresh adsorbent (Q_s), mL/min	Flow rate of permeate and feed (Q_p), mL/min
1	Granulated	3	5
2	Granulated	3	5
3	Granulated	3	5
1	Powder	3	5
2	Powder	3	5
3	Powder	6	5

Using the granulated adsorbent performed at a rate of replacement for saturated and fresh adsorbents as 3 mL/min and using a flow rate of permeate as 5 mL/min with a granulated adsorbent concentration of 1.0 g adsorbent/L-geothermal water, hybrid tests were carried out. At these conditions, lithium concentration of the permeate was lowered to 0.31 mg Li/L from 10.34 mg Li/L-geothernal water. The results of lithium concentration of permeate versus time and ratio of lithium concentration of permeate at any time to initial lithium concentration of geothermal water versus time were given in Figures 4.35 (a) and (b), respectively.
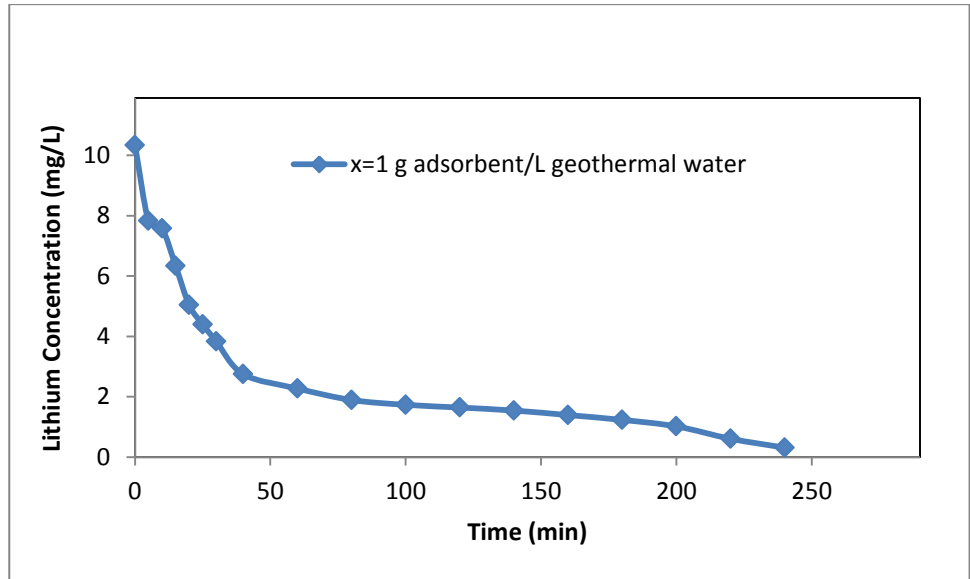
(a)
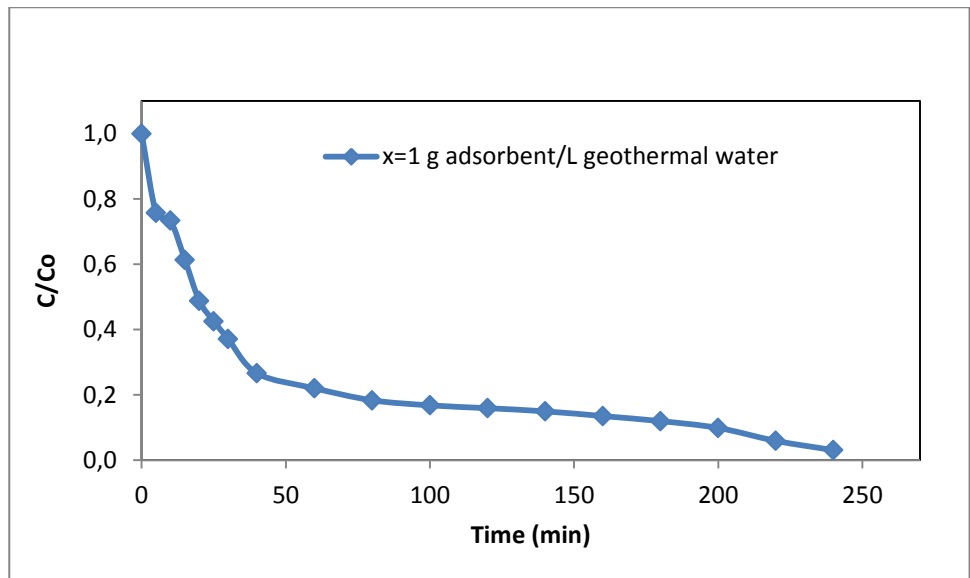
(b)

Figure 4.35. (a) Lithium concentration versus time (b) Ratio of lithium concentration at any time to initial lithium concentration of geothermal water versus time (Adsorbent concentration: 1 g adsorbent/L geothermal water, Qfresh/sat: 3 mL/min, Qfeed/permeate: 5 mL/min)

Under the same conditions, some tests were performed with 2.0 g adsorbent/L-geothermal water. At the end of the test, lithium concentration in the permeate was lowered to almost 0 mg Li/L from 10.53 mg Li/L-geothermal water in 40 minutes. The results of lithium concentration of the permeate versus time and the ratio of lithium concentration of permeate at any time to initial lithium

concentration of geothermal water versus time were given in Figures 4.36 (a) and (b), respectively.
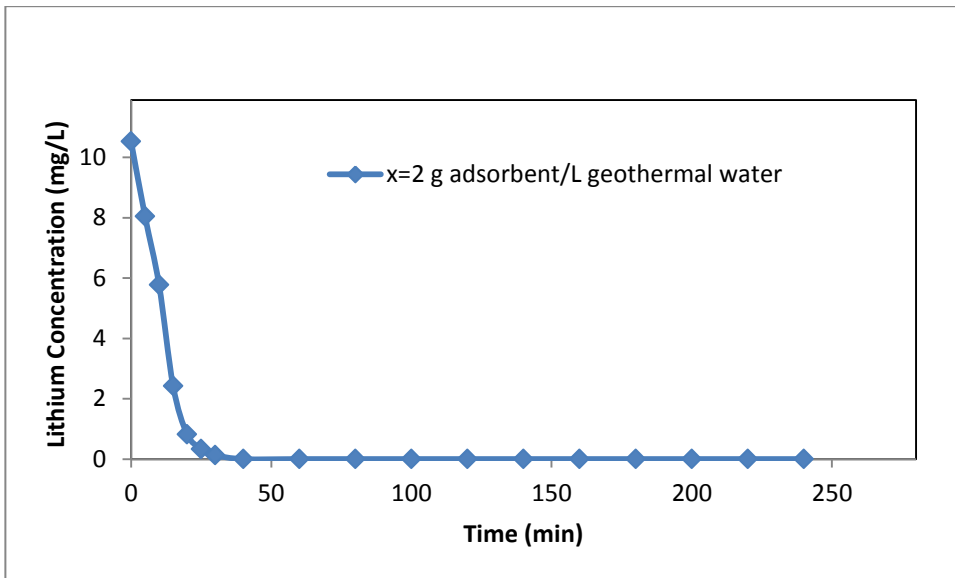
(a)
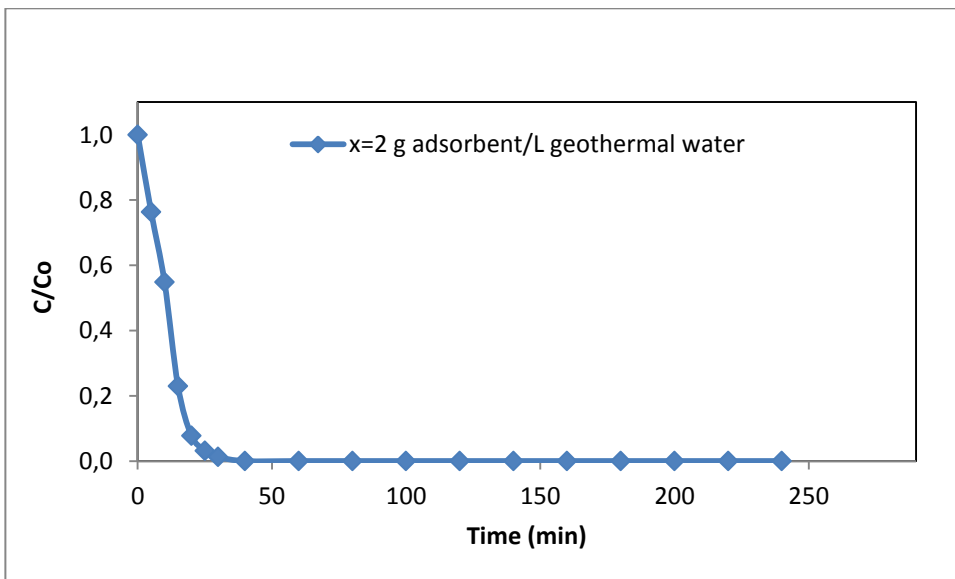
(b)

Figure 4.36. (a) Lithium concentration versus time (b) Ratio of lithium concentration at any time to initial lithium concentration of geothermal water versus time (Adsorbent concentration: 2 g adsorbent/L geothermal water, Qfresh/sat: 3 mL/min, Qfeed/permeate: 5 mL/min)

The next experiment was performed using the same flow rates at an adsorbent concentration of 3.0 g adsorbent/L geothermal water. Increasing the

adsorbent amount gave positive effect on lithium removal and lithium concentration in the permeate was lowered to almost 0 mg Li/L-geothermal water from 10.15 mg Li/L in 40 minutes. The results of lithium concentration of permeate versus time and ratio of lithium concentration of permeate at any time to initial lithium concentration of geothermal water versus time were given in Figures 4.37 (a) and (b), respectively.
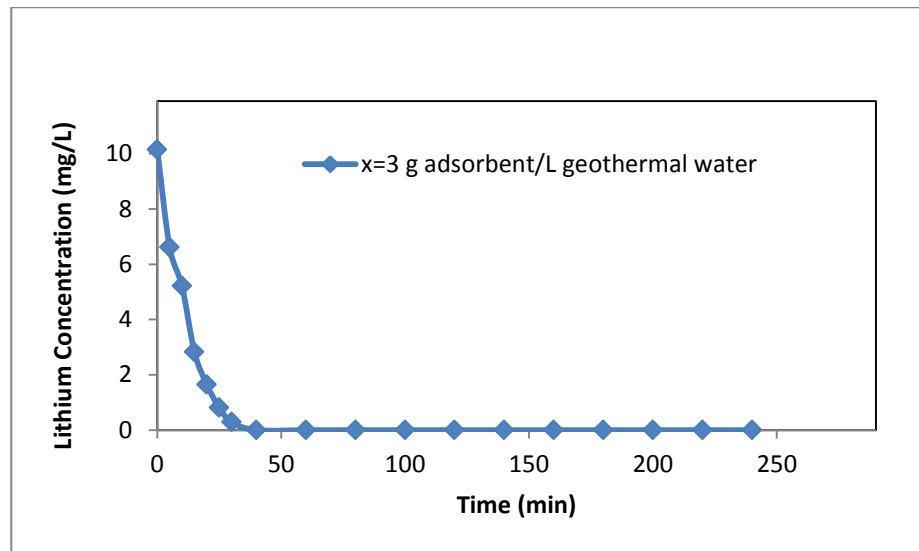
(a)
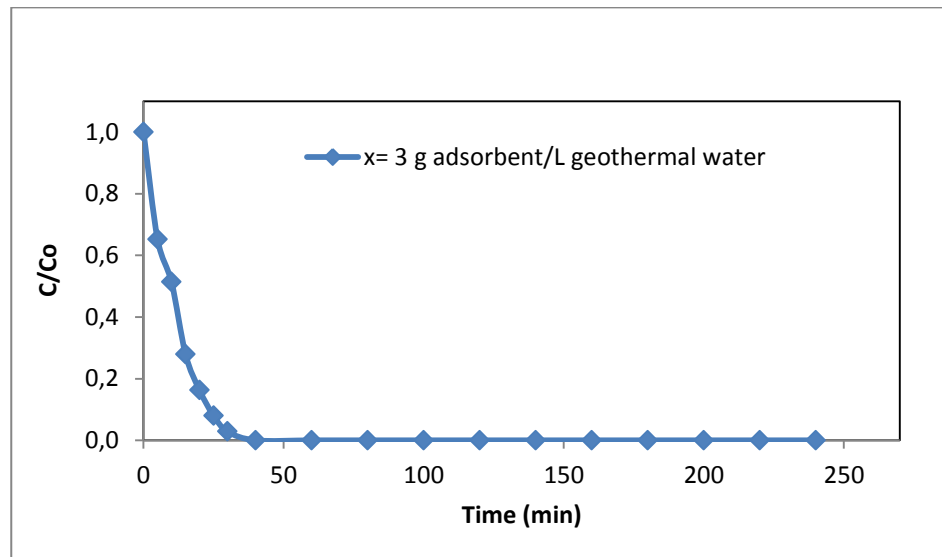
(b)

Figure 4.37. (a) Lithium concentration versus time (b) Ratio of lithium concentration at any time to initial lithium concentration of geothermal water versus time (Adsorbent concentration: 3 g adsorbent/L geothermal water, Qfresh/sat: 3 mL/min, Qfeed/permeate: 5 mL/min).

Figure 4.38 shows the effect of adsorbent concentration on lithium separation by granulated adsorbent. Increasing the adsorbent concentration was shown positive effect on lithium removal. Increasing the adsorbent amount from 2 g adsorbent/L-geothermal water to 3 g adsorbent/L-geothermal water did not give much effect for lithium separation.
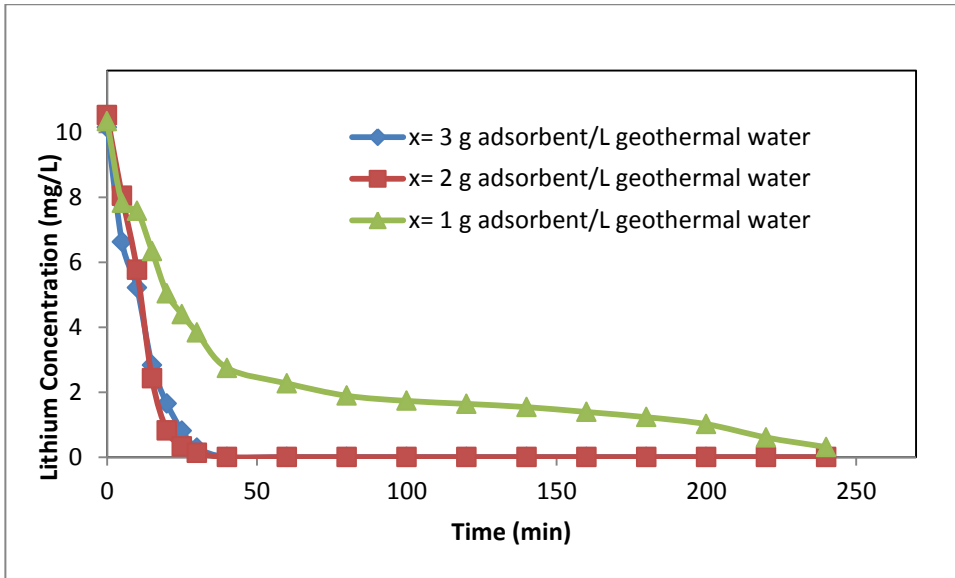
(a)
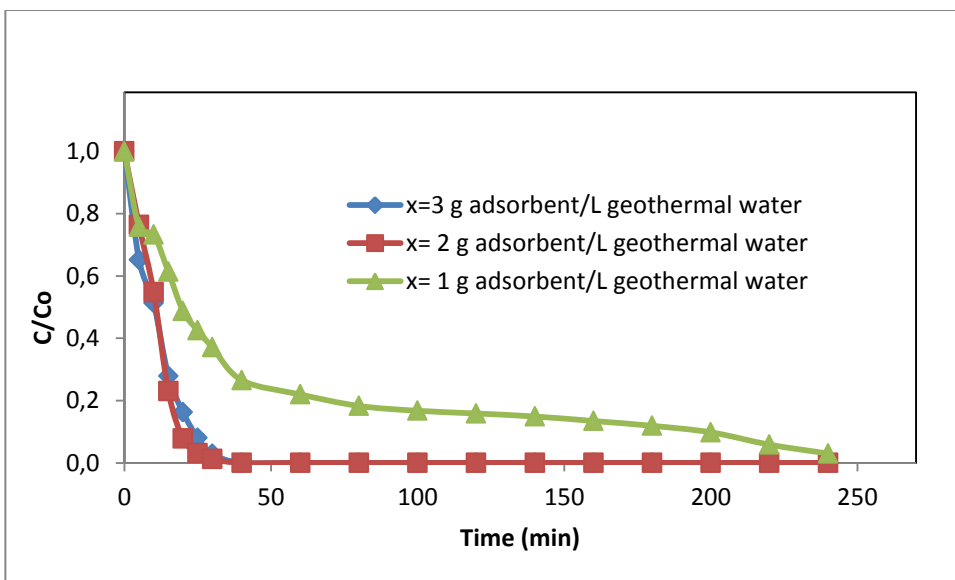
(b)

Figure 4.38. Effect of adsorbent concentration on lithium separation from geothermal water (a) Lithium concentration versus time (b) Ratio of lithium concentration at any time to initial lithium concentration of geothermal water versus time (Qfresh/sat: 3 mL/min, Qfeed/permeate:5mL/min)

Next tests were performed using powder λ-MnO_2 adsorbent using 1.0 g adsorbent/L geothermal water, 3 mL/min of fresh/saturated adsorbent replacement rate and 5 mL/min of permeate flow rate test were performed. Lithium concentration in the permeate was lowered to 5.54 mg Li/L-geothermal water from 10.35 mg Li/L-geothermal water at the end. The results of lithium concentration in the permeate versus time and ratio of lithium concentration in the permeate at any time to initial lithium concentration in the geothermal water versus time were given in Figures 4.39 (a) and (b), respectively.
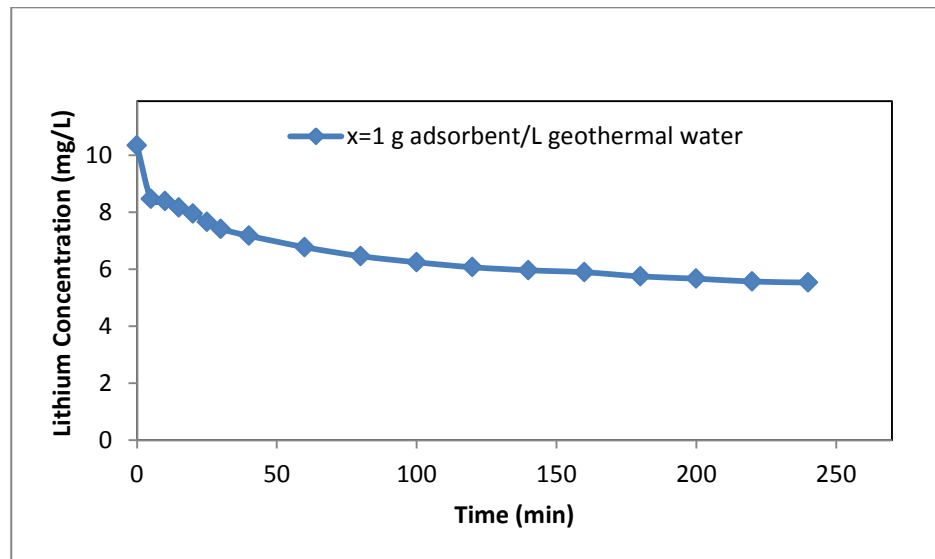
(a)
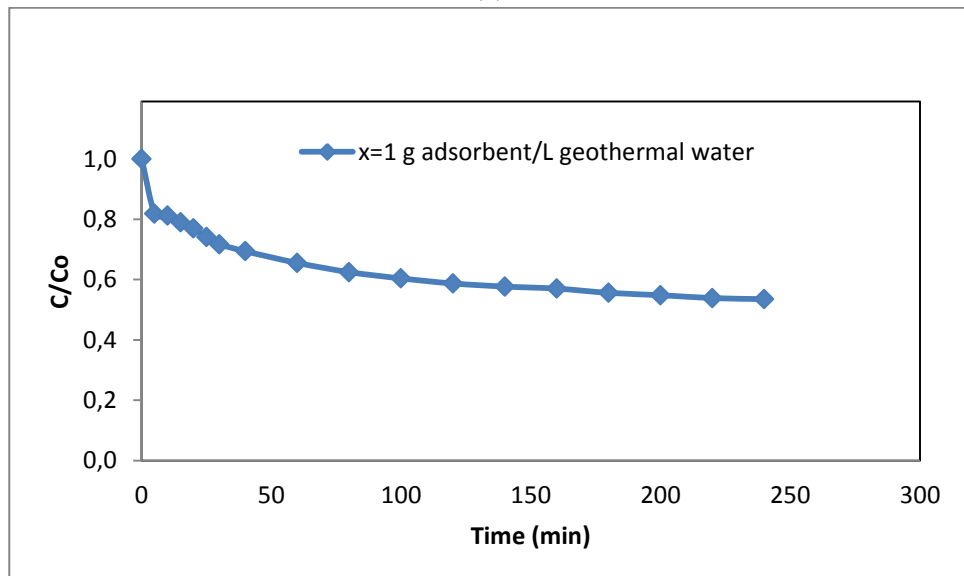
(b)

Figure 4.39. (a) Lithium concentration versus time (b) Ratio of lithium concentration at any time to initial lithium concentration of geothermal water versus time (Adsorbent concentration: 1 g adsorbent/L geothermal water, Qfresh/sat: 3 mL/min, Qfeed/permeate: 5 mL/min).

The next experiment was performed using the same operational conditions with adsorbent concentration of 2.0 g adsorbent/L geothermal water. Lithium removal was effective with increasing adsorbent concentration and lithium concentration in the permeate was lowered to 3.94 mg Li/L-geothermal water from 10.85 mg Li/L-geothermal water. The results of lithium concentration of permeate versus time and ratio of lithium concentration of permeate at any time to initial lithium concentration of geothermal water versus time were given in Figures 4.40 (a) and (b), respectively.
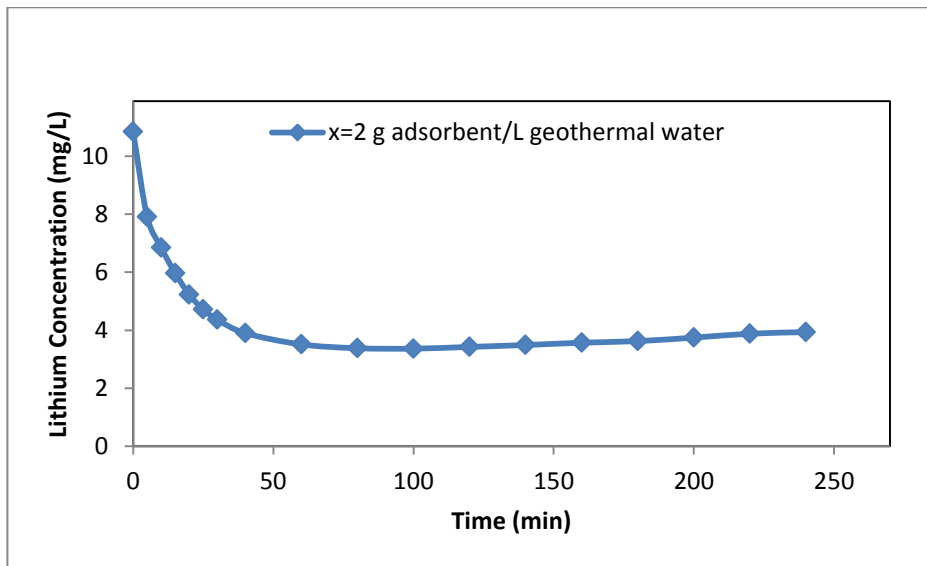
(a)
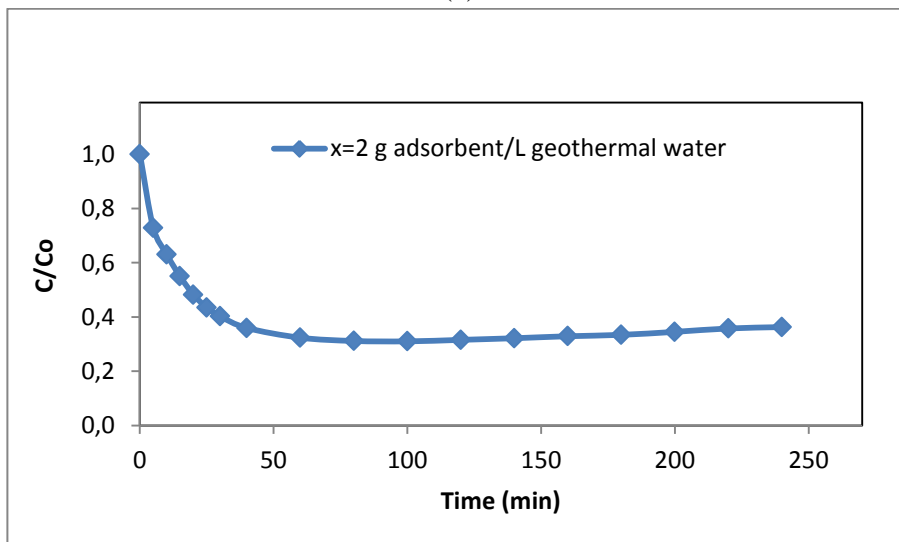
(b)

Figure 4.40. (a) Lithium concentration versus time (b) Ratio of lithium concentration at any time to initial lithium concentration of geothermal water versus time (Adsorbent concentration: 2 g adsorbent/L geothermal water, Qfresh/sat: 3 mL/min, Qfeed/permeate: 5 mL/min).

Later, the test was performed using the flow rates of saturated and fresh adsorbents of 6 mL/min while the flow rates of feed and permeate were kept constant as 5 mL/min using with adsorbent concentration of 3.0 g adsorbent/L geothermal water. Lithium concentration of the permeate was lowered to 0.68 mg Li/L-geothermal water from 10.57 mg Li/L-geothermal water. The results of lithium concentration of permeate versus time and ratio of lithium concentration of permeate at any time to initial lithium concentration of geothermal water versus time were given in Figures 4.41 (a) and (b), respectively.
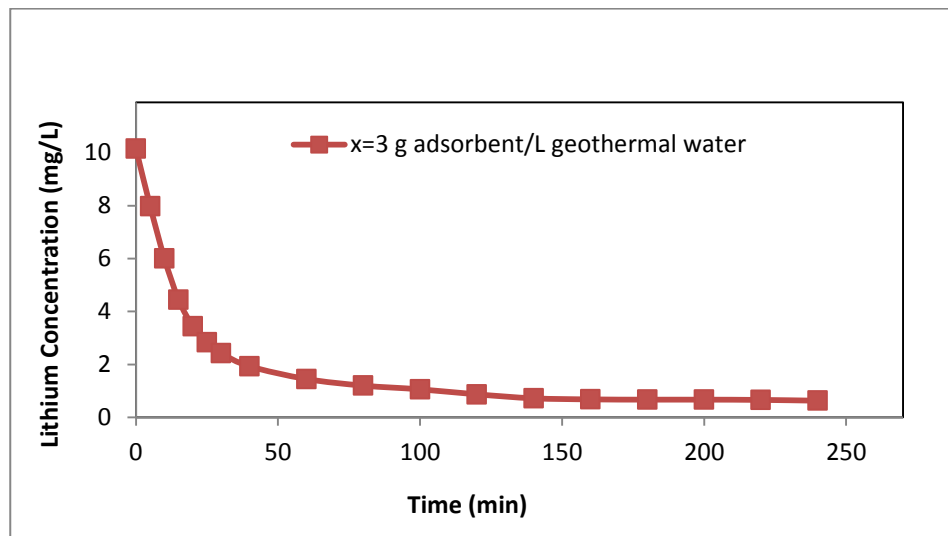
(a)
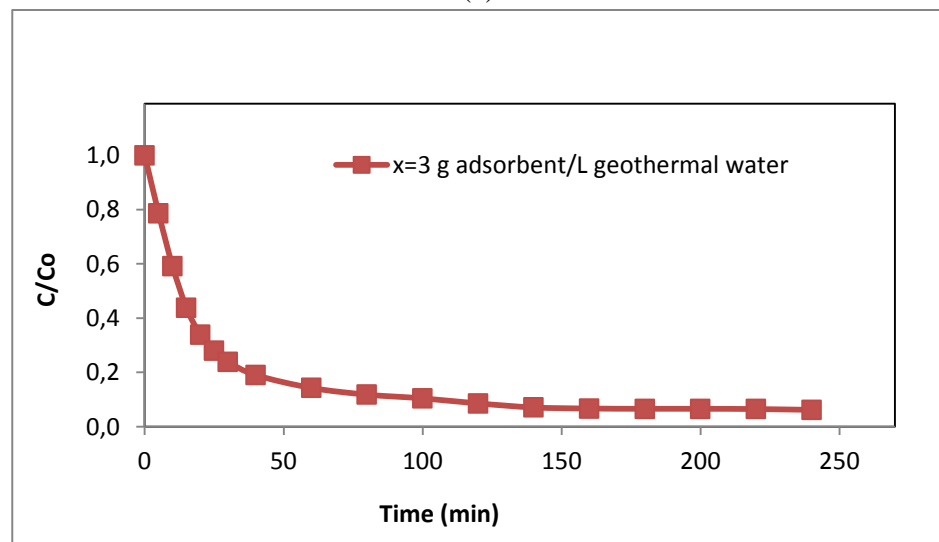
(b)

Figure 4.41. (a) Lithium concentration versus time (b) Ratio of lithium concentration at any time to initial lithium concentration of geothermal water versus time (Adsorbent concentration: 3 g adsorbent/L geothermal water, Qfresh/sat: 6 mL/min, Qfeed/permeate: 5 mL/min).

Figure 4.42 shows the effect of adsorbent concentration on lithium separation by powder adsorbent. Increasing adsorbent concentration had positive effect of lithium removal from geothermal water.
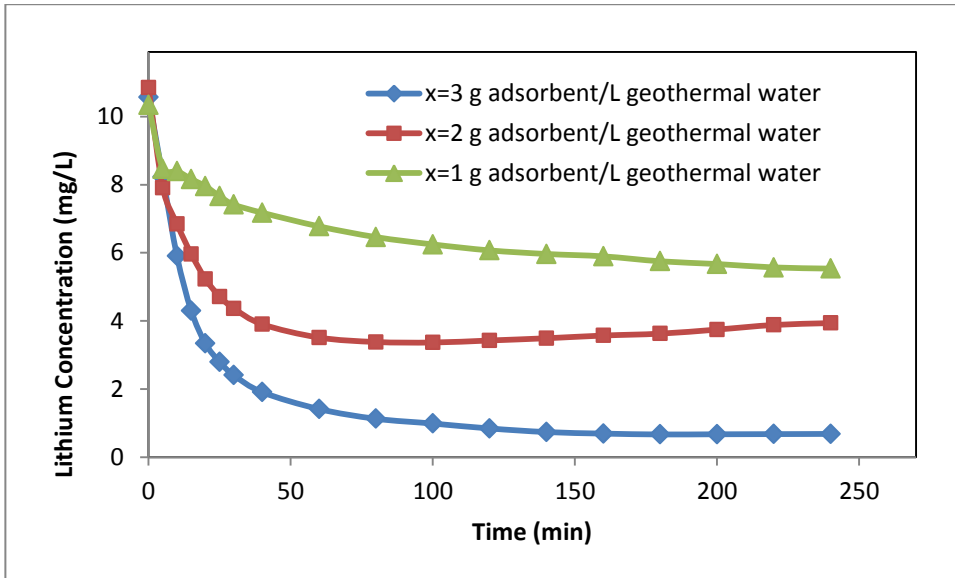
(a)
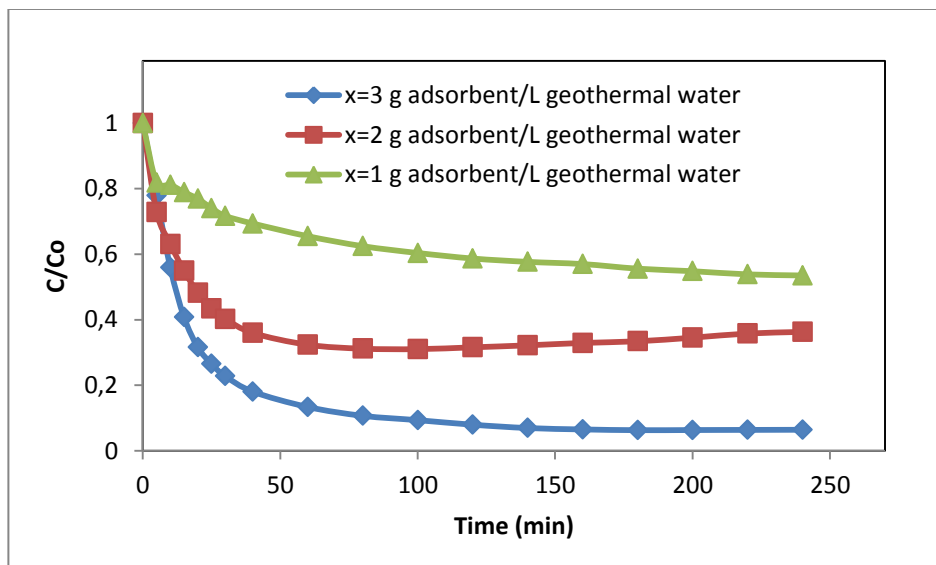
(b)

Figure 4.42. Effect of adsorbent concentration on lithium separation from geothermal water (a) Lithium concentration versus time (b) Ratio of lithium concentration at any time to initial lithium concentration of geothermal water versus time.

Increasing the adsorbent amount from 2 g adsorbent/L to 3 g adsorbent/L geothermal water did not give much effect on lithium removal for granulated adsorbent, whereas increasing the adsorbent amount from 2 g adsorbent/L to 3 g

adsorbent/L-geothermal water gave positive effect for powder adsorbent. These results were caused by the particle size of powder adsorbent that gives more interaction and bigger contact surface opportunities.

As seen in Figure 4.43, the graphs of lithium concentration versus time using 1.0 g granulated adsorbent/L geothermal water and 1.0 g powder adsorbent/L geothermal water. Lithium concentration was reduced below 0.31 mg Li/L and 5.54 mg Li/L for the experiments performed by using 1.0 g granulated adsorbent/L geothermal water and 1.0 powder adsorbent/L geothermal water, respectively.
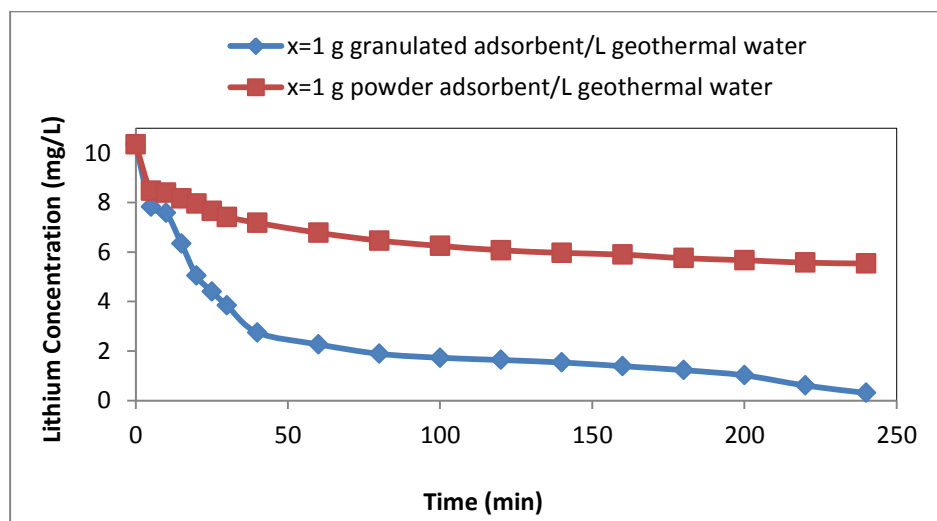
Figure 4.43. Comparison of lithium concentration versus time using granulated and powder adsorbents.

As seen in Figure 4.44, the graphs of lithium concentration versus time using 2.0 g granulated adsorbent/L geothermal water and 2.0 g powder adsorbent/L geothermal water. Lithium concentration was lowered to almost 0 mg Li/L in 40 minutes and 3.90 mg Li/L in 40 minutes for the experiments performed by using 2.0 g granulated adsorbent/L geothermal water and 2.0 powder adsorbent/L geothermal water, respectively.
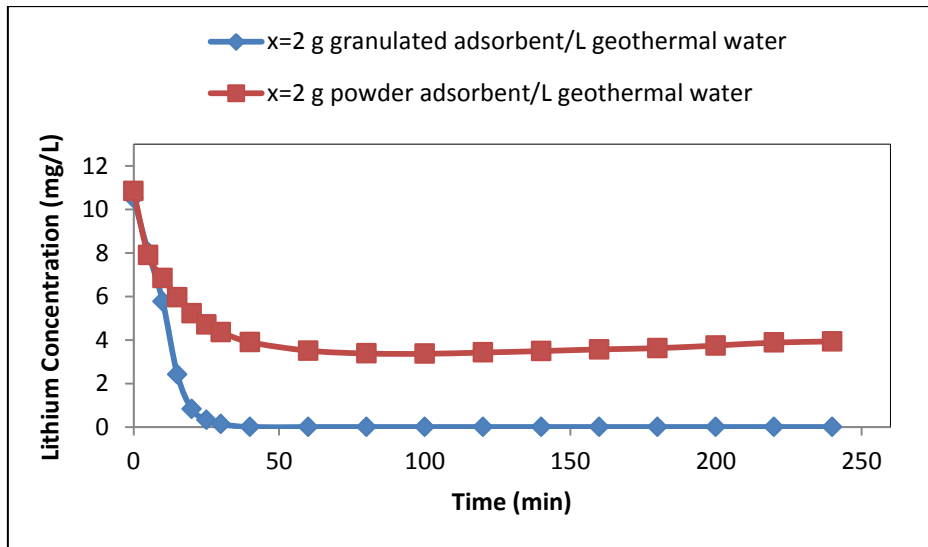
Figure 4.44. Comparison of lithium concentration versus time using granulated and powder adsorbents.

Another comparison was performed in order to see whether we can get reproducible results with λ-MnO_2 adsorbents using hybrid method. Test 1 was carried out in 2011, whereas test 2 was in 2012 under same laboratory conditions to check the reproducibility of investigations for lithium separation as shown in Figures from 4.45 to 4.50.
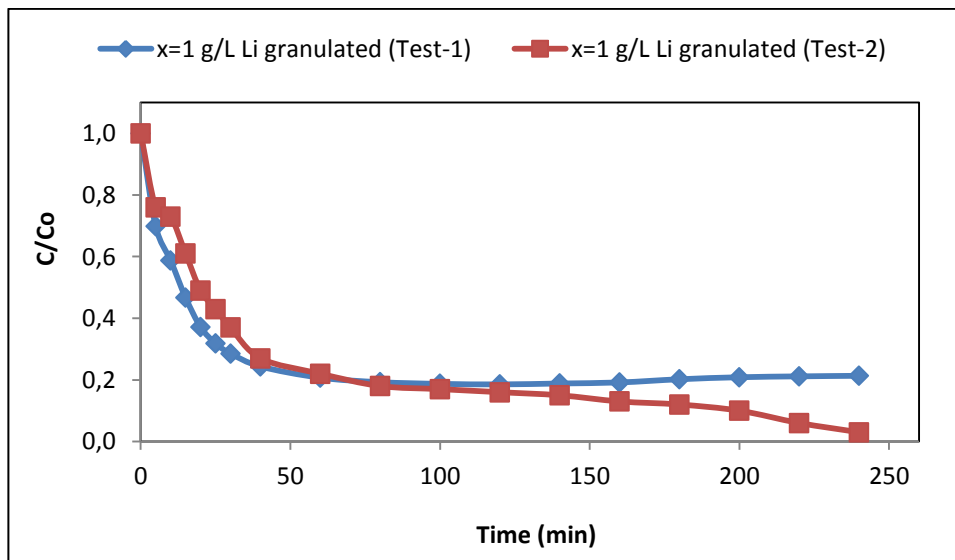
Figure 4.45. Comparison of Test-1 and Test-2 (Adsorbent concentration: 1 g adsorbent/L geothermal water).
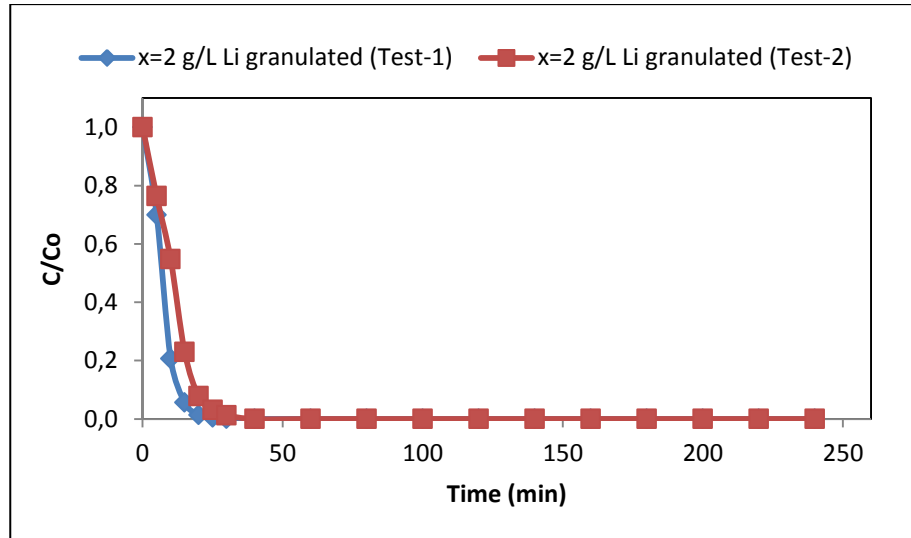
Figure 4.46. Comparison of Test-1 and Test-2 (Adsorbent concentration: 2 g adsorbent/L geothermal water)
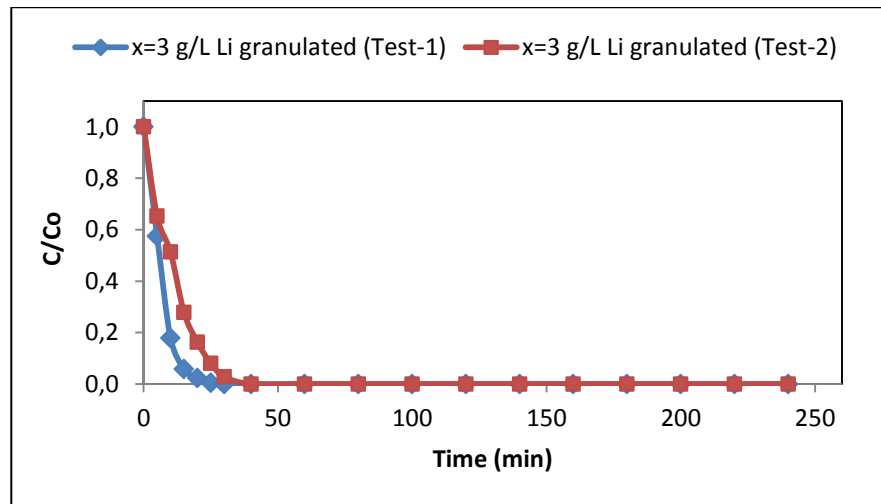
Figure 4.47. Comparison of Test-1 and Test-2 (Adsorbent concentration: 3 g adsorbent/L geothermal water)
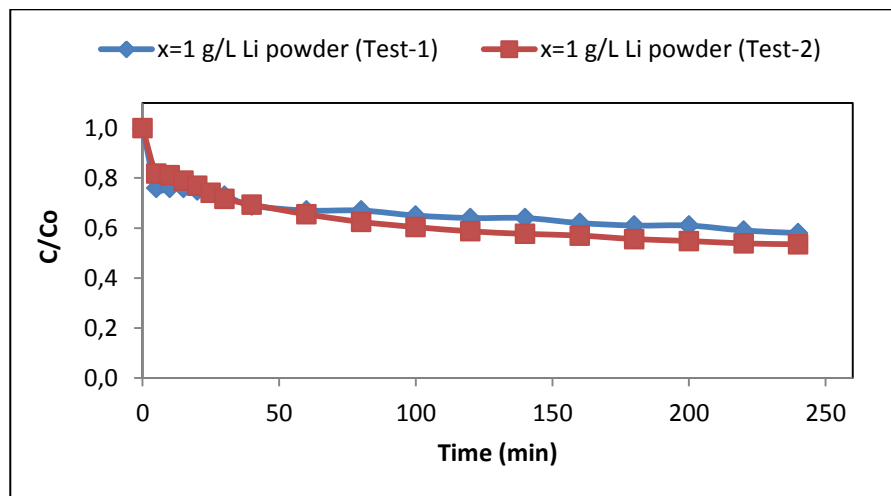
Figure 4.48. Comparison of Test-1 and Test-2 (Adsorbent concentration: 1 g adsorbent/L geothermal water).
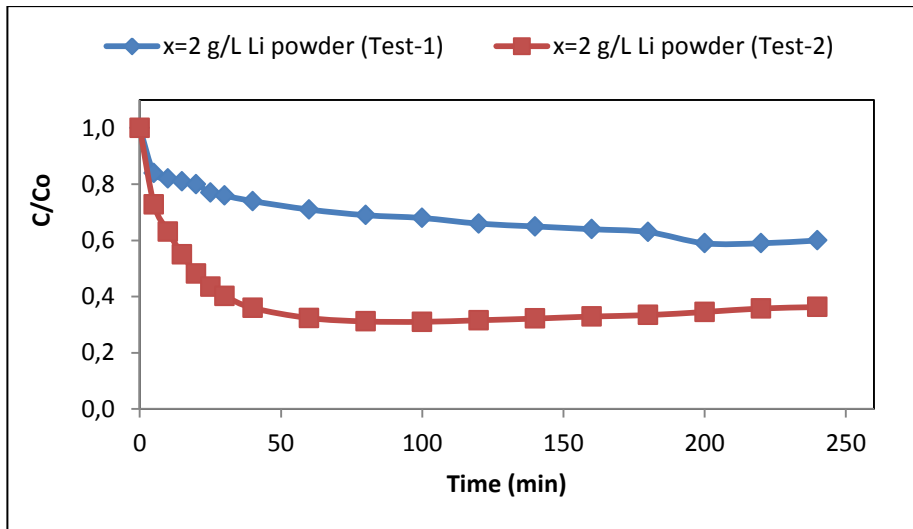
Figure 4.49. Comparison of Test-1 and Test-2 (Adsorbent concentration: 2 g adsorbent/L geothermal water)
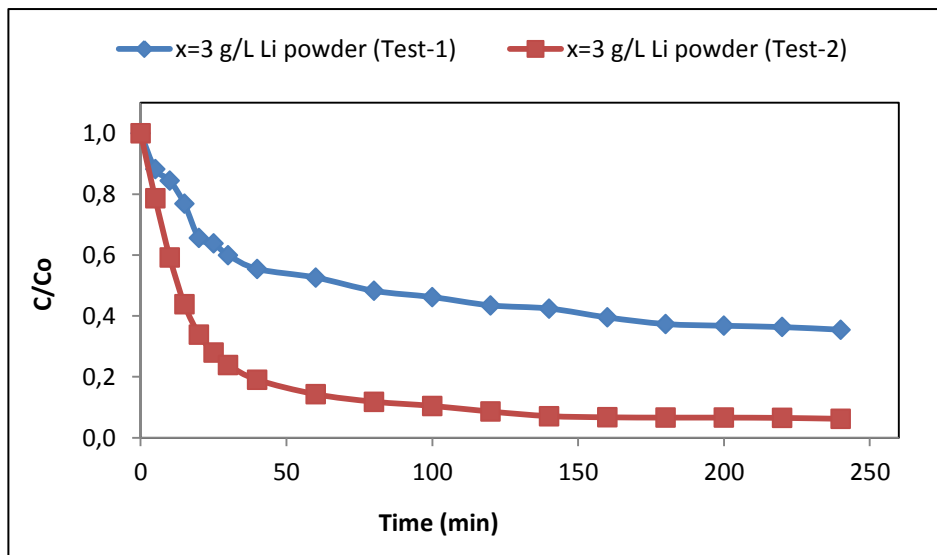
Figure 4.50. Comparison of lithium concentration versus time Test-1 and Test-2 (Adsorbent concentration: 2 g adsorbent/L geothermal water).

The results of Test 2 were generally better than Test 1 for lithium separation from geothermal water by using granulated and powder adsorbents in the doses of 1, 2 and 3 g/L. Moreover, with the dosages of 2 and 3 grams of powder adsorbent/L, the lithium separation results were also better.

4.1.5. Removal of As(V) by Ion Exchange Resins

As(V) removal studies were investigated for P(VbNMDG) and P(ClVBTA) resins that were synthesized in the laboratory of Concepcion University. The performance of sorption for these resins were checked by using batch-mode sorption studies.

4.1.5.1. Characterisation of ion exchange resins

Fig. 4.51 (a) and (b) show the infrared spectra of VbNMDG and ClVBTA resins. The VbNMDG resin showed the characterisic absorpion bands are 1080 cm^{-1} v (C-O), 1455 cm^{-1} v (CH$_2$), 1653 cm^{-1} v (C=C). The ClVBTA resin showed the characterisic absorpion bands at 1117 cm^{-1} v (C-N), 1482 cm^{-1} v (NH$_4$), 1644 cm^{-1} v (C=C).
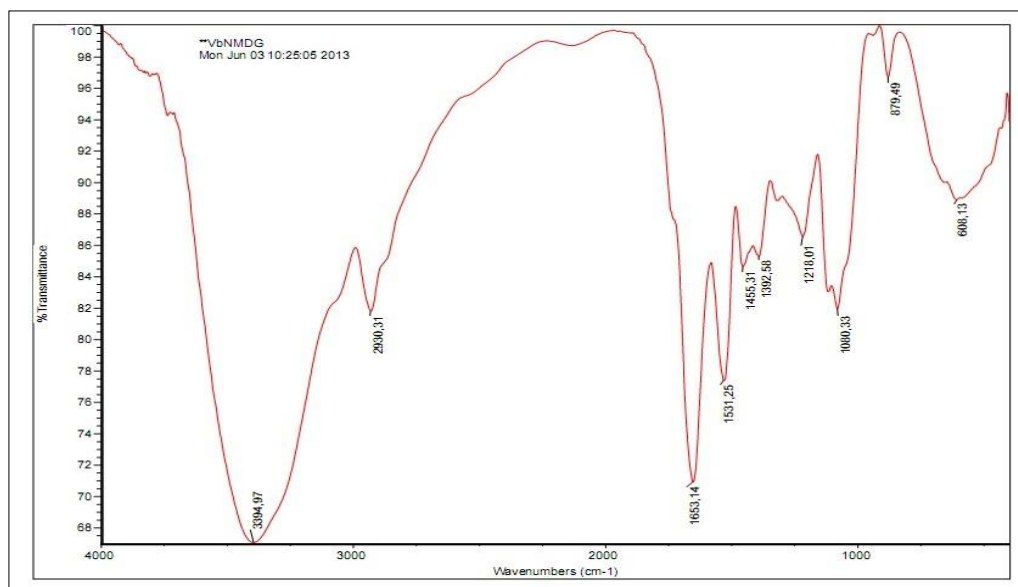
(a)
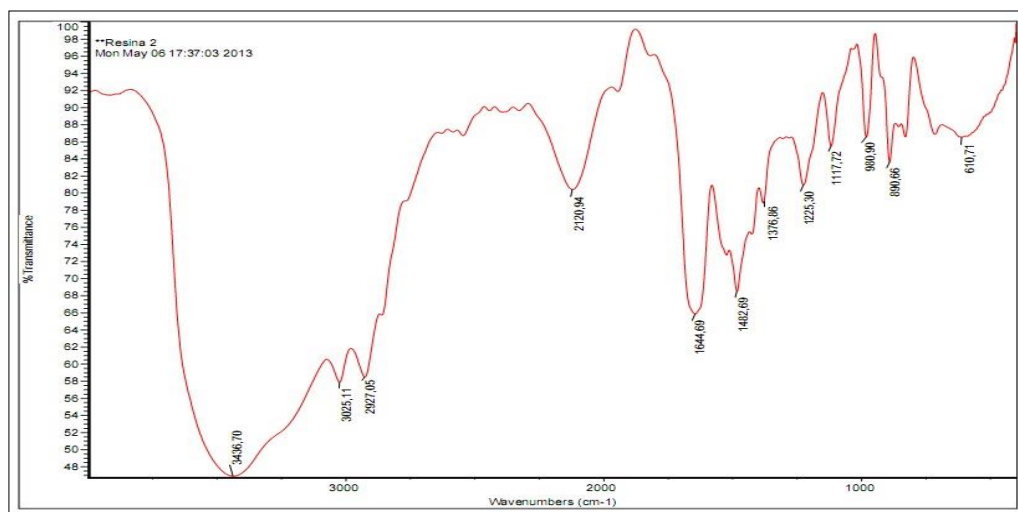
(b)

Figure 4.51. FT-IR spectra of ion exchange resins synthesized (a) P(VbNMDG) and (b) P(ClVBTA).

4.1.5.2. Effect of pH on the sorption of As(V)

Fig. 4.52 shows the effect of pH on arsenate sorption studied with a batch equilibrium procedure. The removal of arsenic increased with increasing amount of resin. For P(ClVBTA) resin, the maximum retention was observed at pH 9 where arsenic is found primarily as $HAsO_4^{2-}$. Strongly basic anion exchange resins with ammonium groups interact better with divalent species of arsenic in the pH range of 8-10. The arsenic removal decreased at pH 6 because $HAsO_4^{2-}$ and $H_2AsO_4^-$ ions exist in the equilibrium. For P(VbNMDG) resin, the maximum retention was observed at pH 3 and pH 6 where arsenic is found primarily as $H_2AsO_4^-$.
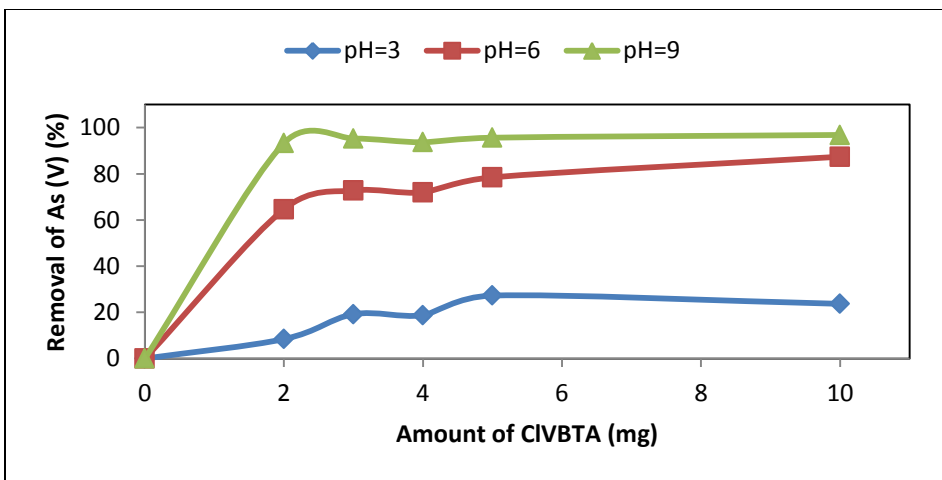
(a)
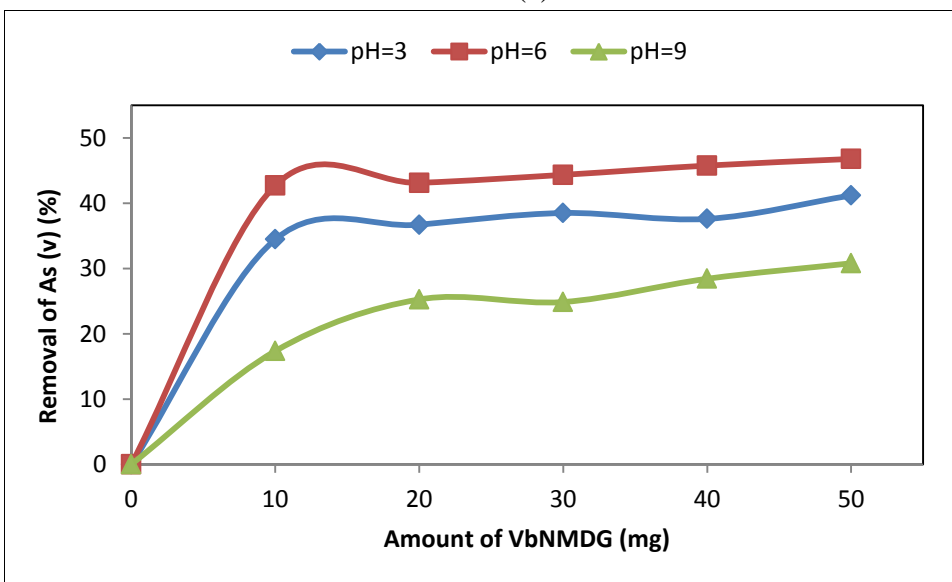
(b)

Figure 4.52. Curves of arsenic removal using (a) ClVBTA (b) VbNMDG resin at pH= 3-9.

Removal of arsenic using P(ClVBTA) resin was obtained higher than using P(VbNMDG) resin because P(ClVBTA) resin was more selective to arsenic. P(ClVBTA) and P(VbNMDG) resins were utilized by mixing at different mole ratios and using solutions different pH values. Figure 4.53 shows removal of As(V) versus different P(VbNMDG):P(ClVBTA) mole ratios.
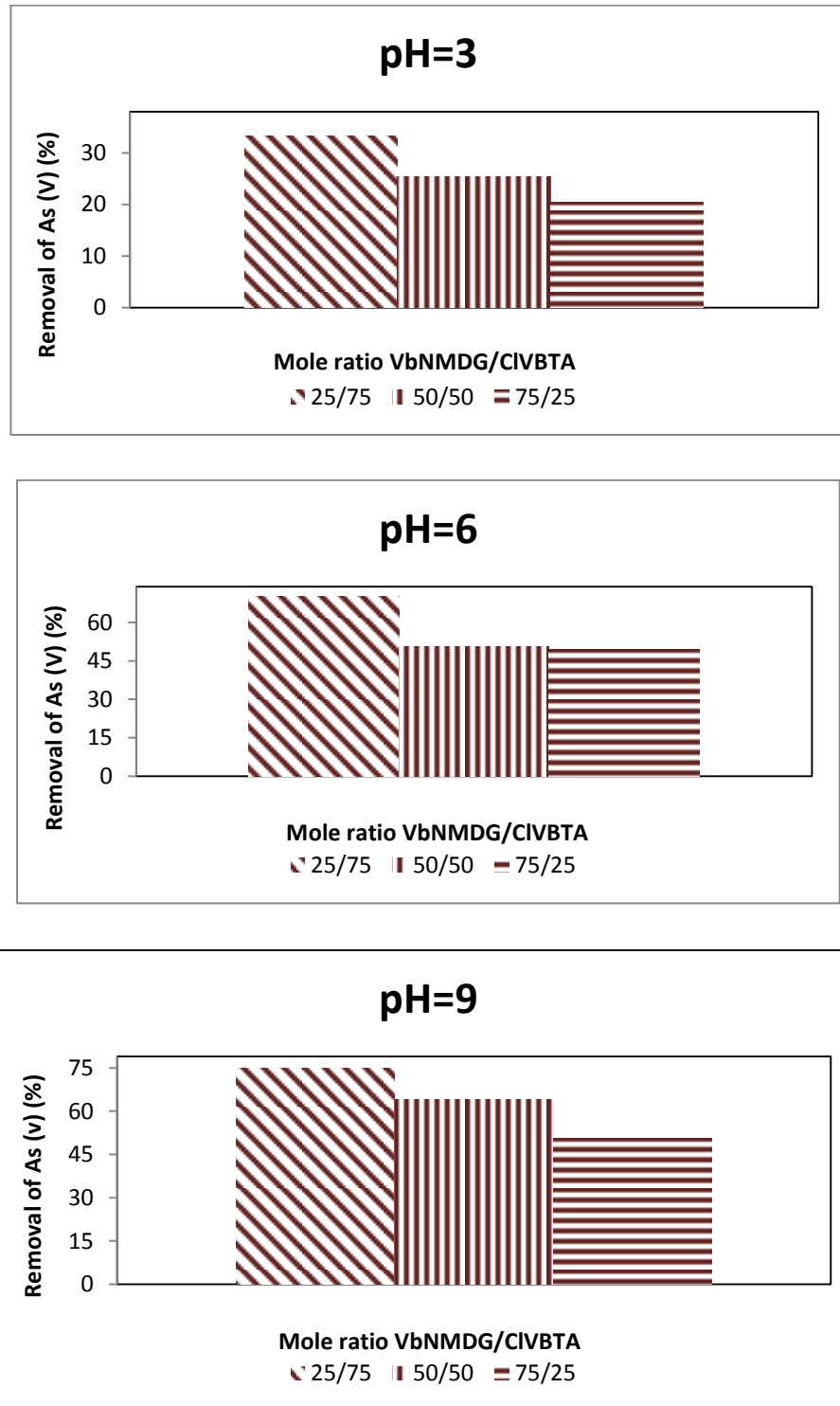
Figure 4.53. Removal of arsenic for different P(VbNMDG):P(ClVBTA) mole ratios such as 25:75, 50:50 and 75:25 at pH= 3-9.

Removal of arsenic of resin at a mole ratio of P(VbNMDG):P(ClVBTA) with 25:75 gave the best results at each pH values.

4.1.5.3. Kinetic tests

The kinetic behavior of resin at a mole ratio of P(VbNMDG):P(ClVBTA) with 25:75 for arsenic removal was investigated with batch-mode sorption tests. Figure 4.54 shows the change of arsenic concentrations as a function of time. After 24 h of contact, for experiments at pH 3, 6 and 9, the percentages of As(V) removal were 37.0%, 66.7%, 67.2%, respectively.
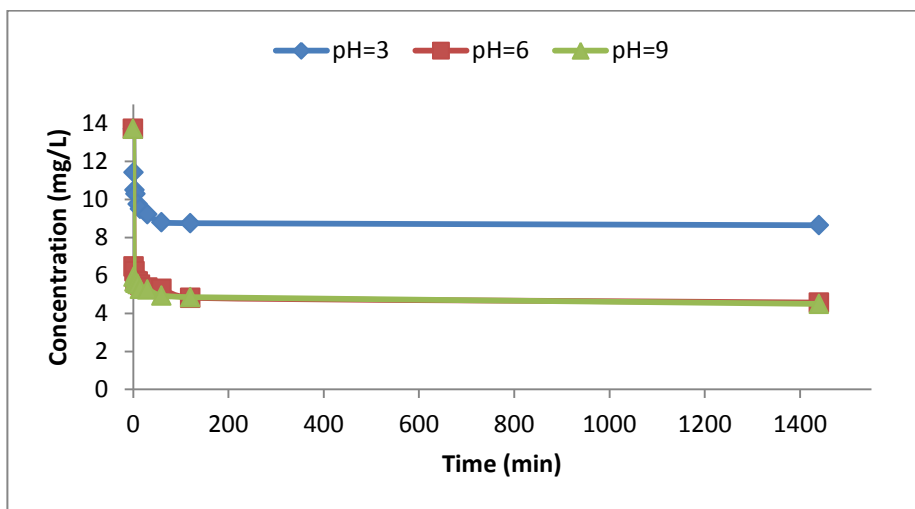
Figure 4.54. Effect of pH on As(V) by a resin mixture of P(VbNMDG):P(ClVBTA) (25:75).

Mathematical modeling

The kinetic studies were evaluated using pseudo-first-order and pseudo-second-order kinetics models using Eqs. 3.2 and 3.5 given in Section 3.1. To obtain the the correlation coefficients, $\log(q_e - q_t)$ versus t and t/q_t where t were plotted for first-order and second-order kinetic models, respecively.

Table 4.8 shows the correlation coefficients (R^2) calculated for resins. The correlation coefficiens of pseudo-second-order kinetics (R^2) are greater than those of pseudo-first-order kinetics for the resin mixture of P(VbNMDG):P(ClVBTA) (25:75).
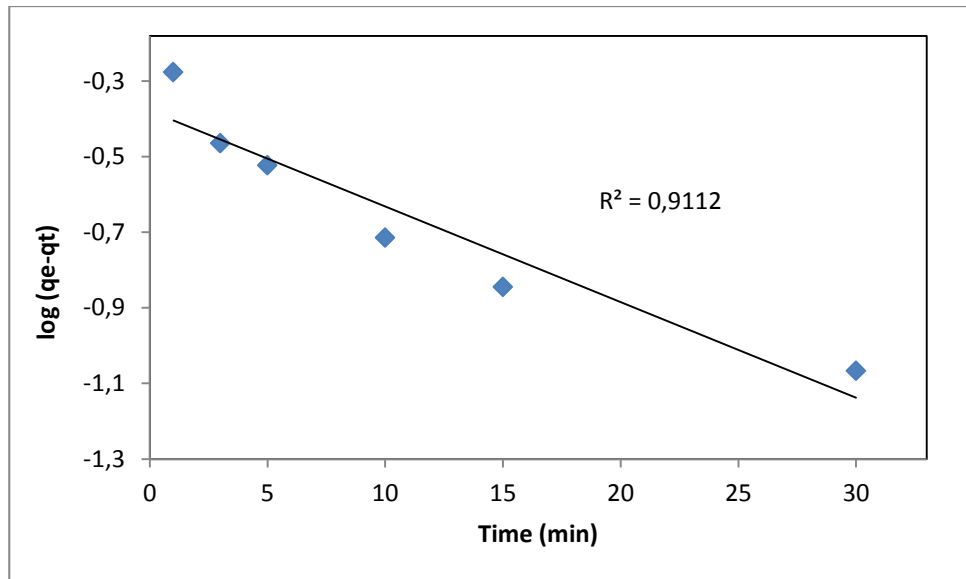
Figure 4.55. Evaluation of kinetic data using pseudo-first-order kinetic model at pH 3.
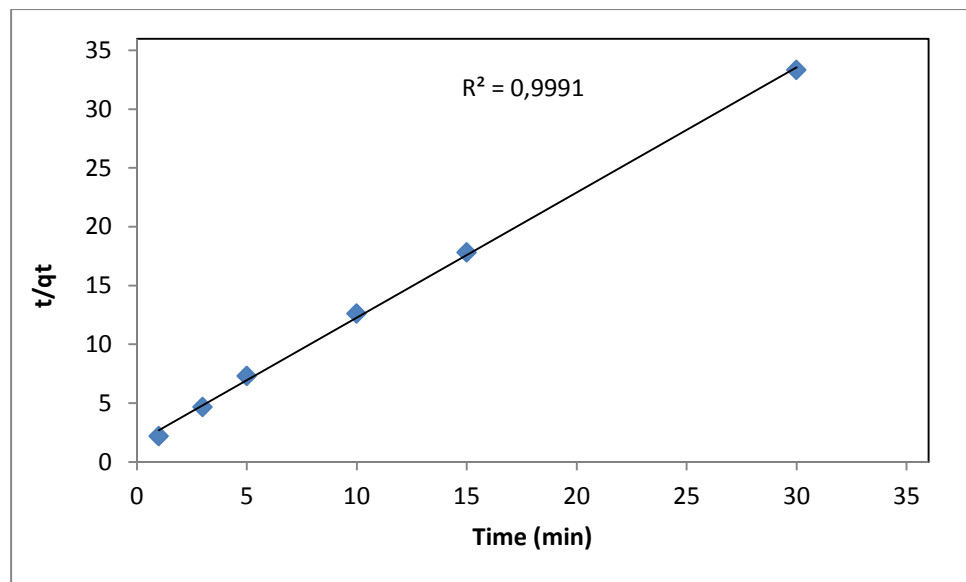
Figure 4.56. Evaluation of kinetic data using pseudo-second-order kinetic model pH 3.
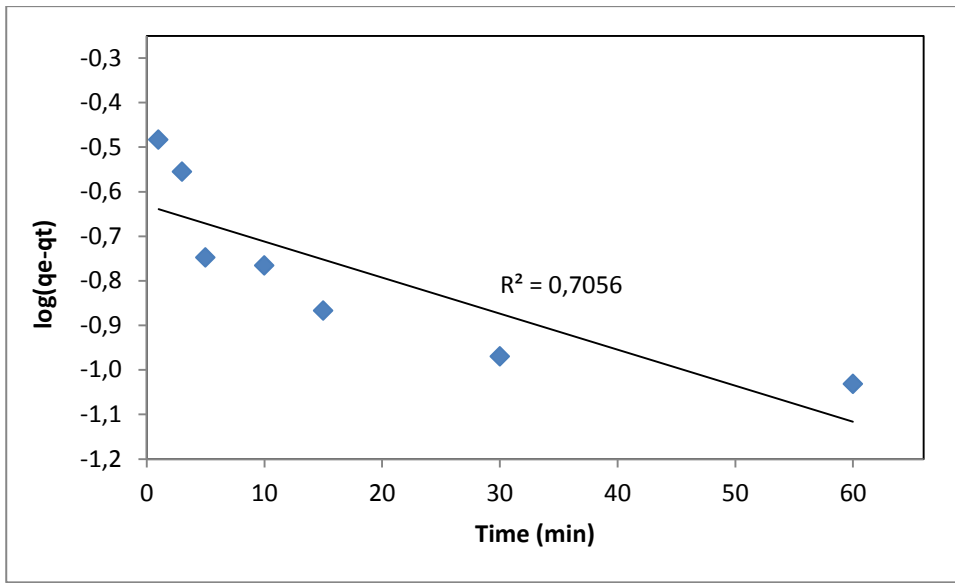
Figure 4.57. Evaluation of kinetic data using pseudo-first-order kinetic model at pH 6.
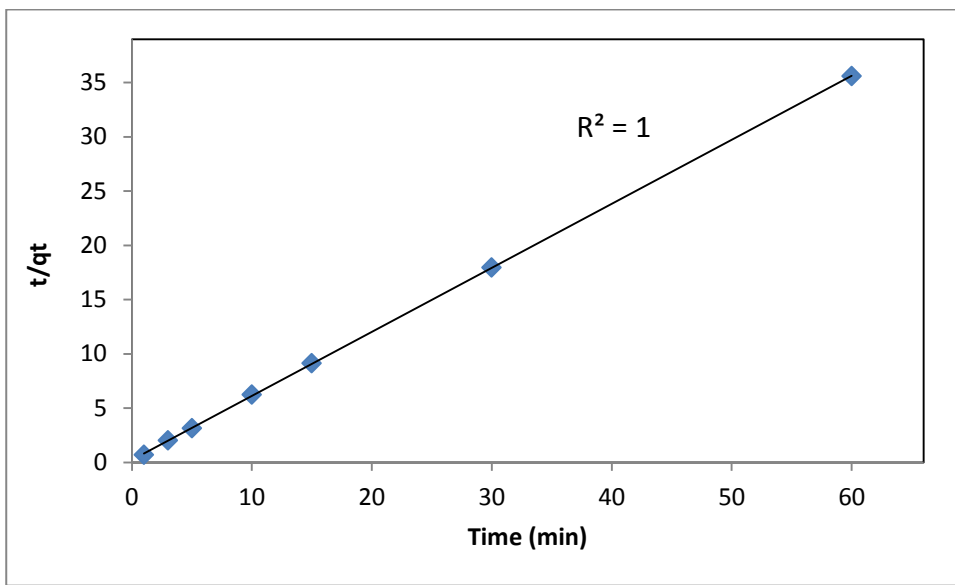
Figure 4.58. Evaluation of kinetic data using pseudo-second-order kinetic model pH 6.
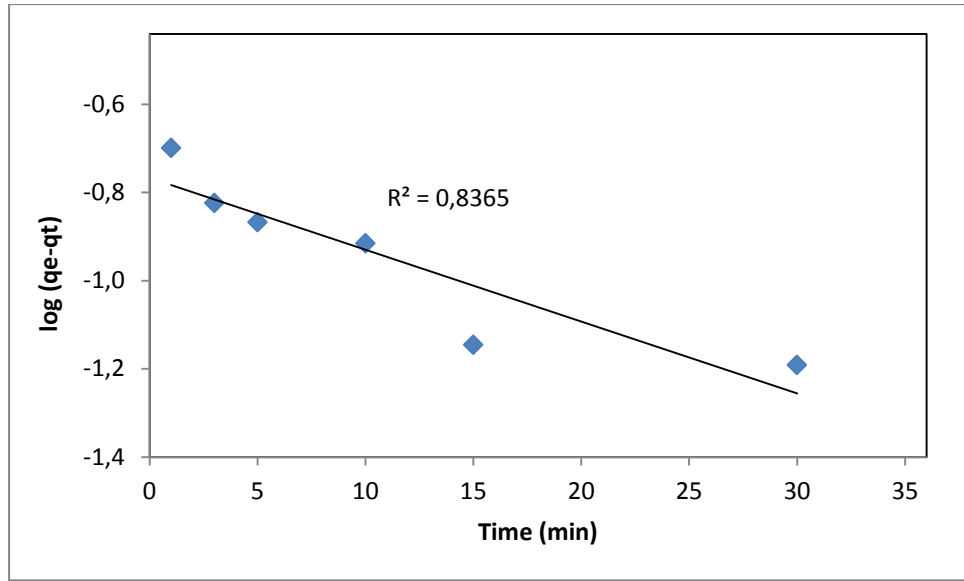
Figure 4.59. Evaluation of kinetic data using pseudo-first-order kinetic model at pH 9.
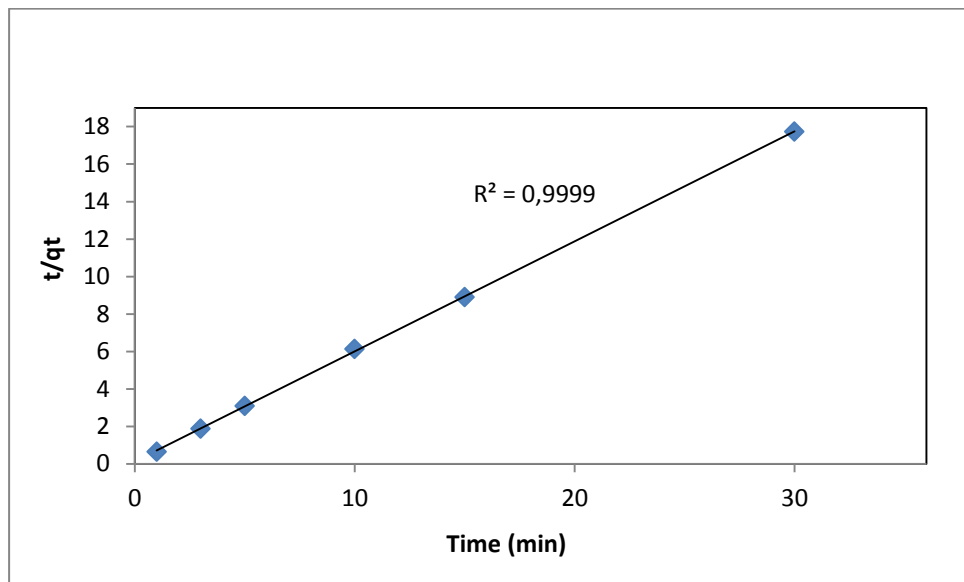
Figure 4.60. Evaluation of kinetic data using pseudo-second-order kinetic model pH 9.

Table 4.8. The correlation coefficients (R^2) for a resin mixture of VbNMDG:ClVBTA (25:75).

pH	R^2	
	Pseudo-first-order	Pseudo-second-order
pH=3	0.9112	**0.9991**
pH=6	0.7056	**1.0000**
pH=9	0.8365	**0.9999**

The kinetic data obtained were also evaluated with diffusional and reaction models resin as explained in Section 3.2. The results were shown in Figures 4.61–4.66.
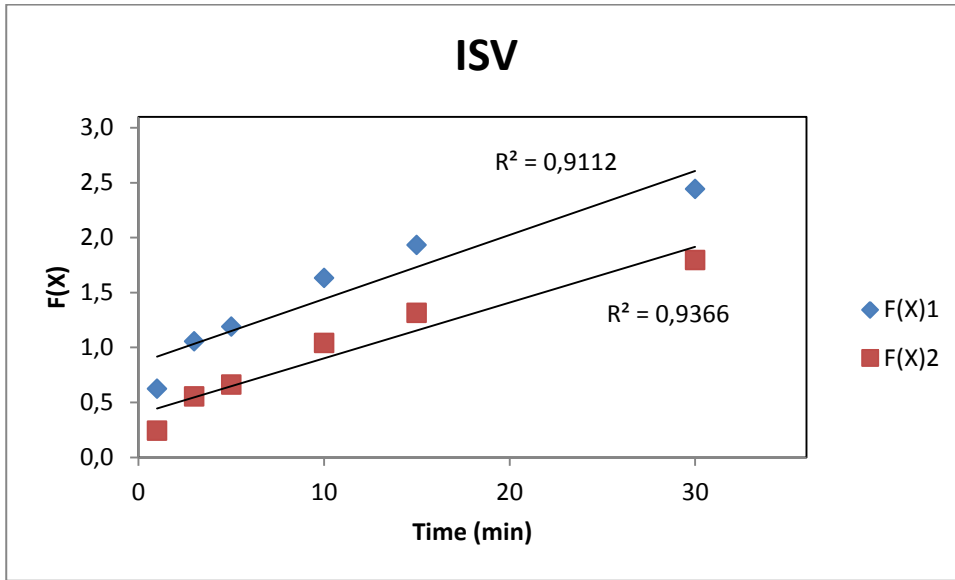
Figure 4.61. Evaluation of kinetic data using infinite solution volume model (ISV) at pH 3.
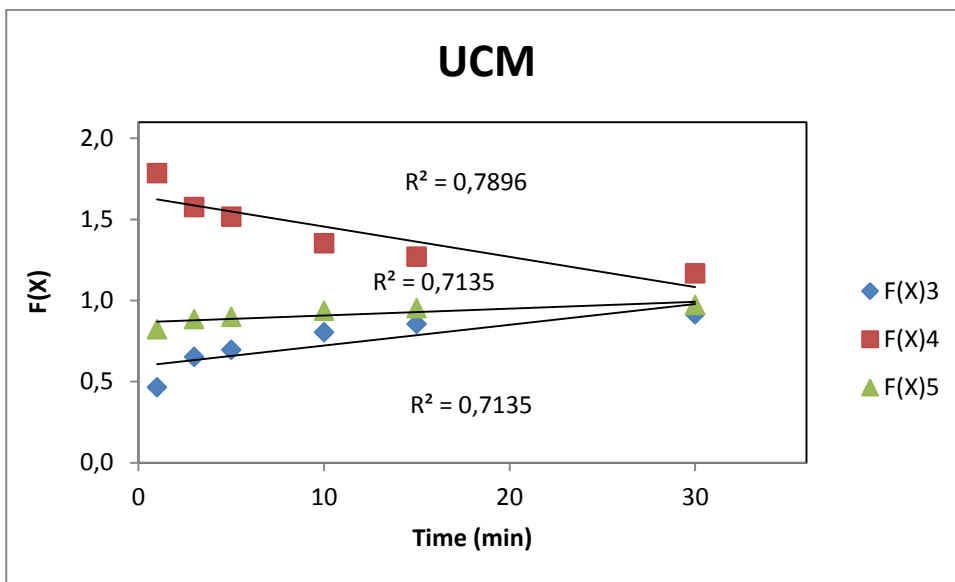
Figure 4.62. Evaluation of kinetic data using unreacted core model (UCM) at pH 3.
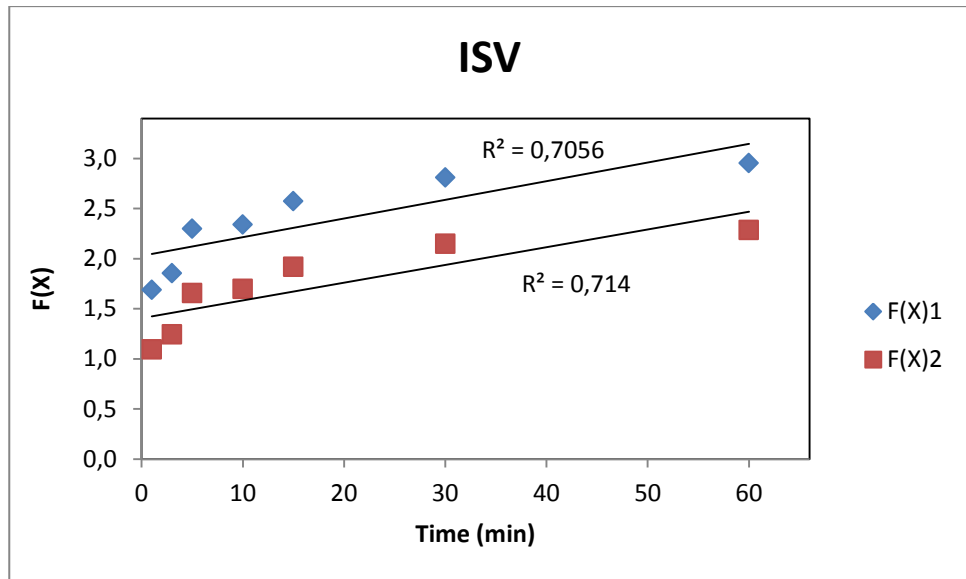
Figure 4.63. Evaluation of kinetic data using infinite solution volume model (ISV) at pH 6.
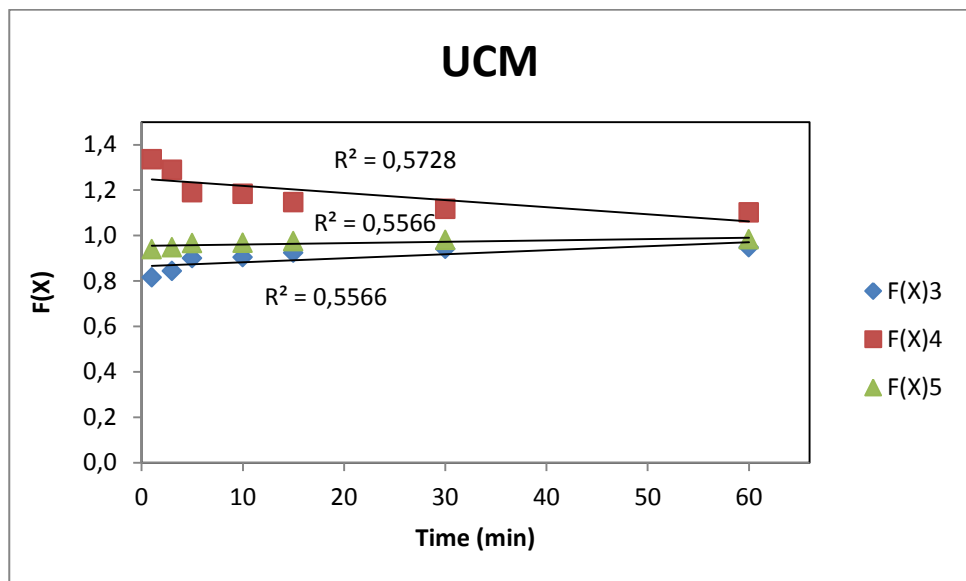
Figure 4.64. Evaluation of kinetic data using unreacted core model (UCM) at pH 6.
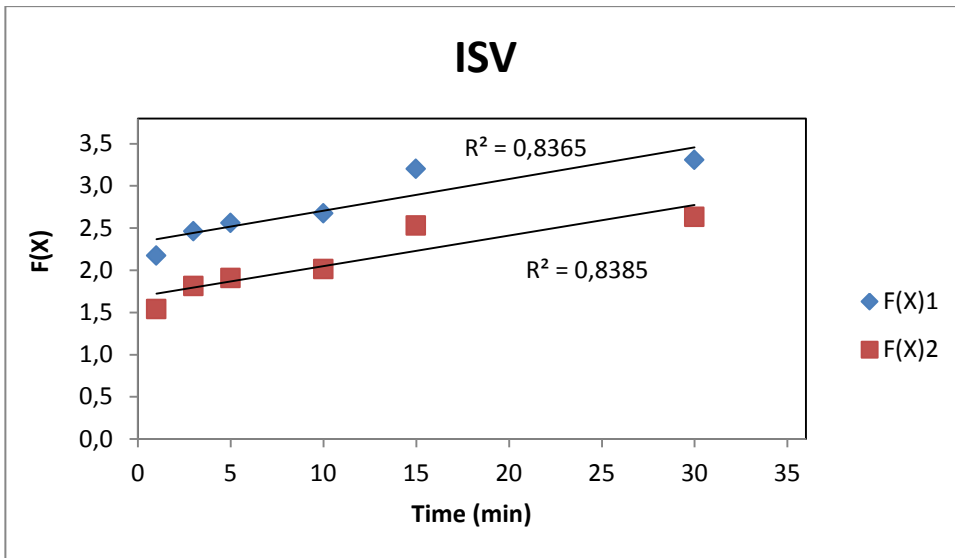
Figure 4.65. Evaluation of kinetic data using infinite solution volume model (ISV) at pH 9.
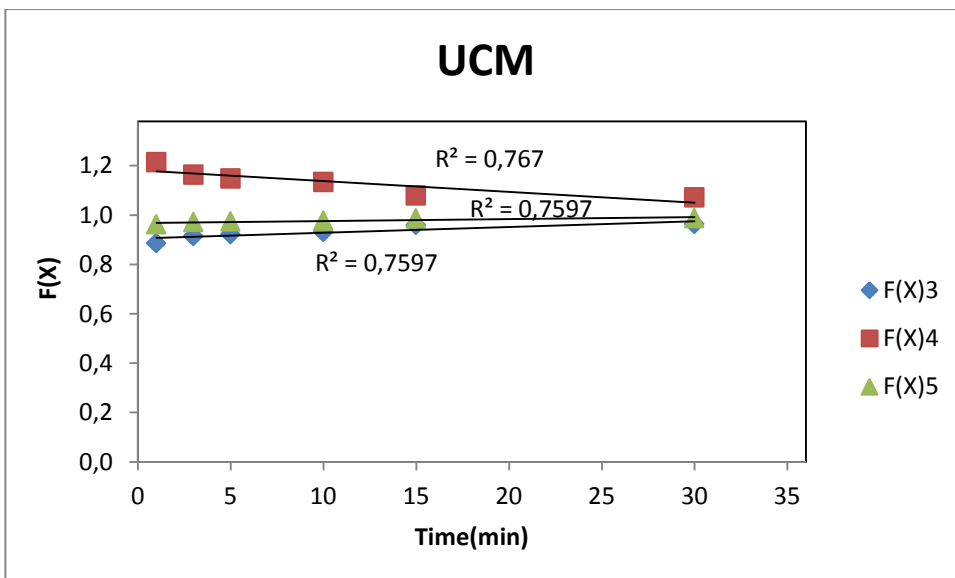
Figure 4.66. Evaluation of kinetic data using unreacted core model (UCM) at pH 9.

The maximum correlation coefficients for the linear models show that the rate is particle diffusion controlled according to ISV models, reacted layer controlled according to UCM models for all pH. Table 4.9 shows the linear correlation coefficients obtained from the plots of F(X) function versus time as shown in (Figures 4.61 – 4.66).

Table 4.9. Linear correlation coefficients for a resin mixture of VbNMDG:ClVBTA (25:75).

pH	R^2				
	ISV		UCM		
	Film diffusion -ln(1-X)	Particle diffusion -ln(1-X^2)	Liquid film X	Reacted layer 3-3(1-X)$^{2/3}$-2X	Chemical reaction 1-(1-X)$^{1/3}$
pH=3	0.9112	**0.9366**	0.7135	**0.7896**	0.7135
pH=6	0.7056	**0.7140**	0.5566	**0.5728**	0.5566
pH=9	0.8365	**0.8385**	0.7597	**0.7670**	0.7597

4.1.5.4. Adsorption Isotherms

The linearized plots of Langmuir and Freundlich isotherms are given in Figures from 4.67 to 4.72. Table 4.10 shows isotherm correlation values (R^2) at different pH values as shown in (Figures 4.67 – 4.72). The experimental data for resin mixture of P(VbNMDG):P(ClVBTA) (25:75) fit well to Freundlich model at each pH.
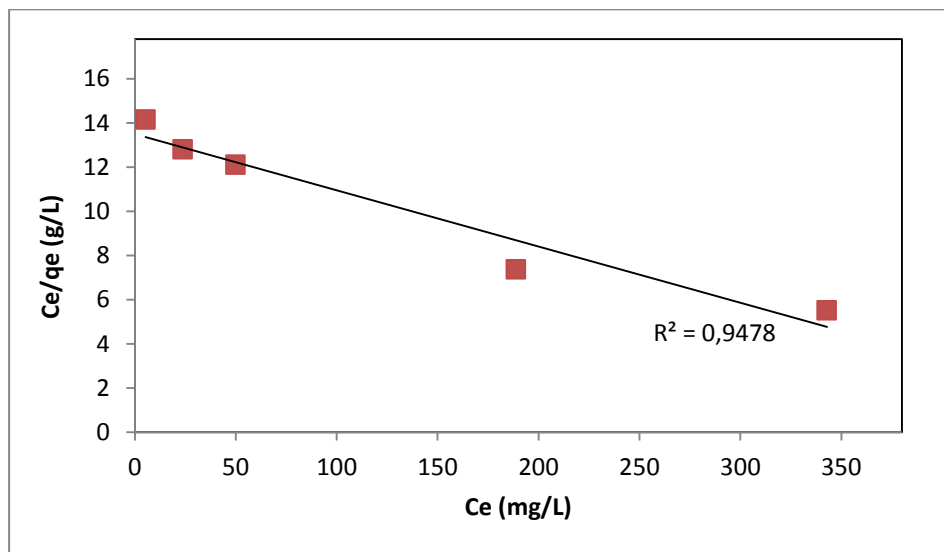
Figure 4.67. Linearized form of Langmuir isotherm at pH 3.
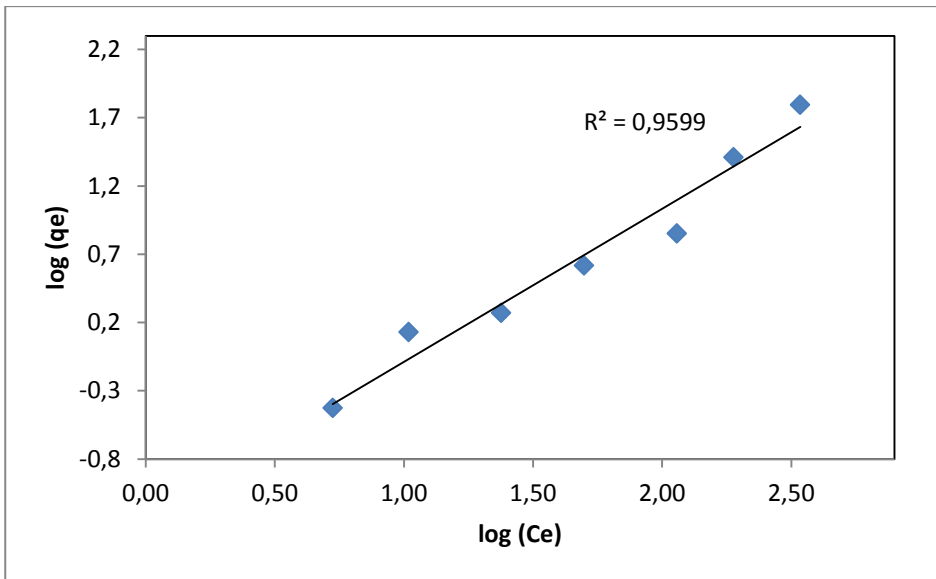
Figure 4.68. Linearized form of Freundlich isotherm at pH 3.
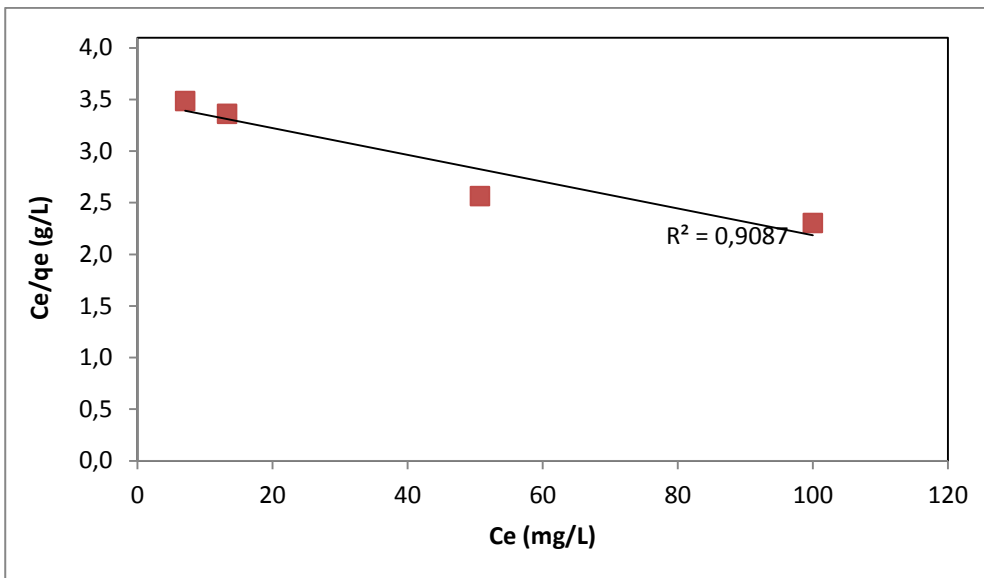
Figure 4.69. Linearized form of Langmuir isotherm at pH 6.
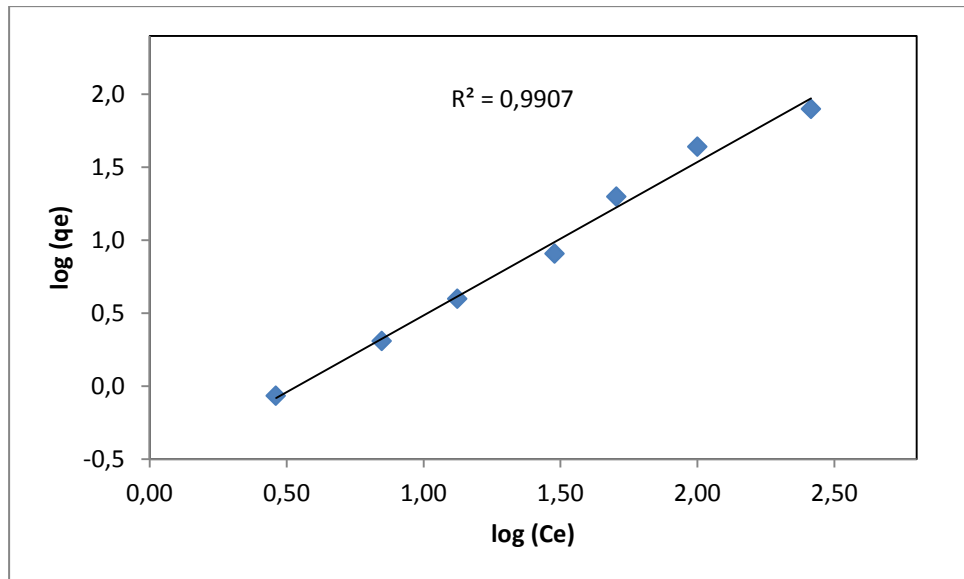
Figure 4.70. Linearized form of Freundlich isotherm at pH 6.
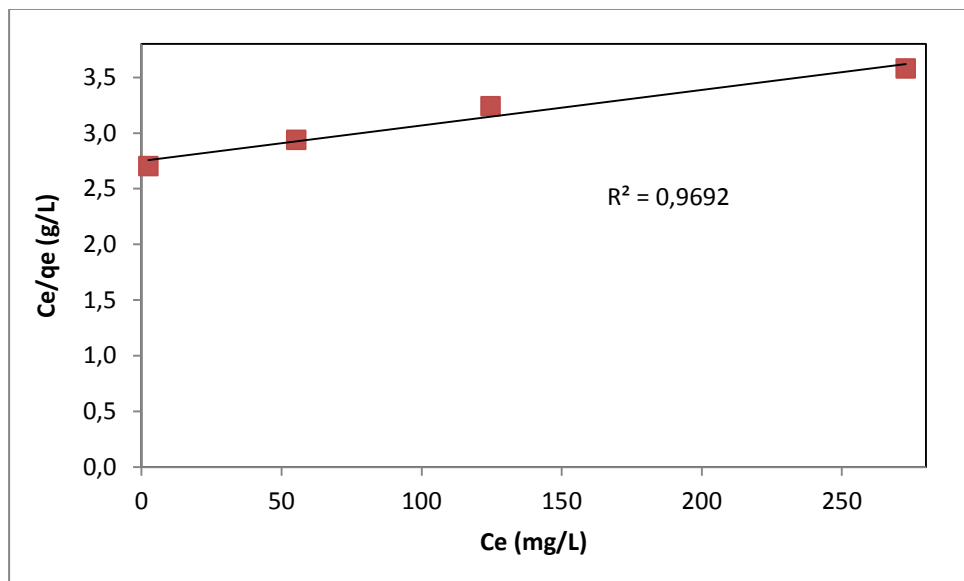
Figure 4.71. Linearized form of Langmuir isotherm at pH 9.
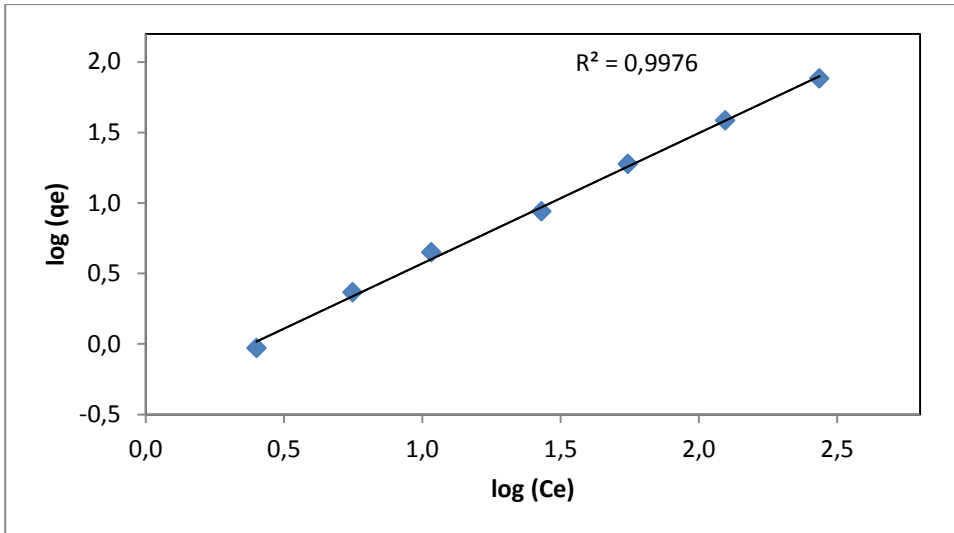
Figure 4.72. Linearized form of Freundlich isotherm at pH 9.

Table 4.10. Isotherm correlation values (R^2) at different pH values.

Adsorption Isotherm	pH=3	pH=6	pH=9
Freundlich	**0.9599**	**0.9907**	**0.9976**
Langmuir	0.9478	0.9087	0.9692

4.1.5.5. Elution studies

After the sorption studies, the elution tests were carried out with a resin mixture of VbNMDG: ClVBTA (25:75). The elution study was performed with 4 M of different acid solutions (HCl, HNO_3 and $HClO_4$). Figure 4.73 shows the elution efficiency of HCl, HNO_3 and $HClO_4$ solutions were 95.96%, 96.09% and 92.33%, respectively.
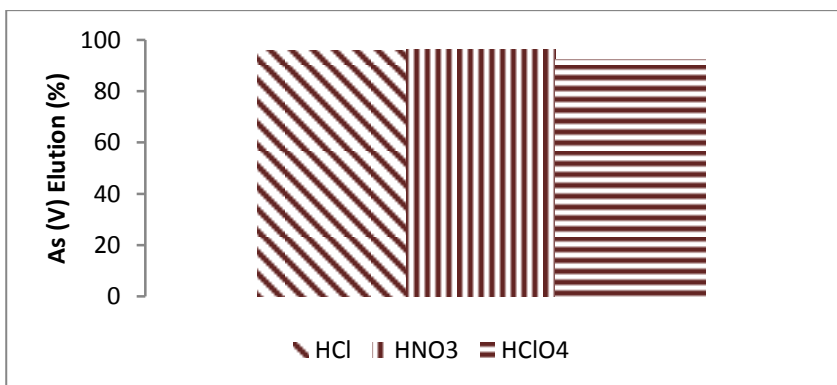
Figure 4.73. Elution profile of arsenic using HCl, HNO_3 and $HClO_4$.

5. CONCLUSIONS

In this thesis, boron removal from geothermal water by using N-methyl-D-glucamine containing Amberlite PWA 10 at a particle size of 0.500-0.710 mm and composite boron selective fiber was investigated. Removal studies were performed using batch and column studies. Also separation of lithium from geothermal water by using (λ-MnO$_2$) adsorbent at ion exchange – membrane filtration hybrid system was studied.

According to the obtained results, removal percentage of boron increased with the increase in adsorbent amount. The results showed that 2.8 g resin/L and 2 g fiber/L solution were found as the optimum adsorbent amounts for removal of boron from geothermal water.

In kinetic tests, the concentration of boron decreased with time and was reduced below 1.0 mg B/L after 180 minutes for Amberlite PWA-10 and after 120 minutes for composite fiber. Fiber adsorbent exhibited a faster kinetic for boron removal than with Amberlite PWA-10 resin.

The batch kinetic data obtained for boron removal were evaluated by using conventional kinetic models. The correlation coefficients of pseudo-first-order kinetics (R^2) are greater than those of pseudo-second-order kinetics for Amberlite PWA 10 and composite fiber. The kinetic data obtained were also evaluated with diffusional and reaction models for Amberlite PWA 10 and composite fiber. The maximum correlation coefficients for the linear models show that the rate is film diffusion controlled according to ISV models and reacted layer controlled according to UCM models for the study done with composite fiber. For Amberlite PWA-10, the rate is particle diffusion controlled according to ISV models and reacted layer controlled according to UCM models for both of the studies done with 2.0 g resin/L and 2.8 g resin/L concentrations, as they have greater linear correlation coefficients.

Cycle studies, were performed to monitor the recycle and sustainability performances of composite fiber and Amberlite PWA-10 resin. In sorption stages during ten cycles, the capacity of sorbed boron for both adsorbents did not change significantly. The elution study was performed with different concentrations of H$_2$SO$_4$ solution. Concentration of H$_2$SO$_4$ that is used to elute boron did not influence adsorption properties both fiber and resin, significantly.

In column-mode tests performed, Amberlite PWA-10 (at a particle size range of 0.355-0.500 mm), Diaion CRB02 (at a particle size range of 0.250-0.355 mm and 0.355-0.500 mm) and boron selective composite fiber were used. The effect of the SV on the column performances for the composite fiber was also studied. Space velocity values of 10, 15 and 25 h^{-1} were tested with composite fiber. In the column-mode study of Amberlite PWA-10, Diaion CRB02 space velocity was adjusted to 15 h^{-1}. All of the elution stages were performed at SV 5 h^{-1} with 5% H_2SO_4 solution.

Amberlite PWA-10 had a breakthrough capacity of 2.04 mg B/mL and a total capacity of 3.52 mg B/mL at SV 15 h^{-1}. The effect of particle size of the resin on the column performances for the Diaion CRB02 was also studied SV 15 h^{-1}. Diaion CRB02 had a breakthrough capacity of 2.46 mg B/mL resin at a particle size range of 0.250-0.355 mm and 2.28 mg B/mL resin at a particle size range of 0.355-0.500 mm. Smaller particles gave better breakthrough profile. The effect of eluting agent concentration on the elution performance of boron from Diaion CRB02 (at a particle size range of 0.355-0.500 mm) was also studied. Boron loaded onto the resin Diaion CRB02 was eluted with 1.0 M and 0.5 M H_2SO_4 solution.

The breakthrough capacities of fiber adsorbent were calculated as 1.35, 1.53 and 2.31 mg B/mL at SV 10, 15 and 25 h^{-1}, respectively. It seems that breakthrough capacity of fiber adsorbent increased with an increase in SV. When the comparison was made considering the column utilization for fiber adsorbent, values calculated were 35%, 44% and 52% at SV 10, 15 and 25 h^{-1}, respectively.

Boron removal from RO permeate of geothermal water was investigated using EDI method. For this, ion exchange resins (Purolite CT175 and Purolite A500) in layered bed configuration were employed. At the end of 3 h, boron concentration was reduced below 0.69 mg B/L and 1.42 mg B/L for the experiments performed by using Amberlite PWA-10 and Purolite CT175/ Purolite A500, respectively.

When ion exchange resins Purolite CT175/ Purolite A500 were employed, the measured boron concentrations after 180 minutes were 0.96 mg/L and 1.42 mg/L for the experiments performed by using model solution (containing 5.0 mg B/L) and RO permeate of geothermal water, respectively.

Hybrid studies were performed to determine the effect of particle size of λ-MnO₂ on lithium separation from geothermal water. With 2 g/L of granulated adsorbent concentration, it was possible to separate all lithium from geothermal water in 40 minutes. On the other hand, with 3 g/L of powder adsorbent concentration, it was possible to separate 93.5% of lithium from geothermal water in 240 min.

The removal of arsenic from aqueous solution was also investigated by ion exchange resins P(VbNMDG) and P(ClVBTA) that were synthesized at University of Concepcion. Effect of pH on the arsenic removal from aqueous solution was investigated for P(VbNMDG) and P(ClVBTA). The highest removal of arsenic was observed at pH 9 and at pH 3-6 for P(ClVBTA) and P(VbNMDG), respectively. The effect of pH on As(V) sorption was studied with different P(VbNMDG):P(ClVBTA) mole ratios such as 25:75, 50:50 and 75:25. The removal of arsenic increased with increasing pH using molar ratio of P(VbNMDG):P(ClVBTA) is 25:75.

The batch kinetic data obtained for As(V) removal was evaluated by using conventional kinetic models. The correlation coefficients of pseudo-second-order kinetics (R^2) are greater than that of pseudo-first-order kinetics for P(VbNMDG):P(ClVBTA) (25:75). The kinetic data obtained were also evaluated with diffusional and reactional models for P(VbNMDG):P(ClVBTA) (25:75). The maximum correlation coefficients for the linear models show that the rate is particle diffusion controlled according to ISV models and reacted layer controlled according to UCM models at all pH.

Equilibrium data were obtained for arsenate sorption onto resin. The equilibrium data were evaluated using Langmuir and Freundlich adsorption isotherm models. The experimental data for resin mixture of P(VbNMDG):P(ClVBTA) (25:75) fit well to Freundlich model at all pH.

The elution tests were also carried out for ion exchange resin mixture. The results show that the elution efficiency of HCl, HNO₃ and HClO₄ solutions of 4 M were 96%, 96 % and 92%, respectively.

REFERENCES

Abe, M. and Chitrakar, R., 1987, Recovery of lithium from seawater and hydrothermal water by titanium (IV) antimonate cation exchanger, *Hydrometallurgy*, 19: 117-128pp.

Aral, H., 2007, Lithium and sulphate in the waste streams of Sons of Gwalia's Greenbushes Operations—Part2. Unpublished CSIRO Minerals Report, DMR-3248,43pp.

Aredes, S., Klein, B. and Pawlik, M., 2013, The removal of arsenic from water using natural ironoxide minerals, *Journal of Cleaner Production,* 60:71-76pp.

Ayers, P., Dudeney, W. L. and Kahraman, A., 1981, Solvent extraction of boron with 2-ethyl-1,3-hexanediol and 2-chloro-4-(1,1,3,3-tetra methyl butyl)-6-methylol phenol, *Journal of Nuclear Chemistry*, 43:2097-2100pp.

Badruk, M., Kabay, N., Demircioglu, M., Mordogan, H. and Ipekoglu, U., 1999, Removal of boron from wastewater of geothermal power plant by selective ion-exchange resins. I. Batch sorption-elution studies, *Separation Science Technology*, 34 (13):2553-2569pp.

Banasiak, L.J. and Schafer, A.I., 2009, Removal of boron fluoride and nitrate by electrodialysis in the presence of organic matter, *Journal of Membrane Science,* 334:101-109pp.

Bicak, N., Bulutcu, N., Senkal, B.F. and Gazi, M., 2001, Modification of cross linked glycidyl methacrylate-based polymers for boron-spefic column extraction, *Reactive and Functional Polymer,* 47: 175-184pp.

Bicak, N., Gazi, M. and Bulutcu, N., 2003, N,N-bis(2,3-dihydroxypropyl) octadecylamine for liquid-liquid extraction of boric acid, *Separation Science and Technology*, 38:165-173pp.

Bicak, N., Gazi, M. and Senkal, B.F., 2005, Polymer suorted aminobis-(cis-propan 2,3 diol) functions for removal of trace boron from water, *Reaction and Function Polymer, 65*:143-148pp.

REFERENCES (continued)

Bicak, N., Ozbelge, O., Yilmaz, L. and Senkal, B.F., 2000, Cross linked polymer gels for boron extraction derived from N-glucidol-N-methyl-2-hydroxy propyl methacrylate, *Macromolecules Chemistry and Physics*, 201:577-584pp.

Bick, A. and Oron, G., 2005, Post-treatment design of seawater reverse osmosis plants boron removal technology selection for potable water production and environmental control, *Desalination*, 178:233-246pp.

Bissen, M. and Frimmel, F.H., 2003a, Arsenic - a review, Part I, Occurance, toxicity, speciation, mobility, *Acta Hydrochemistry Hydrobiology,* 31(2): 9–18pp.

Bissen, M. and Frimmel, F.H., 2003b, Arsenic - a review, PartII: oxidation of arsenic and its removal in water treatment, *Acta Hydrochimica Hydrobiologica,* 31: 97-107pp.

Bodek, I., Lyman, W.J., Reehl, W.F. and Rosenblatt, D.H., 1998, *Environmental Inorganic Chemistry: Properties, Processes and Estimation Methods*, Pergamon Press, USA.

Borgono, J.M. and Greiber, R., 1971, Epidemiological study of arsenicism in the city of Autofagasta, *Trace Substances Environmental Health* 5: 13–24pp.

Bouhabila, E.H., Ben Aim R. and H. Buisson, 1998, Microfiltration of activated sludge using submerged membrane with air bubbling (alication to waste-water treatment), *Desalination,* 118: 315–322pp.

Brodd, R., 2002, Comments on the history of lithium-ion batteries.

Brown, P.H. and Hu, H., 1997, Does boron play only a structural role in the growing tissues of higher plants, *Plant Soil,* 196: 211-215pp.

Burkel, R.S. and R.C.Stoll, 1999, Naturally occurring arsenic in sand stone aquifer water suly wells of North Eastern Wisconsin, *Ground Water Monitoring Remediation,* 19: 114–121pp.

REFERENCES (continued)

Cebrian, M.E., Albores, A., Aguilar, M. and Blakely, E., 1983, Chronic arsenic poisoning in the North of Mexico, *Human Toxicology,* 2: 121–133pp.

Chakraborti, D., Rahman, M.M., Das, B., Murrill, M., Dey, S., Mukherjee, S.C., Dhar, R.K., Biswas, B.K., Chowdhury, U.K. and Ro S., 2010, Status of ground water arsenic contamination in Bangladesh: A 1 year study report, *Water Resources*, 44: 5789-5802pp.

Chitrakar, R., Kanoh, H., Miyai, Y. and Kenta Ooi, K., 2001, Recovery of lithium from seawater using manganese oxide adsorbent ($H_{1.6}Mn_{1.6}O_4$) derived from $Li_{1.6}Mn_{1.6}O_4$, *Ind. Eng. Chem. Res.,* 40:2054-2058pp.

Clifford, D., 1999, Ion exchange and inorganic adsorption, In: Letterman, A.(Ed.), Water Quality and Treatment, AWWA, McGraw Hill, NewYork (Chapter 9).

Dambies, L., Vincent, T. and Guibal, E., 2002, Treatment of arsenic-containing solutions using chitosan derivatives: uptake mechanism and sorption performance, *Water Research,* 36: 3699-3710pp.

Daus Wennrich, R. and Weiss, H., 2004, Sorption materials for arsenic removal from water: a comparative study, *Water Resources,* 38: 2948–2954pp.

Deliyanni, E. A., Bakoyannakis, D. N., Zouboulis, A.I. and K.A. Matis, 2003, Sorption of As(V) ions by akaganeite-type nanocrystals, *Chemosphere,* 50: 155–163pp.

Deliyanni, E.A., Bakoyannakis, D.N., Zouboulis, A.I., Matis, K.A. and Nalbandian, L., 2000, Akaganeite-type FeO(OH) nanocrystals: preparation and characterization, *Microporous and Mesoporous Materials,* 42: 49–57pp.

Dhar, R., Biswas, B., Samanta, G., Mandal, B., Chakraborti, D., Roy, S., Jafar, A., Islam, A., Ara, G., Kabir, S., Wadud Khan, A., Akther Ahmed, S. and Abdul Hadi, S., 1997, Ground water arsenic calamity in Bangladesh, *Curriculum Science,* 73: 4859-4866pp.

REFERENCES (continued)

Dhar, R.K., Biswas, B.K. and Samanta, G., 1997, Ground water arsenic calamity in Bangladesh, *Curriculum of Science,* 73: 48–59pp.

Dominguez, L., Economy J., Benak, K. and Mangun, C. L., 2003, Anion exchange fibers for arsenate removal derived from a vinylbenzyl chloride precursor, *Polymer Advantage Technology,* 14: 632–637pp.

Edzwald, J.K. and Haarhoff, J., 2011, Sea water pretreatment for reverse osmosis: chemistry, contaminants, and coagulation, *Water Research,* 45: 5428-5440pp.

Eguez, H.E. and Cho, E.H., 1987, Adsorption of arsenic on activated charcoal, *Journal of Metallurgical Study and Research,* 39: 38–41pp.

Erdöl Aydın, N., 2013, Boron removal by means precipitation process with magnesium hydroxide, *Advanced Materials Research,* 699: 262-267pp.

Ergican, E., Gecol, H. and Fuchs, A., 2005, The effect of co-occurring inorganic solutes on the removal of arsenic (V) from water using cationic surfactant micelles and an ultraltration membrane, *Desalination,* 181: 9-14pp.

Farahbakhsh, K., Svrcek, C., Guest, R.K. and Smith, D.W., 2004, A review of the impact of chemical pretreatment on low-pressure water treatment membranes, *Journal of Environmental Engineering Science,* 3: 237-253pp.

Feenstra, L., van Erkel, J. and Vasak,L., 2007, Arsenic in ground water: Overview and evaluation of removal methods, *Utrecht: International Groundwater Resources Assessment Centre*, 2-23pp.

Ficklin, W.H., 1983, Separation of arsenic(III) and arsenic (V) in ground waters by ion- exchange, *Talanta,* 30: 371–373pp.

Fortuny, A., Coll, M.T. and Sastre, A.M., 2012, Use of methyltrioctyl/decylammonium bis 2,4,4 (trimethylpentyl) phosphinate ionic liquid (ALiCY IL) on the boron extraction in chloride media, *Separation and Purification Technology,* 97: 137-141pp.

REFERENCES (continued)

Glueckstern, P. and Priel, M., 2003, Optimization of boron removal in old and new SWRO systems, *Desalination,* 156: 219-228pp.

Guo, C., Zhang, F. and Yang, X., 2000, Treatment of As-containing wastewater by lime-polyferric sulfate coagulating process, *Gongye Shuichuli,* 20: 27–29pp.

Habashi, F., 1997, Handbook of Extractive Metallurgy, vol.4. Wiley-VCH, NewYork.

Han, B., Runnells, T., Zimbron, J. and Wickramasinghe R., 2002, Arsenic removal from drinking water by flocculation and microfiltration, *Desalination*, 145: 293–298pp.

Hering, J.G., Chen, P.Y., Wilkie, J.A., Elimelech, M. And Liang, S., 1996, Arsenic removal by ferric chloride, *Journal of AWWA,* 88: 155–167pp.

Hijazi A. A., Dembitsky M. V. and Morris S., 2005, Contemporary Aspects of Boron: *Chemistry and Biological Aplications.*

Hilal, N., Kim, G.J. and Samereld, C., 2011, Boron removal from saline water: a comprehensive review, *Desalination,* 272: 23-35pp.

Hosgoren, H., Tural, S., Kahraman, F., Togrul, M. and Karakaplan, M., 1997, Solvent extraction of boron with 1,2-Dihydroxy-4-Oxadodecane (Dud) in D-Amyl alcohol, *Solvent Extraction and Ion Exchange,* 15(2): 249-257pp.

Huang, C.P. and Fu, P.L.K, 1984, Treatment of arsenic (V) containing water by the activated carbon process, *Journal of Water Pollution Control Federation,* 56: 233–242pp.

Hwang, B.J., Santhanam, R., Huang, C.P., Tsai, Y.W. and Lee, J.F., 2002, $LiMn_2O_4$ core surrounded by $LiCo_xMn_{2-x}O_4$ shell material for rechargeable lithium batteries, *Journal of Electrochemical Society,* 149: 694-698pp.

Iesan, C., Bapat, S.S. , Fries, B., Coman, D. and Florea, D., 2004, Arsenic removal from drinking water by ion exchange resins, *Environmental Engineering and Management Journal,* 3: 283-291pp.

REFERENCES (continued)

Itakuta, T., Sasai, R. and Itoh, H., 2005, Precipitation recovery of boron from wastewater by hydrotermal mineralization, *Water Research,* 39: 2543-2548pp.

Jain, C.K. and Ali, I., 2000, Arsenic: occurrence, toxicity and speciation techniques, *Water Resources,* 34: 4304–4312pp.

Jay Murray, F. 1995, A human health risk assessment of boron (boric acid and borax) in drinking water, *Regulatory Toxicology and Pharmacology,* 22: 221-230pp.

Johnston, R. And Heijnen, H., 2001, Safe water technology for arsenic removal, In technologies for arsenic removal from drinking water, *Technologies for Arsenic Removal from Drinking Water*, 7-12pp.

Kabata-Pendias, A. and Pendias, H., 2000, *Trace Elements in Soils and Plants*, CRC Press, Boca Raton, FL.

Kabay, N., Arar, O., Acara, F., Ghazal, A., Yuksel, U. and Yuksel, M., 2008, Removal of boron from water by electrodialysis: effect of feed characteristics and interferingions, *Desalination,* 223: 63-72pp.

Kabay, N., Güler, E. and Bryjak, M., 2010, Boron in seawater and methods for its separation — A review, *Desalination,* 261: 212-217pp.

Kabay, N., Yılmaz, I., Yamac, S., Samatya, S., Yuksel, M., Yuksel, U., Arda, M., Sağlam, M., Iwanaga, T. and Hirowatari, K., 2004, Removal and recovery of boron from geothermal wastewater by selective ion exchange resins. I. Laboratory tests, *Reactive & Functional Polymers,* 60: 163-170pp.

Kabay, N., Yilmaz I., Yamac, S., Yuksel, M., Yuksel, U., Yildirim, N., Aydogdu, O., Iwanaga, T. and Hirowatari, K., 2004a, Removal and recovery of boron from geothermal wastewater by selective ion-exchange resins - II. Field tests, *Desalination,* 167:427-438pp.

REFERENCES (continued)

Kabay, N., Yilmaz, I., Bryjak, M. and Yuksel, M., 2006, Removal of boron from aqueous solutions by hybrid ion exchange-membrane process, *Desalination,* 198: 158-165pp.

Kabay, N., Yilmaz-Ipek, I., Soroko, I., Makowski, M., Kirmizisakal, O., Yag, S., Bryjak, M. and Yuksel, M., 2009, Removal of boron from Balcova geothermal water by ion-exchange-microfiltration hybrid process, *Desalination,* 241:167-173pp.

Kang, M., Kawasaki, M., Tamada, S., Kamei, T. and Magara, Y., 2000, Effect of pH on the removal of arsenic and antimony using reverse osmosis membranes, *Desalination,* 131: 293–298pp.

Karcher, S., Caceres, L., Jekel, M. and Contreras, R., 1999, Arsenic removal from water sulies in northern Chile using ferric chloride coagulation, *Journal of Chartered Institute Water Environmental Management,* 13:164–169pp.

Karim, M.M., 2000, Arsenic in ground water and health problems in Bangladesh, *Water Resources,* 34: 304–310pp.

Kartinen, E. and Christopher, M., 1995, An overview of arsenic removal processes, *Desalination,* 103: 79-85pp.

Koltuniewicz A.B., Anna Witek, A. and Bezak K., 2004, Efficiency of membrane-sorption integrated processes, *Journal of Membrane Science,* 239: 129–141pp.

Koltuniewicz, A.B. and Bezak, K., 2000, Membrane bio- sorber: the new integrated system with biosorption and ultrafiltration, *Euromembrane*, Jerusalem, Israel, 27–30pp.

Koltuniewicz, A.B. and Bezak, K., 2001a, Biosorption of cadmium, lead and copper ions-comparison between whole and disrupted cells of Saccharomyces cere- visiae, *Chem. Agriculture,* 2: 164–170pp.

REFERENCES (continued)

Koltuniewicz, A.B. and Bezak, K., 2001b, Removal of metal ions from contaminated waters by means of integrated system with biosorption and ultrafiltration, *American Water Works Association*, San Antonio, TX.

Korngold, E., Belayev, N. and Aronov L., 2001, Removal of arsenic from drinking water by anion exchangers, *Desalination,* 141: 81-84pp.

Koseoglu, H., Kabay, N., Yüksel, M., Sarp, S., Arar, Ö. and Kitis, M., 2008, Boron removal from seawater using high rejection SWRO membranes- impact of pH, feed concentration, pressure, and cross-flow velocity, *Desalination,* 227: 253–263pp.

Kundu, S. and Gupta, A.K., 2005, Analysis and modeling of fixed bed column operations on As(V) removal by adsorption onto iron oxide-coated cement (IOCC)*, Journal of Colloidal Interface Science,* 290: 52-60pp.

Lakshmanan, D., Clifford, D. and Samanta, G., 2008, Arsenic removal by coagulation with aluminum, iron, titanium, and zirconium, *Journal of American Water Works Association,* 100: 76-88pp.

Lee, J.H., Hong, J.K., Jang, D.H., Sun, Y.K. and Oh, S.M., 2000, Degradation mechanisms in doped spinels of $LiM_{0.05}Mn_{1.95}O_4$ (M = Li, B, Al, Co, and Ni) for Li secondary batteries, *Journal of Power Sources,* 89: 7-14pp.

Li, X., Liu, R., Wu, S., Liu, J., Cai, S. and Chen, D., 2011, Efficient removal of boron acid by N-methyl-D-glucamine functionalized silica-polyallylamine composites and its adsorption mechanism, *Journal Colloid Interface Science,* 361: 232-237pp.

Li-Wen Ma, Bai-Zhen Chen, Ya Chen and Xi-Chang Shi, 2011, Preparation, characterization and adsorptive properties of foam-type lithium adsorbent, *Microporous and Mesoporous Materials,* 142: 147−153pp.

REFERENCES (continued)

Loizou, E., Kanari, P.N., Kyriacou, G. and Aletrari, M., 2010, Boron determination in the multi element national water monitoring program: the absence of legal limits, *Journal of Consumer Protection and Food Safety,* 5: 459-463pp.

Mackenzie, E.T., Lamtzy, R.J. and Petorson, V., 1979, Global trace metals cycles and predictions, *Journal of International Associated Mathematical Geology,* 6: 99–142pp.

Maji, S. K., Pal, A. and Pal, T., 2008, Arsenic removal from real-life ground water by adsorption on laterite soil, *Journal of Hazardous Materials,* 151: 811–820pp.

Maji, S.K., Pal, A. and Pal T., 2007, Sorption kinetics of arsenic on laterite soil in aqueous medium, *Journal of Environmental Science Health*, 42: 989-996pp.

Maji, S.K., Pal, A., Pal, T. and Adak, A., 2007, Modeling and fixed bed column adsorption of As(III) on laterite soil, *Separation and Purification Technology,* 56: 284-290pp.

Mandal, B.K. and Suzuki K.T., 2002, Arsenic round the world: a review, *Talanta,* 58: 201–235pp.

Manju, G.N., Raji, C. and Anirudhan, T.S., 1998, Evaluation of coconut husk carbon for the removal of arsenic from water*, Water Resources*, 32: 3062-3070pp.

Marston, C., Busch, M. and Prabhakaren S., 2005, A boron selective resin for sea water desalination in: *Proceedings of European Desalination Society Conference on Desalination and the Environment*, Santa Margerita Ligure, Italy.

Matschullat, J., 2000, Arsenic in the geosphere - a review, *Science Total Environment,* 249 (1–3): 297–312pp.

REFERENCES (continued)

Matsumoto, M., Kondo, K., Hirata, M., Kokubu, S., Hano, T. and Takada, T., 1997, Recovery of boric acid from wastewater by solvent extraction, *Separation Science and Technology,* 32(5): 983-991pp.

Melnik, L., Goncharuk, V., Butnyk, I. and Tsapiuk, E., 2007, Development of the sorption membrane gren technology for boron removal from natural and wastewaters, *Desalination,* 205: 206-213pp.

Melnik, L., Goncharuk, V., Butnyk, I. and Tsapiuk, E., 2005, Boron removal from natural and wastewater susing combined sorption/membrane process, *Desalination,* 185: 147-157pp.

Melnik, L., Vysotskaja, O. and Kornilovich, B., 1999, Boron behavior during desalination of sea and underground water by electrodialysis, *Desalination,* 124: 125-130pp.

Melnik, L.A., Butnik, I.A. and Goncharuk, V.V., 2008, Sorption membrane removal of boron compounds from natural and wastewaters: ecological and economic aspects, *Journal Water Chemistry Technology,* 30 (3): 167-179pp.

Melnyk, L., Goncharuk, V., Butnyk, I. and Tsapiuk, E., 2005, Boron removal from natural and waste waters using combined sorption membrane process, *Desalination,* 185: 147-157pp.

Miyai, Y., Ooi, K., Nishimura, T. and Kumamoto, J., 1994, Lithium adsorptive properties of a new selective adsorbent derived from $Li_{1.33}Mn_{1.67}O_4$, *Journal of Seawater Science Japan* 48: 411-415pp.

Mohan, D. and PittmanJr. C.U., 2007, Arsenic removal from water/wastewater using adsorbent sacritical review, *Journal of Hazardous Materials,* 142: 1-53pp.

Mondal, P., Majumder, C.B. and Mohanty, B., 2006, Laboratory based aroaches for arsenic remediation from contaminated water: recent developments, *Journal of Hazardous Material,* 137: 464–479pp.

Moore, S., 2007, Between rock and salt lake, *Industrial Minerals*, June, 58-69pp.

REFERENCES (continued)

Morisada S., Rin, T., Ogata, T., Kim,Y. H. and Nakano Y, 2011, Adsorption removal of boron in aqueous solutions by amine-modified tannin gel, *Water Research,* 45: 4028-4034pp.

Nable, R.O., Banuelos, G.S. and Paull, J.G., 1997, Boron toxicity, *Plant Soil,* 193: 181-198pp.

Nadav, N., 1999, Boron removal from seawater reverse osmosis permeate utilizing selective ion exchange resin, *Desalination,* 124: 131-135pp.

Nagura, T. and Tozawa, K., 1990, Lithium ion rechargeable battery, *Progress in Batteries and Solar Cells*, 209: 9-15pp.

Neal, C., Fox, K.K., Harrow, M.L. and Neal, M., 1998, Boron in the major UK river sentering the North Sea, *Science of Total Environment,* 210-211: 41-51pp.

Ng, J.C., Wang, J. and Shraim, A., 2003, A global health problem caused by arsenic from natural sources, *Chemosphere,* 52: 1353-1359pp.

Okay, O., Güçlü, H., Soner, E. and Balkaş, T., 1985, Boron pollution in the Simav River, Turkey and various methods of boron removal, *Water Research,* 19(7): 857-862pp.

Ooi, K., Kanoh, H., Sonoda, A. and Hirotsu, T., 1996, Screening of adsorbents for boron in brine, *Journal of Ion Exchange,* 7(3): 166-172pp.

Parschova, H., Mistova, E., Matejka, Z., Jelinek, L., Kabay, N. and Kauinen P., 2007, Comparison of several polymeric sorbents for selective boron removal from reverse osmosis permeate, *Reactive & Functional Polymers,* 67: 1622-1627pp.

Penrose, W.R., 1974, Arsenic in the marine and aquatic environments, Analysis occurrence and significance, *Critical Review Environmental Contr.,* 4: 465-472pp.

Pirnie, M., 2000, Technologies and costs for removal of arsenic from drinking water, US EPA Report 815-R-00-028.

REFERENCES (continued)

Power, P.P. and Woods, W.G., 1997, The chemistry of boron and its speciation in plants, *Plant Soil,* 193: 113-118pp.

Prats, D., Chillon-Arias, M.F. and Rodriguez-Pastor, M., 2000, Analysis of the influence of pH and pressure on the elimination of boron in reverse osmosis, *Desalination,* 128: 269-273pp.

Premanand, R., Durairajan, A., Haran, B., White, R. and Popov, B., 2002, Journal *of Electrochemical Society,* 149: A54-59pp.

Ravenscroft, P., Brammer,H. and Richards, K., 2009, Arsenic pollution: a global synthesis, *Wiley-Blackwell*, Oxford,UK.

Recepoglu, O. and Beker, U., 1991, A preliminary study on boron removal from Kizildere/Turkey geothermal wastewater, *Geothermics,* 20(1-2): 83-89pp.

Redondo, J., Busch, M. and De Witte, J.P., 2003, Boron removal from seawater using Filmtec^{TM} high rejection SWRO membranes, *Desalination,* 156: 229-238pp.

Russeva ,E., Havezov, I. and Detcheva, A., 1993, Arsenic speciation in wastewaters by extraction chromatography followed by atomic absorption spectrometry, *Fresenius Journal of Analytical Chemistry,* 347, 320–323pp.

Sabarudin, A., Oshita, K., Oshima, M. and Motomizu, S., 2005, Synthesis of cross-linked chitosan possessing N-methyl-d-glucamine moiety (CCTS-NMDG) for adsorption/concentration of boron in water samples and its accurate measurement by ICP-MS and ICP-AES, *Talanta,* 66: 136–144pp.

Sahin, S., 2002, A mathematical relationship forthe explanation of ion exchange for boron removal, *Desalination,* 143: 3543-3552pp.

Saitoh, M., Yoshida, S., Yamane, H., Sano, M., Fujita, M., Kifune and K., Kubota, Y., 2003, Capacity fading of the acid-treated lithium manganese oxides in high-temperature storage, *Journal of Power Sources,* 122: 162-168pp.

Sarp, S., 2006, M.S.Thesis, Ege University, Izmir, Turkey.

REFERENCES (continued)

Sato, Y., Kang, M., Kamei, T. and Magara, Y., 2002, Performance of nanofiltration for arsenic removal, *Water Resources,* 36: 3371–3377pp.

Sayiner, G., Kandemirli, F. and Dimoglo, A., 2008, Evaluation of boron removal by electrocoagulation using iron and aluminum electrodes, *Desalination,* 230: 205-212pp.

Scott, K.N., Green, J.F., Do, H.D. and McLean, S.J., 1995, Arsenic Removal By. Coagulation, *Journal of American Water Works Association* 87: 114-126pp.

Senkal, B.F. and Bicak, N., 2003, Polymer suorted imino dipropylene glycol functions for removal of boron, *Reactive and Functional Polymer,* 55: 27-33pp.

Shen, Y.S., 1973, Study of arsenic removal from drinking water, *Journal of American Water Works Association,* 65: 543-550pp.

Smedley, P.L. and Kinniburgh, D.G., 2002, A review of the source, behaviour and distribution of arsenic in natural waters, *Alied Geochemistry,* 17: 517-568pp.

Smith, A., Hopenhayn-Rich, C., Bates, M., Goeden, H., Hertz-Picciotto, I., Duggan, H., Wood, R., Kosnett, M. and Smith, M., *1992*, Cancer risks from arsenic in drinking water, *Environmental Health Perspectives,* 97: 259-267pp.

Smith, A.H., Lingas, E.O. and Rahman, M., 2000, Contamination of drinking-water by arsenic in Bangladesh: A public health emergency, *Bulletin World Health Organization,* 78: 1093-1103pp.

Song, S., Lopez-Valdivieso, A., Hernandez-Campos, D.J., Peng, C., Monroy-Fernandez, M.G. and Razo-Soto, I., 2006, Arsenic removal from high-arsenic water by enhanced coagulation with ferric ions and coarse calcite, *Water Research,* 40: 364-372pp.

Sorg, J.T. and Logsdon, G.S., 1978, Treatment technology to meet the inter imprimary drinking water regulations for inorganics, Part 2, *Journal of American Water Works Association,* 70: 379–392pp.

REFERENCES (continued)

Striebel, K.A., Sakai, E. and Cairns, E.J., 2002, Impedance studies of the thin film LiMn$_2$O$_4$ / electrolyte interface, *Journal of Electrochemical Society,* 149: 61-67pp.

Şimşek, A., Korkmaz, D., Velioğlu, Y.S. and Ataman, O.Y., 2003, Determination of boron in hazelnut (Corylus avellana L.) varieties by inductively coupled plasma optical emission spectrometry and spectrophotometry, *Food Chemistry,* 83: 293-296pp.

Takano, J., Miwa, K. and Fujiwara, T., 2008, Boron transport mechanisms: collaborationon of channel and transports, *Trends Plant Science,* 13 (8): 451-457pp.

Thomas, S.Y., Choong, T.G., Chuah, Y., Robiah, F.L. and Gregory Koay, I., Azni, 2007, Arsenic toxicity, health hazards and removal techniques from water: an overview, *Desalination,* 217: 139-166pp.

Tsunekawa, H., Tanimoto, S., Marubayashi, R., Fujita, M., Kifune, K. and Sano, M., 2002, Capacity fading of graphite electrodes due to the deposition of manganese ions on them in Li-ion batteries, *Journal of Electrochemical Society,* 149: A1326-1332pp.

Tu, K.L., Ngheim, L.D. and Chivas A.R., 2010, Boron removal by reverse osmosis membranes in seawater desalination, *Separation and Purification Technology,* 75: 87-101pp.

Tu, K.L., Ngheim, L.D. and Chivas, A.R., 2011, Coupling effects of feed solution pH an dionic strength on the rejection of boron by NF/RO membranes, *Chemical Engineering Journal,* 168: 700-706pp.

Tucker, M.C., Reimer, J.A. and Cairns, E.J., 2002, A ^{7}Li NMR study of capacity fade in metal-substituted lithium manganese oxide spinels**,** *Journal of Electrochemical Society,* 149: A574-585pp.

Turek, M., Bandura, B. and Dydo, P., 2008, Electrodialytic boron removal from SWRO permeate, *Desalination,* 223: 17-22pp.

REFERENCES (continued)

Turek, M., Dydo, P., Trojanowska, J. and Bandura, B., 2007, Electrodialytic treatment of boron-containing wastewater, *Desalination,* 205: 185-191pp.

Turek, M., Dydo, P., Ciba, J., Trojanowska, J., Kluczka, J. and Palka-Kupczak, B., 2005, Electrodialytic treatment of boron-containing wastewater with univalent perm selective membranes, *Desalination,* 185: 139-145pp.

Weng, Y.H., Han Chaung-Hsieh, L., Lee, H.H., Li, K.C. and Huang, C.P., 2005, Removal of arsenic and humic substances (HSs) by electro-ultrafiltration (EUF), *Journal of Hazardous Materials,* 122: 171–176pp.

WHO, 2004, Guidelines for Drinking – Water Quality, 3rd edition, World Health Organization, Geneva.

WHO, 2011, Guidelines for Drinking-Water Quality, 4th edition World Health Organization, Geneva.

Wolska, J. and Bryjak, M., 2013, Methods for boron removal from aqueous solutions - A review, *Desalination,* 310: 18-24pp.

Wyness, A.J., Parkaman, R.H. and Neal, C, 2003, A summary of boron surface water quality data throughout the European Union, *Science Total Environment,* 314: 255-269pp.

Xia, Y. and Yoshio, M., 1997, Optimization of spinel Li^{1+} xMn^{2-} yO_4 as a 4 V Li-cell cathode in terms of a Li-Mn-O phase diagram**,** *Journal of Electrochemical Society,* 144: 4186-4195pp.

Yamane, H., Inoue, T., Fujita, M. and Sano, M., 2001, A causal study of the capacity fading of $Li_{1.01}Mn_{1.99}O_4$ cathode at 80^oC, and the suppressing substances of its fading, *Journal of Power Sources,* 99: 60-65pp.

Yamane, H., Saitoh, M., Sano, M., Fujita, M., Sakata, M., Takada, M., Nishibori and E., Tanaka N., 2002, Cycle performance in each state-of-charge in $LiMn_2O_4$, *Journal of Power Sources,* 149 : A1514-1520pp.

REFERENCES (continued)

Yazicigil, Z. and Oztekin, Y., 2006, Boron removal by electrodialysis with anion-exchange membranes, *Desalination,* 190: 71-78pp.

Yilmaz A. E., Boncukcuoğlu, R., Bayar, S., Fil, B. A. and Kocakerim, M.M., 2012, Boron removal by means of chemical precipitation with calcium hydroxide and calcium borate formation, *Korean Journal Chemical Engineering,* 29(10): 1382-1387pp.

Yilmaz, A. E., Boncukcuoglu, R. and Kocakerim, M. M., 2007, A quantitative comparison between electrocoagulation and chemical coagulation for boron removal from boron containing solution, *Journal of Hazardous Materials,* 149: 475-481pp.

Yilmaz, A. E., Boncukcuoglu, R., Kocakerim, M. M., Yilmaz, M.T. and Paluluoğlu, C., 2008, Boron removal from geothermal waters by electrocoagulation, *Journal of Hazardous Materials,* 153: 146-151pp.

Yilmaz-Ipek, I., Koseoglu, P., Yuksel, U., Yasar, N., Yolseven, G., Yuksel, M. and Kabay, N., 2010, Separation of boron from geothermal water using a boron selective macroporous weak base anion exchange resin, *Separation Science and Technology,* 45: 809-813pp.

Zhu, H., Jia, Y., Wu, X. and Wang, H., 2009, Removal of arsenic from water by suorted nanozero-valent ironon activated carbon, *Journal of Hazardous Materials,* 172: 1591-1596pp.

CURRICULUM VITAE

Name	Gülşah ÖZKULA
Date of Birth	27.08.1988
Place of Birth	Bandırma
Nationality	Turkish Republic
Marital Status	Single
Address	Hacıyusuf Mahallesi Adalet Caddesi Rüzgargülü Sitesi No:79/21 Bandırma/BALIKESİR
e-mail	gulsah_ozkula@hotmail.com
MSc	Ege University, Faculty of Science, Department of Chemistry (2011-2014)

Thesis subject: Separation of arsenic, boron and lithium from water by using functional resins, fibers and inorganic ion exchanger λ-MnO$_2$

Supervised by:
Assoc. Prof. Dr. Müşerref ARDA
Prof. Dr. Nalan KABAY
(Chem. Eng. Dept.)

BSc	Ege University, Faculty of Science, Department of Chemistry (2007-2011)

Presentations in National Conferences

Gülşah Özkula, Müşerref Arda, Nalan Kabay, Akio Katakai, Bor Seçimli Fonksiyonel Polimerler ile Jeotermal Sudan Bor Giderilmesi, VI. Ulusal Analitik Kimya Kongresi, Eylül 3-7, 2012, Hatay (poster presentation)

Gülşah Özkula, Müşerref Arda, Nalan Kabay, Mithat Yüksel, Ümran Yüksel, Akio Katakai, Bor Seçimli Kompozit Fiber ile Jeotermal Sudan Bor Giderilmesi, 1. Ege Nanoteknoloji Günleri, 18-19 Nisan 2013, Ege Üniversitesi, İzmir, Türkiye (poster presentation)

SCI Papers Published

P. Santander, B. L. Rivas, B. F. Urbano, İ. Yılmaz İpek, **G. Özkula**, M. Arda, M. Yüksel, M. Bryjak, T. Kozlecki, N. Kabay, Removal of boron from geothermal water by a novel boron selective resin, 2013, Desalination 310, 102–108.

Projects Submitted During Undergraduate Education

2209/A - Üniversite Öğrencileri Yurt İçi Araştırma Projeleri Destek Bursu – (Dimetiletanolamin fonksiyonel grubunu ve kuarterner amonyum fonksiyonel grubunu içeren iki farklı kuvvetli bazik anyon değiştirici reçine kullanılarak sulardan nitrat iyonlarının giderilmesi)

Projects Involved During Graduate Education

1. Project Number: EÜ-2012-FEN-49, Fonksiyonel Reçine, Fiber ve Anorganik İyon Değiştirici λ-MnO$_2$ ile Sulardan Arsenik, Bor ve Lityum Ayrılması

2. Innovative Materials and Methods for Water Treatment-CHILTURPOL2 (supported by FP7-People 2010 IRSES-Marie Curie Actions) (2012-2013) (Faculty of Chemistry, Concepcion University of Chile/ between April 14 - July 8, 2013 financially supported for 3 months as a research staff through this project).

APPENDIX

Appendix 1: Effect of adsorbent amount on boron removal from geothermal water by boron selective resin (0.500-0.710 mm) and fiber

Appendix 2: Effect of adsorbent concentration on boron sorption kinetics. (a) boron concentration versus time, (b) ratio of boron concentration at any time to initial boron concentration of geothermal water. (2.0 g fiber /L and 2.8 g Amberlite PWA-10/L)

Appendix 3: Effect of adsorbent concentration on boron sorption kinetics. (a) boron concentration versus time, (b) ratio of boron concentration at any time to initial boron concentration of geothermal water. (2 g fiber/L and 2g Amberlite PWA-10/L)

Appendix 4: Evaluation of kinetic data using pseudo-first-order model (fiber concentration: 2.0 g/L)

Appendix 5: Evaluation of kinetic data using pseudo-second-order kinetic model (fiber concentration: 2.0 g/L)

Appendix 6: Evaluation of kinetic data using pseudo-first-order model (resin concentration: 2.8 g/L)

Appendix 7: Evaluation of kinetic data using pseudo-second-order kinetic model (resin concentration: 2.8 g/L)

Appendix 8: Evaluation of kinetic data using pseudo-first-order model (resin concentration: 2.0 g/L)

Appendix 9: Evaluation of kinetic data using pseudo-second-order kinetic model (resin concentration: 2.0 g/L)

Appendix 10: Evaluation of kinetic data using infinite solution volume model (ISV) (fiber concentration: 2 g/L)

Appendix 11: Evaluation of kinetic data using unreacted core model (UCM) (fiber concentration: 2 g/L)

Appendix 12: Evaluation of kinetic data using infinite solution volume model (ISV) (resin concentration: 2.8 g/L)

Effect of adsorbent amount on boron removal from geothermal water

Appendix 1: Effect of adsorbent amount on boron removal from geothermal water by boron selective resin (0.500-0.710 mm) and fiber. (**Figure 4.2**)

Amount of adsorbent (g)	Fiber			Amberlite PWA-10			g adsorbent/L geothermal water
	Ci (mg/L)	Ceq. (mg/L)	Removal of B (%)	Ci (mg/L)	Ceq. (mg/L)	Removal of B (%)	
0.005	10.39	7.89	24.03	10.92	8.78	19.60	0.2
0.01	10.39	5.76	44.57	10.92	7.57	30.68	0.4
0.02	10.39	1.98	80.91	10.92	4.10	62.45	0.8
0.05	10.39	0.33	96.87	10.92	0.78	92.86	2.0
0.06	10.39	0.20	98.03	10.92	0.70	93.59	2.4
0.07	10.39	0.15	98.51	10.92	0.36	96.70	2.8
0.10	10.39	0.06	99.43	10.92	0.10	99.08	4.0

Appendix 2: Effect of adsorbent concentration on boron sorption kinetics. (a) boron concentration versus time, (b) ratio of boron concentration at any time to initial boron concentration of geothermal water. (2.0 g fiber /L and 2.8 g Amberlite PWA-10/L). (**Figure 4.3**)

Time (min)	C (Fiber) mg/L	C/Co (Fiber)	C (Amberlite PWA-10) mg/L	C/Co (Amberlite PWA-10) mg/L
0	9.25	1.00	9.31	1.00
5	7.72	0.83	6.45	0.69
10	7.13	0.77	6.11	0.66
15	6.06	0.66	5.48	0.59
20	5.50	0.59	4.99	0.54
30	4.62	0.50	4.39	0.47
45	4.18	0.45	3.37	0.36
60	2.47	0.27	2.67	0.29
120	0.86	0.09	1.25	0.13
180	0.51	0.06	0.79	0.08
240	0.29	0.03	0.58	0.06
360	0.25	0.03	0.39	0.04
480	0.21	0.02	0.23	0.02
1440	0.13	0.01	0.11	0.01

Appendix 3: Effect of adsorbent concentration on boron sorption kinetics. (a) boron concentration versus time, (b) ratio of boron concentration at any time to initial boron concentration of geothermal water. (2 g fiber/L and 2g Amberlite PWA-10/L) (**Figure 4.4**)

Time (min)	C (Fiber) mg/L	C/Co (Fiber)	C (Amberlite PWA-10) mg/L	C/Co (Amberlite PWA-10) mg/L
0	9.25	1.00	9.42	1.00
5	7.72	0.83	7.82	0.83
10	7.13	0.77	7.34	0.77
15	6.06	0.66	6.96	0.65
20	5.50	0.59	6.58	0.59
30	4.62	0.50	5.73	0.50
45	4.18	0.45	4.97	0.45
60	2.47	0.27	4.26	0.27
120	0.86	0.09	2.61	0.09
180	0.51	0.06	1.71	0.06
240	0.29	0.03	1.34	0.03
360	0.25	0.03	0.82	0.03
480	0.21	0.02	0.63	0.02
1440	0.13	0.01	0.21	0.01

Appendix 4: Evaluation of kinetic data using pseudo-first-order model (fiber concentration: 2.0 g/L). (**Figure 4.5**)

Time (min)	q_e (mg/g)	q_t (mg/g)	q_e-q_t	$\log(q_e$-$q_t)$
5	4.37	0.77	3.61	0.56
10	4.37	1.06	3.31	0.52
15	4.37	1.60	2.78	0.44
20	4.37	1.88	2.50	0.40
30	4.37	2.32	2.06	0.31
45	4.37	2.54	1.84	0.26
60	4.37	3.39	0.98	-0.01
120	4.37	4.20	0.18	-0.76

Appendix 5: Evaluation of kinetic data using pseudo-second-order kinetic model (fiber concentration: 2.0 g/L). (**Figure 4.6**)

Time (min)	q_t (mg/g)	t/qt
5	0.77	6.54
10	1.06	9.43
15	1.60	9.40
20	1.88	10.67
30	2.32	12.96
45	2.54	17.75
60	3.39	17.70
120	4.20	28.61

Appendix 6: Evaluation of kinetic data using pseudo-first-order model (resin concentration: 2.8 g/L). (**Figure 4.7**)

Time (min)	q_e (mg/g)	q_t (mg/g)	q_e-q_t	log(q_e-q_t)
5	3.12	1.02	2.10	0.32
10	3.12	1.14	1.98	0.30
15	3.12	1.37	1.75	0.24
20	3.12	1.54	1.58	0.20
30	3.12	1.76	1.36	0.13
45	3.12	2.12	1.00	0.00
60	3.12	2.37	0.75	-0.13
120	3.12	2.88	0.24	-0.62
180	3.12	3.04	0.08	-1.12

Appendix 7: Evaluation of kinetic data using pseudo-second-order kinetic model (resin concentration: 2.8 g/L). (**Figure 4.8**)

Time (min)	q_t (mg/g)	t/qt
5	1.02	4.90
10	1.14	8.75
15	1.37	10.97
20	1.54	12.96
30	1.76	17.07
45	2.12	21.21
60	2.37	25.30
120	2.88	41.49
180	3.04	59.15

Appendix 8: Evaluation of kinetic data using pseudo-first-order model (resin concentration: 2.0 g/L). (**Figure 4.9**)

Time (min)	q_e (mg/g)	q_t (mg/g)	q_e-q_t	log(q_e-q_t)
5	4.30	0.80	3.50	0.54
10	4.30	1.04	3.26	0.51
15	4.30	1.23	3.07	0.49
20	4.30	1.42	2.88	0.46
30	4.30	1.85	2.46	0.39
45	4.30	2.23	2.08	0.32
60	4.30	2.58	1.72	0.24
120	4.30	3.41	0.90	-0.05
180	4.30	3.86	0.45	-0.35
240	4.30	4.04	0.26	-0.59

Appendix 9: Evaluation of kinetic data using pseudo-second-order kinetic model (resin concentration: 2.0 g/L). (**Figure 4.10**)

Time (min)	q_t (mg/g)	t/qt
5	0.80	6.25
10	1.04	9.62
15	1.23	12.20
20	1.42	14.08
30	1.85	16.26
45	2.23	20.22
60	2.58	23.26
120	3.41	35.24
180	3.86	46.69
240	4.04	59.41

Appendix 10: Evaluation of kinetic data using infinite solution volume model (ISV) (fiber concentration: 2 g/L). (**Figure 4.11**)

Time (min)	q_e (mg/g)	q_t (mg/g)	$X= q_t/q_e$	$F(X)=-\ln(1-X)$	$F(X)=-\ln(1-X^2)$
5	4.37	0.77	0.175	0.192	0.031
10	4.37	1.06	0.243	0.278	0.061
15	4.37	1.60	0.365	0.454	0.143
20	4.37	1.88	0.429	0.560	0.203
30	4.37	2.32	0.530	0.754	0.329
45	4.37	2.54	0.580	0.868	0.410
60	4.37	3.39	0.776	1.495	0.921
120	4.37	4.20	0.960	3.218	2.545

Appendix 11: Evaluation of kinetic data using unreacted core model (UCM) (fiber concentration: 2 g/L). (**Figure 4.12**)

Time (min)	$X= q_t/q_e$	$F(X)3=X$	$F(X)4=3-3(1-X)^{2/3}-2X$	$F(X)= 1-(1-X)^{1/3}$
5	0.175	0.175	1.969	0.725
10	0.243	0.243	1.941	0.748
15	0.365	0.365	1.867	0.788
20	0.429	0.429	1.816	0.810
30	0.530	0.530	1.719	0.843
45	0.580	0.580	1.663	0.860
60	0.776	0.776	1.398	0.925
120	0.960	0.960	1.078	0.987

Appendix 12: Evaluation of kinetic data using infinite solution volume model (ISV) (resin concentration: 2.8 g/L). (**Figure 4.13**)

Time (min)	q_e (mg/g)	q_t (mg/g)	$X= q_t/q_e$	$F(X)=-\ln(1-X)$	$F(X)=-\ln(1-X^2)$
5	3.12	1.02	0.328	0.397	0.114
10	3.12	1.14	0.367	0.457	0.144
15	3.12	1.37	0.439	0.578	0.214
20	3.12	1.54	0.495	0.683	0.281
30	3.12	1.76	0.564	0.829	0.382
45	3.12	2.12	0.680	1.141	0.622
60	3.12	2.37	0.761	1.430	0.864
120	3.12	2.88	0.923	2.567	1.913
180	3.12	3.04	0.976	3.727	3.046

Appendix 13: Evaluation of kinetic data using unreacted core model (UCM) (resin concentration: 2.8 g/L). (**Figure 4.14**)

Time (min)	$X = q_t/q_e$	F(X)3=X	$F(X)4=3-3(1-X)^{2/3}-2X$	$F(X)= 1-(1-X)^{1/3}$
5	0.328	0.328	1.893	0.776
10	0.367	0.367	1.866	0.789
15	0.439	0.439	1.808	0.813
20	0.495	0.495	1.755	0.832
30	0.564	0.564	1.682	0.855
45	0.680	0.680	1.537	0.893
60	0.761	0.761	1.421	0.920
120	0.923	0.923	1.148	0.974

Appendix 14: Evaluation of kinetic data using infinite solution volume model (ISV) (resin concentration: 2.0 g/L). (**Figure 4.15**)

Time (min)	q_e (mg/g)	q_t (mg/g)	$X = q_t/q_e$	$F(X)=-\ln(1-X)$	$F(X)=-\ln(1-X^2)$
5	4.30	0.80	0.186	0.206	0.035
10	4.30	1.04	0.242	0.277	0.060
15	4.30	1.23	0.286	0.337	0.085
20	4.30	1.42	0.330	0.401	0.115
30	4.30	1.85	0.429	0.560	0.203
45	4.30	2.23	0.517	0.729	0.312
60	4.30	2.58	0.600	0.916	0.446
120	4.30	3.41	0.792	1.570	0.986
180	4.30	3.86	0.897	2.268	1.628
240	4.30	4.04	0.940	2.806	2.143

Appendix 15: Evaluation of kinetic data using unreacted core model (UCM) (resin concentration: 2.0 g/L). (**Figure 4.16**)

Time (min)	$X = q_t/q_e$	F(X)3=X	$F(X)4=3-3(1-X)^{2/3}-2X$	$F(X)= 1-(1-X)^{1/3}$
5	0.186	0.186	1.965	0.729
10	0.242	0.242	1.942	0.747
15	0.286	0.286	1.918	0.762
20	0.330	0.330	1.891	0.777
30	0.429	0.429	1.816	0.810
45	0.517	0.517	1.732	0.839
60	0.600	0.600	1.640	0.867
120	0.792	0.792	1.373	0.931

Appendix 16: Sorption profile of boron using Amberlite PWA-10 for cycle studies. (**Figure 4.17**)

	Sorbed Boron (mg)									
	Cycle-1	Cycle-2	Cycle-3	Cycle-4	Cycle-5	Cycle-6	Cycle-7	Cycle-8	Cycle-9	Cycle-10
1	0.256	0.253	0.249	0.252	0.246	0.249	0.260	0.259	0.263	0.257
2	0.258	0.254	0.250	0.251	0.247	0.249	0.253	0.258	0.259	0.261
3	0.258	0.252	0.249	0.249	0.244	0.241	0.248	0.255	0.255	0.260
4	0.258	0.254	0.247	0.252	0.246	0.245	0.253	0.256	0.262	0.259

Appendix 17: Sorption profile of boron using composite fiber for cycle studies. (**Figure 4.18**)

	Sorbed Boron (mg)									
	Cycle-1	Cycle-2	Cycle-3	Cycle-4	Cycle-5	Cycle-6	Cycle-7	Cycle-8	Cycle-9	Cycle-10
1	0.248	0.256	0.235	0.238	0.236	0.238	0.251	0.250	0.244	0.248
2	0.242	0.253	0.238	0.237	0.236	0.240	0.255	0.244	0.242	0.250
3	0.247	0.250	0.233	0.233	0.233	0.234	0.255	0.248	0.245	0.248
4	0.243	0.254	0.237	0.232	0.234	0.233	0.254	0.250	0.245	0.247

Appendix 18: Elution profile of boron using Amberlite PWA-10 for cycle studies. (**Figure 4.19**)

Acid Conc. (mol/L)	Eluted Boron (mg)									
	Cycle-1	Cycle-2	Cycle-3	Cycle-4	Cycle-5	Cycle-6	Cycle-7	Cycle-8	Cycle-9	Cycle-10
0.1	0.234	0.232	0.227	0.238	0.254	0.254	0.261	0.262	0.239	0.236
0.5	0.239	0.211	0.246	0.238	0.268	0.251	0.256	0.263	0.242	0.241
1	0.234	0.217	0.236	0.244	0.263	0.242	0.261	0.264	0.244	0.247
2	0.227	0.199	0.213	0.233	0.233	0.237	0.246	0.252	0.235	0.234

Appendix 19: Elution profile of boron using composite fiber for cycle studies. (**Figure 4.20**)

Acid Conc. (mol/L)	Eluted Boron (mg)									
	Cycle-1	Cycle-2	Cycle-3	Cycle-4	Cycle-5	Cycle-6	Cycle-7	Cycle-8	Cycle-9	Cycle-10
0.1	0.234	0.247	0.271	0.237	0.235	0.237	0.240	0.248	0.241	0.242
0.5	0.224	0.241	0.262	0.234	0.229	0.238	0.243	0.230	0.242	0.244
1	0.226	0.241	0.260	0.231	0.223	0.230	0.231	0.228	0.246	0.244
2	0.218	0.237	0.246	0.221	0.216	0.221	0.234	0.219	0.235	0.237

Appendix 20: Sorption profile of boron using Amberlite PWA-10 with respect to cycle no (**Figure 4.21**)

Cycle No	% Sorption	Cycle No	% Sorption
1	98.51	6	96.87
2	98.55	7	94.87
3	98.01	8	97.13
4	98.10	9	97.59
5	97.87	10	97.75

Appendix 21: Elution profile of boron using Amberlite PWA-10 with respect to cycle no (**Figure 4.22**)

Cycle No	% Elution	Cycle No	% Elution
1	90.73	6	100.07
2	84.88	7	100.94
3	92.50	8	101.24
4	95.00	9	92.52
5	103.57	10	92.32

Appendix 22: Sorption profile of boron using composite fiber with respect to cycle no. (**Figure 4.23**)

Cycle No	% Sorption	Cycle No	% Sorption
1	94.10	6	95.07
2	96.23	7	97.09
3	95.07	8	96.58
4	95.60	9	96.02
5	95.62	10	97.15

Appendix 23: Elution profile of boron using composite fiber with respect to cycle no. (**Figure 4.24**)

Cycle No	% Elution	Cycle No	% Elution
1	94.10	6	98.03
2	95.41	7	93.44
3	110.23	8	93.20
4	98.20	9	98.85
5	96.19	10	97.35

Column-mode tests of boron removal from geothermal water

Appendix 24: Breakthrough profiles of B by composite fiber at SV 10,15 and 25 h^{-1}. (**Figure 4.25**)

SV:10 h^{-1}

F.No	Total BV	C (mg/L)	F.No	Total BV	C (mg/L)
1	7.43	0	56	420.98	6.74
2	14.88	0	57	428.62	6.83
3	22.34	0	58	436.27	6.96
4	29.79	0	59	443.93	7.06
5	37.26	0	60	451.57	7.07
6	44.72	0	63	474.06	7.55
7	52.18	0	65	489.15	7.77
8	59.66	0	68	511.85	8.00
9	66.04	0	70	527.04	8.05
10	73.55	0	73	549.68	8.11
11	81.07	0	75	564.74	8.19

12	88.60	0	**78**	587.35	8.36
13	96.10	0	**80**	602.48	8.52
14	103.62	0	**83**	625.21	8.69
15	111.12	0.03	**85**	640.38	8.62
16	118.64	0.14	**88**	664.66	8.69
17	126.18	0.30	**90**	679.93	8.71
18	133.70	0.48	**92**	695.23	8.71
19	141.25	0.66	**94**	710.52	8.77
20	148.77	0.83	**95**	718.17	8.74
21	156.31	1.00	**96**	725.83	8.86
22	163.88	1.16	**97**	733.19	8.78
23	171.45	1.41	**99**	748.27	8.98
24	179.02	1.58	**100**	755.83	8.88
25	186.61	1.69	**102**	771.02	9.01
26	194.20	1.90	**103**	778.60	9.00
27	201.79	2.09	**105**	793.87	9.04
28	209.38	2.30	**106**	801.50	9.05
29	216.98	2.56	**108**	816.30	9.05
30	224.56	2.86	**110**	831.47	9.09
32	239.27	3.52	**112**	846.69	9.13
34	254.43	4.32	**113**	854.31	9.19
36	269.59	4.69	**114**	861.92	9.20
37	277.18	4.76	**115**	869.55	9.30
38	284.78	4.88	**117**	884.82	9.40
39	292.40	5.08	**118**	892.47	9.38
40	300.01	5.21	**120**	907.74	9.42
41	307.51	5.44	**123**	930.69	9.37
42	314.63	5.61	**125**	946.02	9.49
43	322.17	5.64	**128**	969.02	9.54
44	329.74	5.60	**129**	976.69	9.36
45	337.31	5.65	**130**	984.40	9.66
46	344.88	5.89	**131**	992.05	9.54
47	352.45	6.07	**132**	999.71	9.61
48	360.02	6.05	**135**	102.,54	10.16
49	367.62	6.22	**138**	1045.41	10.18
50	375.23	6.26	**140**	1059.97	9.93
51	382.86	6.26	**145**	1097.84	9.84
52	390.48	6.43	**148**	1120.65	9.76
53	398.10	6.49	**150**	1135.93	9.73
54	405.72	6.53			
55	413.34	6.53			

SV:15 h^{-1}

F.No	Total BV	C (mg/L)	F.No	Total BV	C (mg/L)
1	7.21	0	45	329.24	5.91
2	14.46	0	46	336.68	6.36
3	21.69	0	47	344.13	6.37
4	28.89	0	48	351.57	6.46
5	36.09	0	49	359.02	6.60
6	43.31	0	50	366.49	6.80
7	50.55	0	51	373.95	6.95
8	57.77	0	52	381.38	6.98
9	65.01	0	53	388.82	7.00
10	72.30	0	54	396.26	7.14
11	79.51	0	55	403.77	7.23
12	86.78	0	56	411.34	7.41
13	94.09	0	57	418.89	7.49
14	101.36	0	58	426.36	7.86
15	108.61	0	59	433.87	7.98
16	115.87	0	60	441.39	8.05
17	123.16	0.00	63	463.73	8.14
18	130.42	0.03	65	478.57	8.26
19	137.70	0.07	68	500.90	8.30
20	145.00	0.15	70	515.70	8.34
21	152.28	0.26	73	538.01	8.40
22	159.58	0.43	75	552.88	8.46
23	166.90	0.74	78	575.29	8.66
24	174.23	1.07	80	590.17	8.52
25	181.54	1.30	83	612.41	8.86
26	188.85	1.62	85	627.26	8.86
27	196.16	1.99	88	649.62	8.89
28	203.49	2.25	90	664.52	8.86
30	218.24	2.90	95	701.79	9.03
32	232.95	3.34	100	739.22	9.08
34	247.65	3.87	105	776.52	9.31
36	262.41	4.34	110	814.05	9.53
37	269.80	4.51	120	888.98	9.08
38	277.21	4.75	125	926.26	9.48
39	284.62	4.89	130	964.10	9.25
40	292.04	5.08	135	1001.92	9.38
41	299.45	5.40	140	1039.78	9.65
42	306.90	5.46	145	1077.83	9.32
43	314.37	5.60	148	1100.75	9.42
44	321.81	5.76	150	1116.06	9.47

SV:25 h^{-1}

F.No	Total BV	C (mg/L)	F.No	Total BV	C (mg/L)
1	8.46	0	49	388.96	5.08
2	16.88	0	50	397.47	5.23
3	25.27	0	51	405.97	5.37
4	33.63	0	52	414.44	5.61
5	41.90	0	53	422.92	5.82
6	50.11	0	54	431.40	5.92
7	58.39	0	55	439.89	6.13
8	66.37	0	56	448.38	6.21
9	74.33	0	57	456.88	6.35
10	81.78	0	58	465.38	6.37
11	88.82	0	59	473.90	6.58
12	95.78	0	60	482.41	6.74
13	102.79	0	63	507.91	7.19
14	109.70	0	65	524.35	7.71
15	116.65	0	68	549.64	8.14
16	123.62	0	70	566.61	8.16
17	130.70	0	73	591.59	8.75
18	137.59	0	75	608.21	8.91
19	144.74	0	78	633.24	9.03
20	151.74	0	80	650.02	9.06
21	158.66	0.01	83	675.27	9.11
22	165.44	0.01	85	691.39	9.16
23	172.60	0.08	88	716.23	9.20
24	181.06	0.10	90	733.05	9.20
25	188.55	0.10	93	758.29	9.22
26	196.61	0.12	95	775.10	9.25
27	204.78	0.12	97	791.89	9.31
28	213.00	0.18	100	817.18	9.31
29	221.42	0.24	103	842.44	9.34
30	229.82	0.29	105	859.28	9.31
32	246.59	0.56	108	884.49	9.40
34	263.27	1.21	110	901.27	9.39
36	279.87	1.96	113	926.42	9.44
37	288.16	2.19	115	943.22	9.56
38	296.45	2.41	118	968.46	9.53
39	304.78	2.74	120	985.35	9.50
40	313.10	3.00	123	1010.82	9.65
41	321.48	3.21	125	1027.75	9.80
42	329.88	3.45	128	1053.02	9.85
43	338.30	3.64	130	1070.04	9.97
44	346.72	3.88	135	1110.65	10.05
45	355.16	4.12	140	1152.51	10.12

46	363.60	4.45	**145**	1193.45	10.18
47	372.04	4.67	**148**	1218.23	9.98
48	380.49	4.85	**150**	1234.85	9.95

Appendix 25: Elution profiles of B by composite fiber at SV 10,15 and 25 h^{-1}. (**Figure 4.26**)

SV:10 h^{-1}

F.No	Total BV	C (mg/L)	F.No	Total BV	C (mg/L)
1	2.73	363.52	8	22.07	0.43
2	5.47	749.82	9	24.86	0.19
3	8.23	146.34	10	27.65	0.09
4	11.00	10.64	11	30.45	0.07
5	13.76	9.25	12	33.24	0.04
6	16.53	2.28	13	36.04	0.03
7	19.30	0.98	14	38.83	0.03

SV:15 h^{-1}

F.No	Total BV	C (mg/L)	F.No	Total BV	C (mg/L)
1	2.632	267.20	9	25.705	0.16
2	5.376	598.39	10	28.450	0.10
3	8.094	80.70	11	31.213	0.07
4	10.850	16.72	12	33.962	0.05
5	14.152	4.98	13	36.725	0.05
6	16.905	1.45	14	39.470	0.05
7	20.201	0.56	15	42.225	0.05
8	22.946	0.26			

SV:25 h^{-1}

F.No	Total BV	C (mg/L)	F.No	Total BV	C (mg/L)
1	3.33	511.75	9	30.43	0.12
2	6.69	675.70	10	33.86	0.12
3	10.05	46.39	11	37.30	0.10
4	13.43	3.94	12	40.74	0.09
5	16.81	0.35	13	44.17	0.06
6	20.19	0.24	14	47.61	0.06
7	23.60	0.16	15	51.06	0.05
8	27.01	0.14			

Appendix 26: Breakthrough profiles of B by composite fiber and Amberlite PWA-10. (**Figure 4.27**)

F.No	BV (Resin)	C (mg/L)	C/C$_o$	F.No	BV (Resin)	C (mg/L)	C/C$_o$
1	9,59	0,00	0,00	30	294,44	3,25	0,31
2	19,31	0,00	0,00	31	304,29	3,74	0,36
3	28,97	0,00	0,00	32	314,14	4,33	0,41
4	38,80	0,00	0,00	33	324,13	4,66	0,45
5	48,64	0,00	0,00	34	334,16	5,06	0,48
6	58,49	0,00	0,00	35	344,15	5,90	0,56
7	68,33	0,00	0,00	36	354,19	6,49	0,62
8	78,22	0,00	0,00	37	364,27	6,89	0,66
9	88,05	0,00	0,00	38	374,35	7,37	0,70
10	97,88	0,00	0,00	39	384,36	7,96	0,76
11	107,70	0,00	0,00	40	394,38	8,45	0,81
12	117,46	0,01	0,00	41	404,07	8,94	0,85
13	127,25	0,02	0,00	42	413,83	9,12	0,87
14	137,08	0,03	0,00	43	423,67	9,51	0,91
15	146,89	0,06	0,01	44	433,57	9,74	0,93
16	156,72	0,10	0,01	45	443,47	9,71	0,93
17	166,56	0,15	0,01	46	453,38	9,71	0,93
18	176,36	0,21	0,02	47	463,22	10,24	0,98
19	186,06	0,31	0,03	48	473,04	10,52	1,00
20	195,77	0,40	0,04	49	482,86	10,42	1,00
21	205,46	0,53	0,05	50	492,71	10,19	0,97
22	215,22	0,70	0,07	54	532,08	10,16	0,97
23	225,06	0,88	0,08	60	591,20	10,29	0,98
24	234,92	1,12	0,11	64	630,70	10,11	0,97
25	244,81	1,39	0,13	68	670,58	10,04	0,96
26	254,74	1,69	0,16	69	680,58	10,00	0,95
27	264,63	2,12	0,20	70	690,67	9,47	0,90
28	274,55	2,39	0,23	72	710,70	9,59	0,92
29	284,47	2,83	0,27	78	771,22	9,98	0,95

Appendix 27: Elution profiles of B by composite fiber and Amberlite PWA-10. (**Figure 4.28**)

F.No	Total BV	C (mg/L)	F.No	Total BV	C (mg/L)
1	3,71	272,32	8	30,57	0,10
2	7,51	417,63	9	34,45	0,06
3	11,33	67,18	10	38,36	0,04
4	15,16	12,02	11	42,27	0,04
5	19,01	2,33	12	46,16	0,04
6	22,86	0,69	13	50,07	0,04
7	26,73	0,26			

Appendix 28: Breakthrough profiles of B by Diaion CRB02 at a particle size range of 0.250-0.355 mm and 0.355-0.500 mm. (**Figure 4.29**)

(particle size range of 0.250-0.355 mm)

F.No	BV	C (mg/L)	C/C_o	F.No	BV	C (mg/L)	C/C_o
1	8,77	0,00	0,00	32	307,90	4,67	0,45
2	17,90	0,00	0,00	33	317,87	5,63	0,54
3	27,05	0,00	0,00	34	327,87	6,65	0,64
4	36,31	0,00	0,00	35	337,95	7,31	0,70
5	45,57	0,00	0,00	36	348,11	7,59	0,73
6	54,84	0,00	0,00	37	358,13	8,45	0,81
7	64,21	0,00	0,00	38	368,18	9,19	0,89
8	73,64	0,00	0,00	39	378,23	9,52	0,92
9	83,04	0,00	0,00	40	387,70	9,89	0,95
10	92,63	0,00	0,00	41	397,60	9,77	0,94
11	102,24	0,00	0,00	42	407,62	9,86	0,95
12	111,80	0,00	0,00	43	417,66	10,23	0,99
13	121,40	0,00	0,00	44	427,66	9,86	0,95
14	131,04	0,00	0,00	45	437,75	9,76	0,94
15	140,65	0,00	0,00	46	447,87	10,21	0,98
16	150,31	0,00	0,00	48	468,03	9,92	0,96
17	159,98	0,00	0,00	50	488,08	9,90	0,95
18	169,63	0,00	0,00	52	508,29	10,07	0,97
19	179,30	0,00	0,00	54	528,57	9,78	0,94
20	189,04	0,00	0,00	56	548,95	9,87	0,95
21	198,73	0,03	0,00	58	569,30	9,84	0,95
22	208,48	0,04	0,00	60	589,52	9,87	0,95
23	218,36	0,10	0,01	62	609,78	9,89	0,95
24	228,30	0,23	0,02	64	630,12	9,99	0,96
25	238,27	0,33	0,03	66	650,53	9,73	0,94
26	248,18	0,72	0,07	68	671,03	9,82	0,95
27	258,14	0,98	0,09	70	691,53	9,76	0,94
28	268,09	1,52	0,15	72	711,89	10,01	0,97
29	278,02	2,18	0,21	73	722,14	9,80	0,94
30	287,97	2,84	0,27	75	741,32	9,61	0,93
31	297,93	3,76	0,36				

(particle size range of 0.355-0.50 mm)

F.No	BV	C (mg/L)	C/C_o	F.No	BV	C (mg/L)	C/C_o
1	9,61	0,00	0,00	30	293,13	3,87	0,38
2	19,31	0,00	0,00	31	302,92	4,69	0,46
3	29,09	0,00	0,00	32	312,72	5,32	0,52
4	38,89	0,00	0,00	33	322,52	6,09	0,60
5	48,72	0,00	0,00	34	332,32	6,67	0,65
6	58,55	0,00	0,00	35	342,17	7,22	0,71
7	68,38	0,00	0,00	36	352,00	7,40	0,72
8	78,22	0,00	0,00	37	361,81	8,12	0,79
9	88,04	0,00	0,00	38	371,61	8,58	0,84
10	97,95	0,00	0,00	39	381,37	8,90	0,87
11	107,73	0,00	0,00	40	390,95	8,93	0,87
12	117,50	0,00	0,00	41	400,57	9,63	0,94
13	127,25	0,00	0,00	42	410,31	9,79	0,96
14	136,99	0,03	0,00	43	420,03	9,70	0,95
15	146,74	0,04	0,00	44	429,76	9,17	0,90
16	156,48	0,04	0,00	45	439,50	9,52	0,93
17	166,20	0,06	0,01	46	449,28	10,09	0,99
18	175,91	0,09	0,01	47	459,09	10,05	0,98
19	185,60	0,13	0,01	48	468,84	9,76	0,96
20	195,27	0,20	0,02	49	478,61	9,88	0,97
21	204,99	0,21	0,02	50	488,22	9,92	0,97
22	214,73	0,27	0,03	60	586,08	9,57	0,94
23	224,48	0,47	0,05	64	625,19	9,65	0,94
24	234,28	0,92	0,09	68	664,44	9,64	0,94
25	244,06	1,21	0,12	70	684,17	9,87	0,97
26	253,85	1,62	0,16	72	703,88	9,65	0,94
27	263,69	2,09	0,20	74	723,81	9,47	0,93
28	273,50	2,71	0,27	78	763,65	9,88	0,97
29	283,33	3,31	0,32				

Appendix 29: Elution profiles of B by Diaion CRB02 at a particle size range of 0.250-0.355 mm and 0.355-0.500 mm. (**Figure 4.30**)

(particle size range of 0.250-0.355 mm)

F.No	Total BV	C (mg/L)	F.No	Total BV	C (mg/L)
1	3,99	311,33	9	34,99	0,08
2	7,80	279,70	10	38,90	0,06
3	11,66	39,41	11	42,83	0,09
4	15,53	7,99	12	46,75	0,09
5	19,39	1,75	13	50,68	0,08
6	23,26	0,49	14	54,62	0,09
7	27,19	0,13	15	58,56	0,07
8	31,09	0,09			

(particle size range of 0.355-0.50 mm)

F.No	Total BV	C (mg/L)	F.No	Total BV	C (mg/L)
1	3,73	341,71	8	31,84	0,54
2	7,70	297,45	9	35,89	0,26
3	11,69	56,16	10	39,94	0,14
4	15,71	13,69	11	44,01	0,05
5	19,73	6,40	12	48,07	0,04
6	23,77	1,29	13	52,13	0,02
7	27,80	1,24			

Appendix 30: Comparison of eluting agent concentration for elution of B by Diaion CRB02 at a particle size range of 0.355-0.500 mm. (**Figure 4.31**)

	1 M H_2SO_4		0.5 M H_2SO_4	
F.No	**Total BV**	**C (mg/L)**	**Total BV**	**C (mg/L)**
1	3,88	318,09	3,73	341,71
2	8,04	263,49	7,70	297,45
3	12,16	37,18	11,69	56,16
4	16,38	6,19	15,71	13,69
5	20,34	1,17	19,73	6,40
6	24,47	0,25	23,77	1,29
7	28,58	0,10	27,80	1,24
8	32,78	0,07	31,84	0,54
9	37,03	0,05	35,89	0,26
10	41,28	0,06	39,94	0,14
11	45,53	0,05	44,01	0,05
12	49,76	0,04	48,07	0,04
13	54,02	0,04	52,13	0,02

EDI tests of boron removal from RO permeate of geothermal water

Appendix 31: Comparison of boron concentrations in the stream of central compartment with respect to time (a) boron concentration versus time, (b) ratio of boron concentration at any time to initial boron concentration of RO permeate.(**Figure 4.32**)

	Amberlite PWA-10		Purolite CT 175-A500	
Time (min)	**C (mg/L)**	**C/C_o**	**C (mg/L)**	**C/C_o**
0	3.98	1.00	4.00	1.00
15	1.85	0.46	3.69	0.92
30	1.77	0.44	3.51	0.88
45	1.52	0.38	3.29	0.82
60	1.41	0.35	3.01	0.75
90	1.22	0.31	2.51	0.63
120	1.10	0.28	2.22	0.55
150	0.89	0.22	1.97	0.49
180	0.69	0.17	1.42	0.35

Appendix 32: Boron concentration in the anode compartment versus time with Amberlite PWA-10 and Purolite CT 175-A500. (**Figure 4.33**)

	Amberlite PWA-10	**Purolite CT 175-A500**
Time (min)	C (mg/L)	C (mg/L)
0	0.002	0.017
15	0.046	0.042
30	0.041	0.068
45	0.044	0.086
60	0.072	0.117
90	0.063	0.146
120	0.086	0.179
150	0.069	0.232
180	0.064	0.308

Appendix 33: Comparison of boron concentrations in central compartment with respect to time (a) boron concentration versus time, (b) ratio of boron concentration at any time to initial boron concentration of RO permeate and model solution containing 5.0 mg B/L. (**Figure 4.34**)

	Model Solution		**RO permeate**	
Time (min)	C (mg/L)	C/C_o	C (mg/L)	C/C_o
0	5.02	1.00	4.00	1.00
15	4.94	0.98	3.69	0.92
30	4.18	0.83	3.51	0.88
45	3.96	0.79	3.29	0.82
60	3.45	0.69	3.01	0.75
90	2.68	0.53	2.51	0.63
120	2.01	0.40	2.22	0.55
150	1.41	0.28	1.97	0.49
180	0.96	0.19	1.42	0.35

Removal of lithium with ion exchange-membrane filtration hybrid system

Appendix 34: (a) Lithium concentration versus time (b) Ratio of lithium concentration at any time to initial lithium concentration of geothermal water versus time (Adsorbent concentration: 1 g adsorbent/L geothermal water, Qfresh/sat: 3 mL/min, Qfeed/permeate: 5 mL/min) (**Figure 4.35**)

Time (min)	C (mg/L)	C/C_o	Time (min)	C (mg/L)	C/C_o
0	10,34	1.00	**80**	1,89	0,18
5	7,83	0,76	**100**	1,73	0,17
10	7,58	0,73	**120**	1,64	0,16
15	6,34	0,61	**140**	1,54	0,15
20	5,04	0,49	**160**	1,39	0,13
25	4,4	0,43	**180**	1,23	0,12
30	3,84	0,37	**200**	1,02	0,10
40	2,75	0,27	**220**	0,61	0,06
60	2,27	0,22	**240**	0,31	0,03

Appendix 35: (a) Lithium concentration versus time (b) Ratio of lithium concentration at any time to initial lithium concentration of geothermal water versus time (Adsorbent concentration: 2 g adsorbent/L geothermal water, Qfresh/sat: 3 mL/min, Qfeed/permeate: 5 mL/min) (**Figure 4.36**)

Time (min)	C (mg/L)	C/C$_o$	Time (min)	C (mg/L)	C/C$_o$
0	10,53	1.00	80	0.00	0.00
5	8,04	0,76	100	0.00	0.00
10	5,77	0,55	120	0.00	0.00
15	2,42	0,23	140	0.00	0.00
20	0,82	0,08	160	0.00	0.00
25	0,33	0,03	180	0.00	0.00
30	0,13	0,01	200	0.00	0.00
40	0.00	0.00	220	0.00	0.00
60	0.00	0.00	240	0.00	0.00

Appendix 36: (a) Lithium concentration versus time (b) Ratio of lithium concentration at any time to initial lithium concentration of geothermal water versus time (Adsorbent concentration: 3 g adsorbent/L geothermal water, Qfresh/sat: 3 mL/min, Qfeed/permeate: 5 mL/min). (**Figure 4.37**)

Time (min)	C (mg/L)	C/C$_o$	Time (min)	C (mg/L)	C/C$_o$
0	10,15	1.00	80	0.00	0.00
5	6,62	0,65	100	0.00	0.00
10	5,21	0,51	120	0.00	0.00
15	2,83	0,28	140	0.00	0.00
20	1,65	0,16	160	0.00	0.00
25	0,81	0,08	180	0.00	0.00
30	0,29	0,03	200	0.00	0.00
40	0.00	0.00	220	0.00	0.00
60	0.00	0.00	240	0.00	0.00

Appendix 37: (a) Lithium concentration versus time (b) Ratio of lithium concentration at any time to initial lithium concentration of geothermal water versus time (Adsorbent concentration: 1 g adsorbent/L geothermal water, Qfresh/sat: 3 mL/min, Qfeed/permeate: 5 mL/min). (**Figure 4.39**)

Time (min)	C (mg/L)	C/C$_o$	Time (min)	C (mg/L)	C/C$_o$
0	10,35	1.00	80	6,46	0,62
5	8,47	0,82	100	6,25	0,60
10	8,40	0,81	120	6,07	0,59
15	8,17	0,79	140	5,97	0,58
20	7,96	0,77	160	5,90	0,57
25	7,66	0,74	180	5,75	0,56
30	7,42	0,72	200	5,67	0,55
40	7,18	0,69	220	5,57	0,54
60	6,78	0,65	240	5,54	0,54

Appendix 38: (a) Lithium concentration versus time (b) Ratio of lithium concentration at any time to initial lithium concentration of geothermal water versus time (Adsorbent concentration: 2 g adsorbent/L geothermal water, Qfresh/sat: 3 mL/min, Qfeed/permeate: 5 mL/min). (**Figure 4.40**)

Time (min)	C (mg/L)	C/C$_o$	Time (min)	C (mg/L)	C/C$_o$
0	10,85	1.00	80	3,38	0,31
5	7,91	0,73	100	3,37	0,31
10	6,85	0,63	120	3,43	0,32
15	5,97	0,55	140	3,49	0,32
20	5,23	0,48	160	3,57	0,33
25	4,72	0,43	180	3,63	0,33
30	4,37	0,40	200	3,75	0,35
40	3,90	0,36	220	3,88	0,36
60	3,51	0,32	240	3,94	0,36

Appendix 39: (a) Lithium concentration versus time (b) Ratio of lithium concentration at any time to initial lithium concentration of geothermal water versus time (Adsorbent concentration: 3 g adsorbent/L geothermal water, Qfresh/sat: 6 mL/min, Qfeed/permeate: 5 mL/min). (**Figure 4.41**)

Time (min)	C (mg/L)	C/C$_o$	Time (min)	C (mg/L)	C/C$_o$
0	10,57	1.00	80	1,13	0,11
5	8,23	0,78	100	0,99	0,09
10	5,90	0,56	120	0,84	0,08
15	4,30	0,41	140	0,74	0,07
20	3,34	0,32	160	0,69	0,07
25	2,80	0,27	180	0,67	0,06
30	2,41	0,23	200	0,67	0,06
40	1,91	0,18	220	0,68	0,06
60	1,41	0,13	240	0,68	0,06

Appendix 40: Comparison of lithium concentration versus time Test-1 and Test-2 (Adsorbent concentration: 1 g adsorbent/L geothermal water) (**Figure 4.45**)

	Test-1	Test-2
Time (min)	C/C$_o$	C/C$_o$
0	1,00	1.00
5	0,70	0,76
10	0,59	0,73
15	0,47	0,61
20	0,37	0,49
25	0,32	0,43
30	0,29	0,37
40	0,24	0,27
60	0,21	0,22
80	0,19	0,18
100	0,19	0,17
120	0,19	0,16
140	0,19	0,15
160	0,19	0,13
180	0,20	0,12
200	0,21	0,10
220	0,21	0,06
240	0,21	0,03

Appendix 41: Comparison of lithium concentration versus time Test-1 and Test-2 (Adsorbent concentration: 2 g adsorbent/L geothermal water) (**Figure 4.46**)

Time (min)	Test-1 C/C_o	Test-2 C/C_o
0	1	1.00
5	0,70	0,76
10	0,21	0,55
15	0,06	0,23
20	0,01	0,08
25	0,01	0,03
30	0,00	0,01
40	0,00	0.00
60	0,00	0.00
80	0,00	0.00
100	0,00	0.00
120	0,00	0.00
140	0,00	0.00
160	0,00	0.00
180	0,00	0.00
200	0,00	0.00
220	0,00	0.00
240	0,00	0.00

Appendix 42: Comparison of lithium concentration versus time Test-1 and Test-2 (Adsorbent concentration: 3 g adsorbent/L geothermal water) (**Figure 4.47**)

Time (min)	Test-1 C/C_o	Test-2 C/C_o
0	1,00	1.00
5	0,57	0,65
10	0,18	0,51
15	0,06	0,28
20	0,02	0,16
25	0,01	0,08
30	0,00	0,03
40	0,00	0.00
60	0,00	0.00
80	0,00	0.00
100	0,00	0.00
120	0,00	0.00
140	0,00	0.00
160	0,00	0.00
180	0,00	0.00
200	0,00	0.00
220	0,00	0.00
240	0,00	0.00

Appendix 43: Comparison of lithium concentration versus time Test-1 and Test-2 (Adsorbent concentration: 1 g adsorbent/L geothermal water) (**Figure 4.48**)

	Test-1	Test-2
Time (min)	C/C_o	C/C_o
0	1.00	1.00
5	0,76	0,82
10	0,76	0,81
15	0,76	0,79
20	0,75	0,77
25	0,74	0,74
30	0,73	0,72
40	0,69	0,69
60	0,67	0,65
80	0,67	0,62
100	0,65	0,60
120	0,64	0,59
140	0,64	0,58
160	0,62	0,57
180	0,61	0,56
200	0,61	0,55
220	0,59	0,54
240	0,58	0,54

Appendix 44: Comparison of lithium concentration versus time Test-1 and Test-2 (Adsorbent concentration: 2 g adsorbent/L geothermal water) (**Figure 4.49**)

	Test-1	Test-2
Time (min)	C/C_o	C/C_o
0	1.00	1.00
5	0,84	0,73
10	0,82	0,63
15	0,81	0,55
20	0,8	0,48
25	0,77	0,43
30	0,76	0,40
40	0,74	0,36
60	0,71	0,32
80	0,69	0,31
100	0,68	0,31
120	0,66	0,32
140	0,65	0,32
160	0,64	0,33
180	0,63	0,33
200	0,59	0,35
220	0,59	0,36
240	0,6	0,36

Appendix 45: Comparison of lithium concentration versus time Test-1 and Test-2 (Adsorbent concentration: 3 g adsorbent/L geothermal water). (**Figure 4.50**)

	Test-1	Test-2
Time (min)	C/C_o	C/C_o
0	1,00	1
5	0,88	0,79
10	0,84	0,59
15	0,77	0,44
20	0,66	0,34
25	0,64	0,28
30	0,60	0,24
40	0,55	0,19
60	0,53	0,14
80	0,48	0,12
100	0,46	0,10
120	0,43	0,09
140	0,42	0,07
160	0,39	0,07
180	0,37	0,07
200	0,37	0,07
220	0,36	0,07
240	0,35	0,06

Batch-mode sorption for arsenic removal

Appendix 46: Curves of arsenic removal using (a) ClVBTA (b) VbNMDG resin at pH= 3-9. (**Figure 4.52**)

ClVBTA resin						
	pH 3		pH 6		pH 9	
Amount of resin (mg)	C (mg/L)	Removal of As(V) (%)	C (mg/L)	Removal of As(V) (%)	C (mg/L)	Removal of As(V) (%)
0	14.28	0.00	15.78	0.00	16.21	0.00
2	13,08	8.43	5.58	64.66	1.09	93.28
3	11.54	19.20	4.29	72.79	0.77	95.25
4	11.60	18.75	4.42	71.97	1.03	93.67
5	10.38	27.28	3.40	78.47	0.71	95.65
10	10.90	23.69	1.99	87.41	0.51	96.84

VbNMDG resin						
	pH 3		pH 6		pH 9	
Amount of resin (mg)	C (mg/L)	Removal of As(V) (%)	C (mg/L)	Removal of As(V) (%)	C (mg/L)	Removal of As(V) (%)
0	14.28	0.00	15.78	0.00	16.21	0.00
2	9.36	34.47	9.04	42.73	13.40	17.36
3	9.04	36.71	8.97	43.13	12.12	25.27
4	8.78	38.50	8.78	44.35	12.18	24.87
5	8.91	37.61	8.56	45.77	11.60	28.43
10	8.40	41.20	8.40	46.79	11.22	30.80

Appendix 47: Removal of arsenic for different VbNMDG:ClVBTA mole ratios such as 25:75, 50:50 and 75:25 at pH= 3-9. (**Figure 4.53**)

Resin1/Resin2 mol ratio	pH 3		pH 6		pH 9	
	C (ppm)	Removal of As(V) (%)	C (ppm)	Removal of As(V) (%)	C (ppm)	Removal of As(V) (%)
0/100	8.40	41.20	8.40	46.79	11.22	30.80
25/75	9.52	33.34	4.68	70.35	4.04	75.09
50/50	10.64	25.49	7.82	50.45	5.83	64.02
75/25	11.35	20.55	7.95	49.63	8.01	50.57
100/0	10.90	23.69	1.99	87.41	0.51	96.84

Appendix 48: Effect of pH on As(V) by a resin mixture of VbNMDG:ClVBTA (25:75). (**Figure 4.54**)

Time (min)	pH 3 C (mg/L)	pH 6 C (mg/L)	pH 9 C (mg/L)
0	13,71	13,71	13,71
1	11,43	6,46	5,93
3	10,50	6,21	5,68
5	10,29	5,71	5,61
10	9,75	5,68	5,54
15	9,50	5,50	5,29
30	9,21	5,36	5,25
60	8,79	5,29	4,93
120	8,75	4,82	4,86
1440	8,64	4,57	4,50

Appendix 49: Evaluation of kinetic data using pseudo-first-order kinetic model at pH 3. (**Figure 4.55**)

Time (min)	q_e (mg/g)	q_t (mg/g)	$\log(q_e-q_t)$
1	0,99	0,46	-0,277
3	0,99	0,64	-0,465
5	0,99	0,69	-0,523
10	0,99	0,79	-0,715
15	0,99	0,84	-0,845
30	0,99	0,9	-1,067

Appendix 50: Evaluation of kinetic data using pseudo-second-order kinetic model pH 3. (**Figure 4.56**)

Time (min)	q_t (mg/g)	t/qt
1	0,46	2,19
3	0,64	4,67
5	0,69	7,29
10	0,79	12,61
15	0,84	17,80
30	0,9	33,33

Appendix 51: Evaluation of kinetic data using pseudo-first-order kinetic model at pH 6. (**Figure 4.57**)

Time (min)	q_e (mg/g)	q_t (mg/g)	$\log(q_e-q_t)$
1	1,78	1,45	-0,483
3	1,78	1,50	-0,555
5	1,78	1,60	-0,748
10	1,78	1,61	-0,766
15	1,78	1,64	-0,867
30	1,78	1,67	-0,970
60	1,78	1,69	-1,032

Appendix 52: Evaluation of kinetic data using pseudo-second-order kinetic model pH 6. (**Figure 4.58**)

Time (min)	q_t (mg/g)	t/qt
1	1,45	0,690
3	1,50	2,000
5	1,60	3,125
10	1,61	6,222
15	1,64	9,130
30	1,67	17,949
60	1,69	35,593

Appendix 53: Evaluation of kinetic data using pseudo-first-order kinetic model at pH 9. (**Figure 4.59**)

Time (min)	q_e (mg/g)	q_t (mg/g)	$\log(q_e-q_t)$
1	1,76	1,56	-0,699
3	1,76	1,61	-0,824
5	1,76	1,62	-0,867
10	1,76	1,64	-0,916
15	1,76	1,69	-1,146
30	1,76	1,69	-1,192

Appendix 54: Evaluation of kinetic data using pseudo-second-order kinetic model pH 9. (**Figure 4.60**)

Time (min)	q_t (mg/g)	t/qt
1	1,557	0,642
3	1,607	1,867
5	1,621	3,084
10	1,636	6,114
15	1,686	8,898
30	1,693	17,722

Appendix 55: Evaluation of kinetic data using infinite solution volume model (ISV) at pH 3. (**Figure 4.61**)

Time (min)	q_e (mg/g)	q_t (mg/g)	X= q_t/q_e	F(X)=-ln(1-X)	F(X)=-ln(1-X^2)
1	0,99	0,46	0.464	0,623	0,242
3	0,99	0,64	2	1,056	0,554
5	0,99	0,69	0,696	1,190	0,662
10	0,99	0,79	0,804	1,631	1,041
15	0,99	0,84	0,855	1,932	1,314
30	0,99	0,9	0,913	2,442	1,794

Appendix 56: Evaluation of kinetic data using unreacted core model (UCM) at pH 3. (**Figure 4.62**)

Time (min)	X= q_t/q_e	F(X)3=X	F(X)4=3-3(1-X)$^{2/3}$-2X	F(X)= 1-(1-X)$^{1/3}$
1	0,464	0,464	1,785	0,821
3	0,652	0,652	1,575	0,884
5	0,696	0,696	1,516	0,899
10	0,804	0,804	1,353	0,935
15	0,855	0,855	1,269	0,952
30	0,91	0,91	1,166	0,971

Appendix 57: Evaluation of kinetic data using infinite solution volume model (ISV) at pH 6. (**Figure 4.63**)

Time (min)	q_e (mg/g)	q_t (mg/g)	X= q_t/q_e	F(X)=-ln(1-X)	F(X)=-ln(1-X^2)
1	1,78	1,45	0,815	1,689	1,093
3	1,78	1,50	0,843	1,854	1,242
5	1,78	1,60	0,900	2,299	1,657
10	1,78	1,61	0,904	2,339	1,696
15	1,78	1,64	0,924	2,573	1,919
30	1,78	1,67	0,940	2,809	2,147
60	1,78	1,69	0,948	2,953	2,286

Appendix 58: Evaluation of kinetic data using unreacted core model (UCM) at pH 6. (**Figure 4.64**)

Time (min)	X= q_t/q_e	F(X)3=X	F(X)4=3-3(1-X)$^{2/3}$-2X	F(X)= 1-(1-X)$^{1/3}$
1	0,815	0,815	1,335	0,938
3	0,843	0,843	1,289	0,948
5	0,900	0,900	1,191	0,967
10	0,904	0,904	1,183	0,968
15	0,924	0,924	1,147	0,975
30	0,940	0,940	1,117	0,980
60	0,948	0,948	1,102	0,983

Appendix 59: Evaluation of kinetic data using infinite solution volume model (ISV) at pH 9. (**Figure 4.65**)

Time (min)	q_e (mg/g)	q_t (mg/g)	X= q_t/q_e	F(X)=-ln(1-X)	F(X)=-ln(1-X^2)
1	1,76	1,56	0,886	2,173	1,539
3	1,76	1,61	0,915	2,461	1,811
5	1,76	1,62	0,923	2,561	1,907
10	1,76	1,64	0,931	2,672	2,014
15	1,76	1,69	0,959	3,203	2,530
30	1,76	1,69	0,963	3,308	2,633

Appendix 60: Evaluation of kinetic data using infinite solution volume model (ISV) at pH 9. (**Figure 4.66**)

Time (min)	X= q_t/q_e	F(X)3=X	F(X)4=3-3(1-X)$^{2/3}$-2X	F(X)= 1-(1-X)$^{1/3}$
1	0,886	0,886	1,215	0,962
3	0,915	0,915	1,163	0,972
5	0,923	0,923	1,149	0,974
10	0,931	0,931	1,133	0,977
15	0,959	0,959	1,080	0,986
30	0,963	0,963	1,072	0,988

Appendix 61: Linearized form of Langmuir isotherm at pH 3. (**Figure 4.67**)

C_i (mg/L)	C_e (mg/L)	Sorbed As(V) (mg)	q_e (mg/g)	C_e/q_e (g/L)
7,2	5,30	0,019	0,38	14,14
17,2	10,45	0,067	1,35	7,76
33,1	23,79	0,093	1,86	12,81
70,5	49,91	0,206	4,13	12,10
149,6	114,11	0,355	7,11	16,06
317,1	188,93	1,282	25,64	7,37
654,3	342,86	3,114	62,29	5,50

Appendix 62: Linearized form of Freundlich isotherm at pH 3. (**Figure 4.68**)

C_i (mg/L)	C_e (mg/L)	Sorbed As(V) (mg)	q_e (mg/g)	Log(q_e)	Log(C_e)
7,2	5,30	0,019	0,38	-0,43	0,72
17,2	10,45	0,067	1,35	0,13	1,02
33,1	23,79	0,093	1,86	0,27	1,38
70,5	49,91	0,206	4,13	0,62	1,70
149,6	114,11	0,355	7,11	0,85	2,06
317,1	188,93	1,282	25,64	1,41	2,28
654,3	342,86	3,114	62,29	1,79	2,54

Appendix 63: Linearized form of Langmuir isotherm at pH 6. (**Figure 4.69**)

C_i (mg/L)	C_e (mg/L)	Sorbed As(V) (mg)	q_e (mg/g)	C_e/q_e (g/L)
7,2	2,89	0,04	0,86	3,38
17,2	7,05	0,10	2,03	3,48
33,1	13,29	0,20	3,96	3,36
70,5	30,18	0,40	8,07	3,74
149,6	50,71	0,99	19,79	2,56
317,1	100,00	2,17	43,43	2,30
654,3	260,00	3,94	78,86	3,30

Appendix 64: Linearized form of Freundlich isotherm at pH 6. (**Figure 4.70**)

C_i (mg/L)	C_e (mg/L)	Sorbed As(V) (mg)	q_e (mg/g)	Log(q_e)	Log(C_e)
7,2	2,89	0,04	0,86	-0,07	0,46
17,2	7,05	0,10	2,03	0,31	0,85
33,1	13,29	0,20	3,96	0,60	1,12
70,5	30,18	0,40	8,07	0,91	1,48
149,6	50,71	0,99	19,79	1,30	1,71
317,1	100,00	2,17	43,43	1,64	2,00
654,3	260,00	3,94	78,86	1,90	2,41

Appendix 65: Linearized form of Langmuir isotherm at pH 9. (**Figure 4.71**)

C_i (mg/L)	C_e (mg/L)	Sorbed As(V) (mg)	q_e (mg/g)	C_e/q_e (g/L)
7,2	2,52	0,05	0,93	2,70
17,2	5,61	0,12	2,31	2,42
33,1	10,79	0,22	4,46	2,42
70,5	26,96	0,44	8,71	3,09
149,6	55,36	0,94	18,86	2,94
317,1	124,64	1,93	38,50	3,24
654,3	272,86	3,81	76,29	3,58

Appendix 66: Linearized form of Freundlich isotherm at pH 9. (**Figure 4.72**)

C_i (mg/L)	C_e (mg/L)	Sorbed As(V) (mg)	q_e (mg/g)	Log(q_e)	Log(C_e)
7,2	2,52	0,05	0,93	-0,03	0,40
17,2	5,61	0,12	2,31	0,36	0,75
33,1	10,79	0,22	4,46	0,65	1,03
70,5	26,96	0,44	8,71	0,94	1,43
149,6	55,36	0,94	18,86	1,28	1,74
317,1	124,64	1,93	38,50	1,59	2,10
654,3	272,86	3,81	76,29	1,88	2,44

Appendix 67: Elution profile of arsenic using HCl, HNO_3 and $HClO_4$. (**Figure 4.73**)

	Sorption (mg)	Elution (mg)	% Elution	
Sorption-1	3.23	3.10	95.96	HCl
Sorption-2	3.53	3.40	96.09	HNO_3
Sorption-3	3.72	3.44	92.33	$HClO_4$